

**Extreme Helium Stars:  
Model atmospheres and a NLTE  
abundance analysis of BD+10°2179**

**DIPLOMA THESIS**

of

**Thomas Kupfer**

from

Happurg, Germany

Performed at

Dr. Karl Remeis-Sternwarte Bamberg  
Astronomical Institute of the University of Erlangen-Nuremberg  
Sternwartstraße 7  
96049 Bamberg

**Friedrich-Alexander-Universität  
Erlangen-Nürnberg**



**ERLANGEN CENTRE  
FOR ASTROPARTICLE  
PHYSICS**

Supervised by  
Prof. Dr. Ulrich Heber  
PD Dr. Norbert Przybilla



### Abstract

Extreme helium stars are hydrogen-deficient supergiants of spectral types A and B. The atmospheres are strongly enriched in helium, carbon, nitrogen and neon, while hydrogen is highly depleted by a factor of 10 000 or more. Therefore they must be in a very late stage of evolution, that is they are immediate progenitors of white dwarfs. Two different formation scenarios have been discussed over the decades. The first one is the late thermal pulse model, where a He shell flash on the white dwarf cooling sequence forces the star to expand to become a supergiant and start the post-asymptotic giant branch evolution again. The second model invokes the merger of a helium white dwarf with a more massive C/O white dwarf in a close binary. The final aim of this work is to perform a detailed quantitative spectral analysis for the prototype BD+10°2179 of this class of rare stars using high quality spectra of unprecedented quality which cover the full optical range obtained at the European Southern Observatory with the 8.2m telescope at Paranal Observatory and the 2.2m telescope at La Silla Observatory.

To get started an overview about the interesting field of hydrogen-deficient stars both with respect to spectroscopic properties and with respect to probable evolutionary scenarios is presented. Furthermore the theoretical aspects are introduced which are closely related to this work and necessary to understand the concepts of radiation transport, line formation or the principles of non-local thermodynamic equilibrium (NLTE).

In order to cope with high quality observations the atmosphere models have to be improved. We targeted two issues:

- The UV metal line blanketing has a strong impact on the temperature-density stratification. Therefore we applied ATLAS12 code, which provides the most complete metal line blanketing to extreme composition models for the first time, testing it against the benchmark code STERNE.
- NLTE effects can affect individual spectral lines strongly. We used the DETAIL/SURFACE suite of programs to compute the synthetic spectrum treating 14 ions in NLTE.

The STERNE model atmosphere code has been developed for applications to extreme helium stars and provides a benchmark against which other codes can be tested. A detailed comparison of ATLAS12 and STERNE was mandatory since ATLAS12 has never been before applied to such unusual conditions. ATLAS12 is a general purpose code which is more complete with respect to line blanketing effects. The results obtained with both codes are compared in order to verify this. We found a wrong treatment of the line broadening of the CII line at 651.3 Å for ATLAS12. This erroneous wings dominate the whole EUV<sup>1</sup>. However, a comparison of NLTE line profiles shows no differences between STERNE and ATLAS12 which leads to the assumption that the incorrect EUV-flux has no impact on the line formation.

A LTE analysis of BD+10°2179 is described in full detail and the remaining problems are explained. Except the high value of  $\log g$  we could confirm the results obtained by Pandey et al. (2006). The high phosphorus abundance, the wide spread of abundances of heavy elements and the poor match for some lines like e.g. H $_{\alpha}$  still remain unresolved.

---

<sup>1</sup>extreme-UV means the range between the Lyman (910 Å) and the HeI ground state edge (508 Å)

Strong NLTE effects are seen in several lines which means that these effects are not negligible. We carried out a quantitative spectroscopic analysis treating line-formation in NLTE. The stellar parameters changed significantly, effective temperature by about 1 000 K and gravity by about 0.5 dex. For the first time macroturbulence was detected, in addition to microturbulence and rotation, to match the observation. The synthetic spectrum and the observation now match perfectly for most lines including the notorious ones like e.g.  $H_\alpha$  and abundances of 9 elements in NLTE were determined.

## Zusammenfassung

Extreme Heliumsterne sind wasserstoffarme Überriesen vom Spektraltyp A und B. Ihre Atmosphären sind stark mit Helium, Kohlenstoff, Stickstoff und Neon angereichert, während Wasserstoff um einen Faktor von 10 000 oder mehr abgereichert ist. Dies bedeutet, dass sie sich in einem späten Entwicklungsstadium befinden und damit unmittelbare Vorläufer von Weißen Zwergen sind. Zwei unterschiedliche Entstehungsszenarien wurden über die Jahrzehnte diskutiert. Das erste ist das "Später thermische Puls" - Modell, bei dem ein Helium-flash auf der Abkühlsequenz den Stern zu einem Überriesen aufbläht um die post-AGB Entwicklung erneut zu starten. Das zweite Modell beinhaltet die Verschmelzung von einem Helium Weißen Zwerg mit einem massereicheren C/O Weißen Zwerg in einem engen Doppelsternsystem. Das endgültige Ziel dieser Arbeit ist eine detaillierte spektrale Analyse des Prototyps dieser Klasse von seltenen Sternen, BD+10°2179, durchzuführen. Die Spektren sind von bisher unerreichter Qualität und überdecken den kompletten optischen Bereich. Sie wurden an der Europäischen Südsternwarte mit dem 8,20m Teleskop am Paranal Observatorium und dem 2,20m Teleskop am La Silla Observatorium aufgenommen.

Zu Beginn wird ein Überblick über das interessante Feld der wasserstoffarmen Sterne im Bezug auf spektroskopische Eigenschaften und mögliche Evolutionsszenarien präsentiert. Des Weiteren werden die theoretischen Aspekte, wie Konzepte des Strahlungstransports, Linienentstehung und Prinzipien des nicht lokalen thermodynamischen Gleichgewichts (NLTE) eingeführt. Diese stehen im direkten Zusammenhang zu dieser Arbeit und müssen verstanden sein.

Um der hohen Qualität der Spektren gerecht zu werden, mussten die Modell Atmosphären weiterentwickelt werden.

- Das line-blanketing von Metallen im UV hat einen erheblichen Einfluss auf die Temperatur-Dichte-Struktur. ATLAS12 unterstützt das vollständigste line-blanketing von Metallen für extreme Zusammensetzungen. Zum ersten Mal wurde ATLAS gegen den Code STERNE getestet, der Maßstab für Modell Atmosphären mit extreme Zusammensetzungen ist.
- NLTE Effekte beeinflussen individuelle Spektrallinien stark. Wir verwendeten die Programmfolge DETAIL/SURFACE um synthetische Spektren zu berechnen, die 14 Ionen im NLTE behandelt.

Der STERNE Modell Atmosphären Code wurde für die Analyse von extremen Heliumsterne entwickelt und stellt einen Maßstab gegen den andere Codes getestet werden können. Ein detaillierter Vergleich zwischen ATLAS12 und STERNE war essentiell, weil ersterer nie für diese ungewöhnliche Gegebenheiten verwendet wurde. ATLAS12 ist ein Allzweck-Code, der in Bezug auf line-blanketing Effekte vollständiger ist. Die Ergebnisse der beiden Codes wurden verglichen, um dies zu überprüfen. Wir fanden, dass die Linienverbreiterung einer CII bei 651.3 Å in ATLAS12 falsch behandelt wird. Die fehlerhaften Flügel dominieren den kompletten EUV<sup>1</sup>. Allerdings hat ein Vergleich von NLTE Linienprofile keine Unterschiede zwischen ATLAS12 und STERNE gezeigt. Das bedeutet, dass der fehlerhafte EUV-Fluss keinen Einfluss auf die Linienentstehung hat.

---

<sup>1</sup>extremes UV meint den Bereich zwischen der Lyman- (910 Å) und der HeI Grundzustandskante (508 Å)

Eine LTE Analyse von BD+10°2179 wird im Zusammenhang mit ausstehenden Problemen im Detail beschrieben. Abgesehen von dem hohen  $\log g$  Wert konnten wir die Ergebnisse von Pandey et al. (2006) bestätigen. Die hohe Phosphorhäufigkeit, die große Streuung der Häufigkeiten für schwere Metalle und die schlechte Übereinstimmung für einige Linien wie z.B.  $H_\alpha$  bleiben weiterhin ungelöst.

Starke NLTE Effekte werden in einigen Linien beobachtet. Das bedeutet, dass diese Effekte nicht vernachlässigbar sind. Eine quantitative spektroskopische Analyse, einschließlich der Behandlung von Linienentstehung im NLTE, wurde von uns durchgeführt. Die Parameter änderten sich wesentlich, die effektive Temperatur um ca. 1 000 K und  $\log g$  um ca. 0.5 dex. Zum ersten Mal wurde neben Mikroturbulenz und Rotation auch Makroturbulenz detektiert. Das synthetische Spektrum passt jetzt hervorragend zur Beobachtung, einschließlich einiger berüchtigter Linien wie z.B.  $H_\alpha$ . Abschließend konnten Häufigkeiten für 9 Elemente in NLTE bestimmt werden.

# Contents

<b>Abstract</b>	<b>III</b>
<b>Zusammenfassung</b>	<b>V</b>
<b>Contents</b>	<b>VII</b>
<b>1 Introduction</b>	<b>1</b>
<b>2 Astrophysical Background</b>	<b>3</b>
2.1 Hydrogen-Deficient Stars: A General Overview . . . . .	3
2.1.1 Spectroscopic Signatures of H-deficient and Extreme Helium Stars . . .	3
2.1.2 Evolutionary Scenarios for H-deficient Stars . . . . .	9
2.2 Stellar Structure and Atmospheres . . . . .	14
2.3 LTE vs. NLTE . . . . .	18
2.4 Radiative Transfer . . . . .	20
2.5 Line Formation . . . . .	21
2.6 Deriving Spectroscopic Parameters . . . . .	25
2.7 Computing Model Atmospheres: ATLAS12 vs. STERNE . . . . .	28
2.8 Calculating Synthetic Spectra in LTE and NLTE: DETAIL + SURFACE/SPECTRUM . . . . .	29
<b>3 Comparison between ATLAS12 and STERNE</b>	<b>31</b>
3.1 Solar Composition . . . . .	31
3.1.1 Temperature and Density Stratification . . . . .	31
3.1.2 Flux Distribution . . . . .	32
3.1.3 Hydrogen and Helium Line Profiles . . . . .	32
3.2 Helium-Rich Atmosphere in LTE . . . . .	34
3.2.1 Temperature and Density Stratification in LTE . . . . .	34
3.2.2 Flux Distribution for ATLAS12 and STERNE . . . . .	35
3.2.3 Helium, Hydrogen and Silicon Line Profiles . . . . .	36
3.3 Helium-Rich Atmosphere in NLTE . . . . .	38
3.3.1 Flux Distribution from ATLAS12 and STERNE . . . . .	38
3.3.2 Comparison of the LTE and NLTE Flux from ATLAS12 . . . . .	40
3.3.3 Comparison of the LTE and NLTE Flux from STERNE . . . . .	41
3.3.4 Comparison of the NLTE Flux from STERNE and ATLAS12 . . . . .	42
3.3.5 Line Profiles computed in LTE and NLTE . . . . .	43
<b>4 Quantitative Spectral Analysis of BD+10°2179</b>	<b>45</b>
4.1 LTE Analysis of BD+10°2179 . . . . .	46
4.1.1 Basic Measurements . . . . .	46
4.1.2 Phosphorus and Aluminium - a Quality Check . . . . .	47
4.1.3 Full LTE Analysis of BD+10°2179 . . . . .	48
4.2 Quantitative NLTE Analysis of BD+10°2179 . . . . .	51

<b>5</b>	<b>Summary and Outlook</b>	<b>59</b>
<b>A</b>	<b>Tables</b>	<b>61</b>
<b>B</b>	<b>Figures</b>	<b>69</b>
<b>C</b>	<b>Acknowledgements</b>	<b>75</b>
<b>D</b>	<b>Bibliography</b>	<b>77</b>
<b>E</b>	<b>Declaration</b>	<b>81</b>

# 1 Introduction

400 years ago in a winter night 1610 the great physicist, mathematician and astronomer Galileo Galilei discovered the four biggest moons around Jupiter with a self-constructed telescope. This was the first observation where objects did not move around the earth and therefore a great contradiction to the geocentric world view but it was the beginning of modern astronomy. The huge developments in knowledge of physics, telescopes, analysing methods etc. since that time have lead to a lot of gorgeous discoveries. We learned that we are not the center of the universe. We found out that our Sun is not unique but like millions of other stars and that we belong to a usual galaxy. We discovered that there is not just our galaxy but millions of others with in some cases totally different structure. And at the end of the last century we learned that our solar system is not unique but that there are lots of other stars which host planets. However we have not reached the end of the road yet. A new class of ground based telescopes like the E-ELT (European Extremely Large Telescope), the TMT (Thirty Meter Telescope) or the GMT (Giant Magellan Telescope) and a new generation of satellites like the James Webb Space Telescope or the Gaia satellite, improved computers and computing techniques will allow us a deeper insight into the universe as it is already possible now.

But before we can understand galaxies, galaxy clusters or probably the universe we need to understand the details. The only way to learn something about the evolution of the galaxies or the universe is to study the stars and the interstellar medium because they drive the cosmic circuit of matter. But when we look at these stars even in our neighbourhood we need to recognize that there are still a lot of open questions. There exist many stars which do not fit in the "normal" evolutionary scenario and show, for example, strange surface abundances. Hydrogen-deficient stars and especially the extreme helium stars belong to this very interesting group of stars with uncommon surface compositions. The second chapter gives an overview about the interesting field of hydrogen-deficient stars on one hand with respect to spectroscopic properties and on the other hand with respect to probable evolutionary scenarios. Binary interaction, high mass loss or strong mixing processes could be responsible for the replacement of almost all hydrogen by helium or other products of nucleosynthesis. Stars with unusual abundance compositions place high demands on synthetic model atmospheres. Therefore they are a good testbed for programs which compute these atmospheres involving the atomic physics. STERNE is one computer code which is optimized to compute model atmospheres for A- and B-type stars with extreme compositions. The other code is ATLAS12 which is the most recent version of the ATLAS package. ATLAS12 is doing opacity sampling like STERNE but includes much more metal lines and therefore should also enable the computation of model atmospheres with extreme compositions but has never been applied to such. An important aspect of the work will be to check how well the helium rich atmospheres computed with both match each other (Sec. 3). The second aspect is to apply these atmospheres to observations of the prototype of the extreme helium stars, BD+10°2179, and do a full spectroscopic LTE and NLTE analysis of high resolution FEROS and UVES spectra using STERNE and ATLAS12 model atmospheres to possibly find an answer of their evolutionary stage, their progenitors or their relation to other classes of evolved stars (Sec. 4).



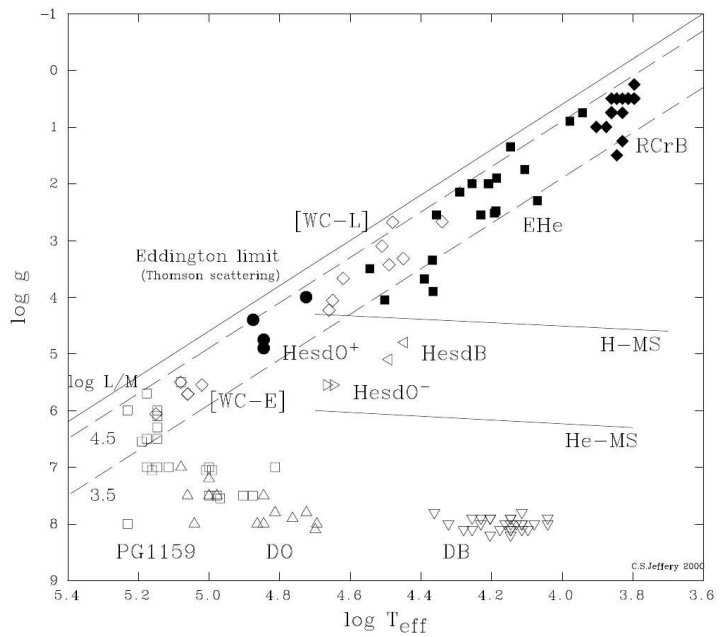
## 2 Astrophysical Background

Before the spectroscopic analysis of BD+10°2179 will be discussed in detail I want to give an overview of the astrophysical topics which are closely related to this work. First, the subclasses of hydrogen-deficient and extreme helium stars are introduced following Jeffery (2008a,b). What we can learn from a spectrum and from the application of spectral analysing methods is discussed in the second part of this chapter, following textbooks.

### 2.1 Hydrogen-Deficient Stars: A General Overview

Hydrogen deficiency has been discovered in a wide range of stars: from Earth-size white dwarfs to supergiants which are several times larger than the Sun, from white dwarfs with masses of about  $0.15 M_{\odot}$  to Wolf-Rayet objects with masses of more than  $50 M_{\odot}$ . Effective temperatures range from about 5 000 K in the R CrB stars up to 200 000 K in the PG1159 stars (Fig. 2.1). An overview of spectroscopic features is discussed first. Evolutionary scenarios are discussed afterwards.

Figure 2.1: Temperature - gravity diagram for hydrogen-deficient stars including R-CrB stars (◆: (Asplund et al. 2000)), EHe stars (■: (Jeffery 1996; Pandey 1999)), low gravity helium-rich sdO stars (HesdO<sup>+</sup>, ●: (Husfeld et al. 1989)), [WC] stars (◇: (Hamann 1996), assuming  $M = 0.6 M_{\odot}$ ), PG1159 stars (□: (Werner et al. 1996)), high-gravity HesdO stars (HesdO<sup>-</sup>, ▷: (Dreizler 1993)), helium-rich sdB stars (HesdB, ◁: (Heber et al. 1988)), DO white dwarfs (△: (Dreizler & Werner 1996)), and the DB white dwarfs (▽: (Wegner & Nelan 1987)). The Eddington limit, loci of constant luminosity over mass ( $L/M$ ), and hydrogen and helium main sequences (H-MS, He-MS) are also shown.



From Jeffery (2000)

#### 2.1.1 Spectroscopic Signatures of H-deficient and Extreme Helium Stars

It was the year 1891 when Williamina Fleming found that “the spectrum of  $\nu$  Sgr is remarkable since the hydrogen lines are very faint and of the same intensity as the additional dark lines” (Fleming 1891). This was the beginning of the research on hydrogen-deficient stars. In the beginning it was believed that the composition of the stellar atmospheres is universal which is

Table 2.1: Various classes of hydrogen-deficient stars, with representative prototypes, the number of known objects and discoverer / classifier.

Prototype	Class	No.	Discovery
<i>Population I</i>			
V1679 Cyg	Wolf-Rayet	~ 230	(Wolf & Rayet 1867)
$\nu$ Sgr	H-deficient binary	5	(Fleming 1891)
$\sigma$ Ori E	Intermediate helium B	~ 30	(Berger 1956)
<i>Low-mass supergiants</i>			
R CrB	R CrB	~ 50	(Pigott 1797; Ludendorff 1906)
HD182040	H-deficient carbon	5	(Curtiss 1916; Rufus 1923)
HD124448	Extreme helium B	17	(Popper 1942)
MV Sgr	Hot RCrB	4	(Woods 1928; Herbig 1964)
FG Sge	Born-again	3	(Hoffmeister 1944)
<i>Hot subdwarfs</i>			
PG1544+488	sdOD / He-sdB	~ 50	(Green et al. 1986; Heber et al. 1988)
BD+75°325	compact He-sdO	~ 50	(Greenstein & Münch 1953)
BD+37°1977	low- $g$ He-sdO	5	(Wolff et al. 1974)
<i>Central stars of planetary nebulae</i>			
BD+30°3639	[WC]	~ 50	(Beals 1938; Smith & Aller 1969)
A66 A30	Of-WR(C)	2	(Cohen et al. 1977)
PG1159-035	O(C) $\equiv$ PG1159	~ 40	(McGraw et al. 1979)
K 1-27	O(He)	4	(Henize & Fairall 1981)
<i>white dwarfs</i>			
HZ 21	DO	~ 50	(Greenstein 1966)
L 930-80	DB	~ 400	(Luyten 1952)
HZ 43	DC	~ 360	(Humason & Zwicky 1947)
	DQ	~ 120	
	DZ	~ 80	
AMCVn	AMCVn binary	21	(Greenstein & Matthews 1957)

From Jeffery (2008b), with modifications

the case for the vast majority of the stars. Hydrogen is with 90% by number the most abundant element in the universe. It required about 50 years until it was accepted that R CrB and  $\nu$  Sgr lost lots of hydrogen. Today there is no doubt that there are stars where all or most of the hydrogen is replaced by helium or other products of nucleosynthesis. Large surveys have produced a huge amount of data for different kinds of hydrogen-deficient stars (Tab. 2.1). They can be separated in five groups:

1. Wolf-Rayet stars, helium rich B-stars or intermediate helium stars, H-deficient or  $\nu$  Sgr binaries belong to the **Population I and Massive Hydrogen-Deficient Stars**.

The Wolf-Rayet stars are exclusively located in spiral arms, OB associations, young clusters and hence are young massive stars. Their spectra show strong emission lines which is due to high mass loss. Two different types are known. Those where the spectra contain mainly nitrogen lines (WN-type) and those where carbon is the dominant element (WC-type). In the Milky Way there are about 230 known. About 100 were found in the Large Magellanic Cloud and a dozen in the Small Magellanic Cloud. Hydrogen was detected in half of the well analysed stars.

He-rich B stars and intermediate helium stars are chemical peculiar main-sequence B stars. In the catalogue of Drilling & Hill (1986) 24 are listed which can be divided in slow and fast rotators. These stars show strong neutral helium lines. Impressive is that the line profiles are variable. The helium/hydrogen ratio varies within 1 - 10 days. The surface abundance distribution is governed by diffusion. Radiation and magnetic field are responsible for a concentration of particular elements at specific locations on the stellar surface. The overabundance in helium is due to helium-enriched spots. It is proven that for one prominent member,  $\sigma$  OriE, the helium ratio is due to strong magnetic fields up to 10 000 G where the field is about  $90^\circ$  inclined to the rotation axis.

Five Hydrogen deficient, or  $\nu$  Sgr binaries, are known today. The spectra are dominated by strong helium lines but also emission in  $H_\alpha$  and  $H_\beta$  and also pulsations were detected. The variations in  $v_{\text{rad}}$  are tens of  $\text{kms}^{-1}$  with orbital periods of 50 to 360 days. All lie not more than 200 pc away from the Galactic plane which means that these systems are not very old.

2. R CrB stars together with the H-deficient carbon stars, "Born-again" stars and the extreme helium stars belong to the group of **Low-Mass Hydrogen-Deficient Supergiants**.

The R CrB stars raised attention not because of their chemical peculiarity but because of strong erratic light variations by five to six magnitudes within days. These impressive variations are caused by surface activity and not by spots as in intermediate helium stars. The spectra are dominated by helium, carbon, the absence of hydrogen and the CH bands are replaced by  $C_2$  molecular features. 35 are known in the Milky Way and 17 in the Large Magellanic Cloud. R CrB shows an infrared excess which originates in a warm dust shell around the star. A few objects show a more extended nebula. A related class are the carbon stars. These stars have similar spectra but no infrared excess and do not show strong light variations. Formerly the carbon stars, extreme helium stars and the R CrB stars were announced to be hydrogen-deficient carbon stars (Warner 1967) but today this name is used just for the cool non-variables.

Extreme helium stars (EHes) are a rare class of low mass supergiants with spectral type A and B. The spectrum is characterised by strong lines of neutral helium but weak or totally absent hydrogen lines. Carbon, nitrogen and for some cases oxygen are strongly overabundant (Jeffery 2008a). There are just 17 EHes known and because of their high luminosity Galactic surveys should be complete. Remarkable is that EHes, carbon stars and the R CrB stars show the same kinematics. They do not share the Galactic rotation. More about the extreme helium stars can be found below.

There are three really impressive stars which evolved from one corner of the Hertzsprung-

Russell diagram to the other and back within a human lifetime. These stars are the so called "Born-again stars". All three show hydrogen-deficiency in the spectrum. FG Sgr was known as a hot white dwarf in the late 19th century and evolved into a cool supergiant in the late 20th century. V4334 Sgr was a faint blue star in 1994. Two years later the star was a yellow supergiant and in the year 1999 the star disappeared in the visual because of a thick dust shell. Radio measurement showed that the star now started a blueward evolution. The analysis of historical data and the current nebula leads to the assumption that the very hot central star of the planetary nebula A58 went through the same evolution like V4334 Sgr. These awesome evolutions are caused by thermonuclear explosions on the surface of a hot white dwarf and with three known objects in one century they are possibly not that rare.

### 3. He-sdB stars, compact He-sdO stars and low gravity He-sdO stars belong to hydrogen-deficient **Hot Subdwarfs**

Helium rich subdwarf B stars (He-sdBs) did not obtain much attention for several years. Twenty years ago just JL87 was discussed in full detail. The spectra show "pure" He I and weak or no hydrogen lines but they are not homogeneous and cover a wide range of hydrogen/helium ratios. Importantly, the double lined binary PG1544+488 consisting of two He-sdBs is the only double lined subdwarf binary which is discussed in full detail, by Ahmad et al. (2004). About 50 He-sdBs are known.

In contrast to the He-sdBs historically much more was known about the Helium rich subdwarf O stars (He-sdOs). They cover a range of two dex in surface gravity which makes the classification not so easy. The higher gravity sdO stars lie close to extreme helium branch stars and therefore are likely to be related to the He-sdB stars. The spectra are dominated by HeI and HeII and show weak hydrogen lines. Like the He-sdBs they show a wide spread in abundances and binarity. There are two main groups one which is carbon rich and the other which is not. Almost all are nitrogen rich. There are several composite binaries and also one which consists of two He-sdO stars (HE0301-3039).

The last group of helium rich hot subdwarfs are the low-gravity He-sdO stars. Just five are known and all have magnitudes brighter than  $V=12$ . No new discoveries were made in recent surveys. A big question is where are the fainter ones? These stars are interesting because R CrB stars and the extreme helium stars should look like these objects during their consecutive evolution to the white dwarf sequence.

### 4. Hydrogen deficient **Central Stars of Planetary Nebula** can be divided into [WC], Of-WR(C), O(He) and the PG1159 stars

The spectra of [WC] stars are similar to the young and massive WC Wolf-Rayet stars. Broad emission of HeI,II, CII,III,IV and NII,III and other light elements dominate the spectra. Because of optical thick winds the effective temperature is hard to derive. But measurements give values for  $T_{\text{eff}}$  of about 22 000 K to 140 000 K.

The spectra of Of-WR(C) stars are characterised by strong carbon emission lines. The HeII4686 line is also strong in emission but narrow for Of(C) and broad for Of-WR(C) stars. Abell 30 and Abell 78 are the only known Of-WR(C) stars.

O(C) stars which spectra are dominated by carbon absorption and the PG1159 stars belong to the same spectral type. Both are known to be with and without planetary nebula. The spectra of PG1159 objects are dominated by carbon and oxygen. They are the hottest known stars with effective temperatures of more than 100 000 K. H1504+065 is remarkable because

it is a naked carbon/oxygen core with no helium in the spectrum and the highest measured effective temperature of about 200 000 K. The PG1159 stars became famous because the prototype PG1159-035 shows multi-periodic pulsations.

The final stars which belong to the hydrogen-deficient central stars of planetary nebula are the O(He) stars. HeII in absorption, CIV, NV and OVI in emission puts the O(He) stars between the [WC] and the PG1159 stars. All four known O(He) do not show pulsations.

#### 5. The last large group are the H-deficient **white dwarfs** with the AM CVn binaries

40 EriB was the first discovered white dwarf (WD). The spectrum was typical for an A star but the absolute magnitude was much too faint. During the years there were a lot suggestions for classifications of white dwarfs. Today the classification scheme which is introduced in Wesemael et al. (1993) is the used one. About 80% of the known white dwarfs are DAs with hydrogen dominated spectra. The other known white dwarfs have no or almost no hydrogen in the atmosphere. DB white dwarfs show just HeI lines. If the white dwarf is hotter helium is ionised and it is therefore classified as a DO white dwarf. DC white dwarfs show just continuum and are believed to be helium white dwarfs. The reason for the absence of lines is that they are too cold to show helium lines. Other "cool" hydrogen-deficient white dwarfs are divided in two groups. Those which show strong features of carbon (DQ) and those which show strong metal lines (DZ).

The AM CVn systems are interacting white dwarf binaries with periods in the range of 5 - 65 min and belong to the most exotic known binary systems. These objects show photometric variations which are different from the orbital period but also the spectra could be totally different. They can be dominated by strong (HZ 29) or broad emission lines of HeI,II (ES Cet). HM Cnc is a AM CVn binary and has the shortest known orbital period with  $P_{\text{orb}} = 321\text{s}$ . Contrary to usual cataclysmic variables the material in AM CVn systems impacts directly on the stellar surface.

Table 2.2: Spectral signatures of hydrogen-deficient white dwarfs

Spectral Type	Characteristics
DB	HeI lines; no H or metals
DC	Continuous spectrum, no lines deeper than 5% in any part of the spectrum
DO	HeII strong; HeI or H present
DZ	Metal lines only; no H or He lines
DQ	Carbon features, either atomic or molecular in any part of the spectrum

From McCook & Sion (1999), with modifications

After an introduction of spectroscopic signatures of hydrogen-deficient stars I will now turn to the extreme helium stars and give an overview of their basic properties.

EHes are low mass supergiants of spectral type B and A. None of the known EHes show radial velocity variations indicating that no close companion exists. The distribution in the Galaxy, the distances and the radial velocities are consistent with an old spherical population strongly

concentrated to the Galactic center. All objects are quite luminous with  $L/M > 4$  and lie therefore close to the Eddington limit. Just a few have  $L/M < 3.5$ . Only 17 (among 3 in the HD catalogue) are known and because of the high luminosity surveys should be complete and just a few are probably hidden behind the spiral arms of the Galaxy. Due to the small number they must be produced by an unusual process or represent a shortlived stage of evolution, or both.

The spectra are dominated by strong neutral helium and weak or absent hydrogen lines. Carbon is highly enriched by a factor of three to ten. Consequently, the material went through the triple alpha process. Nitrogen is also overabundant. The enrichment factor fits well to the expected value if all carbon, nitrogen and oxygen went through the CNO cycle where nitrogen is enriched and oxygen and carbon is depleted. Oxygen fits to the initial metallicity or is overabundant. This fact is not predicted. Due to the CNO cycle oxygen is expected to be depleted. To obtain this abundance there must be some  $\alpha$ -capture of carbon which generates oxygen during the AGB-Phase or the merger. The other possibility could be that the central temperature of the progenitor was not high enough to maintain the NO-bicycle. Elements like Fe, Ni, Mn or Cr which should be unaffected are useful to determine the initial metallicity. The obtained abundances give a wide range of metallicity. Elements like magnesium, sulphur or silicon should follow this metallicity but this is not the case for some stars. Phosphorus and fluorine for example seem to be unexplainable overabundant in some EHes. Probably new NLTE analysis will shed light on this strange range of abundances. The high abundances of processed material lead to the conclusion that these stars are at a very late stage of evolution.

A few extreme helium stars show weak emission lines which might be caused by recombination in a shell or wind close to the star. MV Sgr stands out because it shows a lot of emission lines, some of which are double-lined. These double lines are due to a double stream or a torus around the star. But MV Sgr possibly went through a different evolution due to its erratic light variations it was first classified as a R CrB star. Some show P-Cygni profiles in the resonance lines which are due to stellar winds. Just recently Jeffery & Hamann (2010) measured mass loss rates of six extreme helium stars by fitting the P-Cygni profile of C, N and Si resonance lines. They found mass loss rates in the range of  $10^{-10} - 10^{-7} M_{\odot} \text{yr}^{-1}$ . Jeffery et al. (2001) showed that the effective temperature increases for some EHes because of contraction which is predicted for high  $L/M$  ratios. For evolutionary models the measurements are important and need to be improved. BD+10°2179 for example seems to cool down which would be due to a secular expansion. This can not be completely excluded for early evolution of helium stars but seems to be unlikely.

Small amplitude pulsations have been detected in about three quarters of the extreme helium stars. They can be divided into three major groups, the V652 Her, the FQ Aqr and the V2076 Oph pulsators.

V652 Her and BX Cir belong to the first group. They show low amplitude light and radial velocity variations with a regular period of a few hours. These radial pulsations are driven by the  $\kappa$  mechanism through Z-bump instability.

The cool extreme helium stars which show quasi-periodic low amplitude light variations over 5 - 30 days are the FQ Aqr variables. The radial pulsations are driven by strange-mode instability. Hot extreme helium stars belong to the last group, the V2076 Oph pulsators. They show low amplitude quasi periodic light variations over 0.5 - 5 days. Probably radial velocity and line variations are seen. These variations are due to non-radial g-mode pulsations driven by strange

mode instability.

Some of the EHes do not show any variations on short timescales. BD+10°2179 belongs to this group.

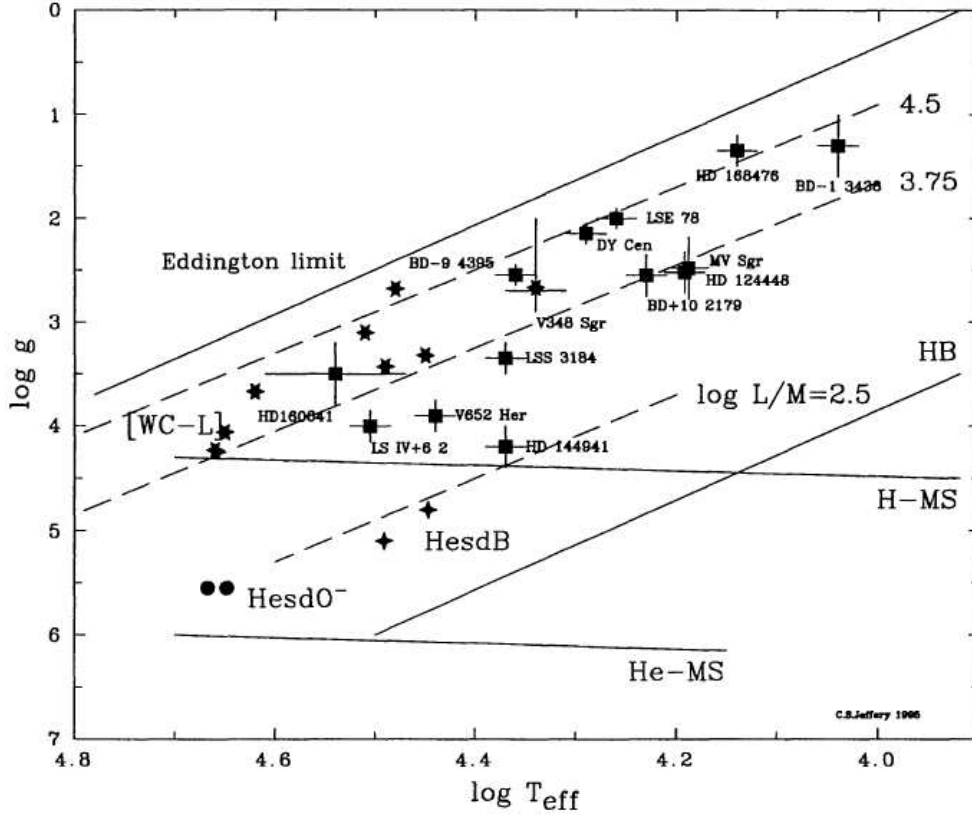


Figure 2.2: The  $\log g - T_{\text{eff}}$  diagram for EHe (squares) and related objects, including HesdB (crosses), HesdO (circles) and [WC-L] (star) stars. Solid lines show the hydrogen and helium main-sequences, the horizontal branch and the Eddington limit for pure Thomson scattering in a helium atmosphere. Broken lines show the loci of stars with the given  $L/M$ .

From Jeffery (1996)

### 2.1.2 Evolutionary Scenarios for H-deficient Stars

High mass loss, mixing processes through thermal pulses or binary interaction can be responsible for the removal of a significant fraction of hydrogen from the surface. For massive hydrogen-deficient stars the formation process is quite well understood. Wolf-Rayet stars lost lots of hydrogen due to strong stellar winds which are driven by high radiation pressure. During their lifetime these stars can lose more than half of their initial mass.  $\nu$  Sgr binary systems lost their envelopes through interaction with the companion. Mass transfer removes the hydrogen rich envelope. The prototype  $\nu$  Sgr was found to be double lined with a primary mass of about  $3 M_{\odot}$ . Therefore it is together with the Wolf-Rayet stars a good candidate for supernovae Ib,c. In the last years the Wolf-Rayet stars went into focus, because of their high mass they are also possible progenitors for Gamma Ray Bursts.

The evolution and the link to progenitors for low mass stars is much more complicated and in some cases still under debate. Helium shell burning occurs in an Asymptotic Giant Branch (AGB) star not stable but in thermal pulses. The huge amount of energy which is produced during a pulse forces the development of a convective zone which mixes helium processed material like carbon and oxygen in the intershell region. The hydrogen burning region is pushed to cooler regions and extinguished. Therefore the envelope convection can proceed in the intershell regions and mixes the carbon and oxygen enriched material to the surface, giving rise to carbon stars. This is called the third dredge up. After the pulse the star contracts and hydrogen burning will start again. This heats up the intershell region and when the helium layer is hot enough another pulse ignites. The time between two pulses is constant but depends on the mass of the star. A more massive star will experience thermal pulses within shorter periods. The post-AGB evolution depends on the fact whether a thermal pulse occurs after the star left the AGB. If no pulse occurs on the post-AGB sequence a DA white dwarf will be formed after the hydrogen burning layer is extinguished. But a thermal pulse can also happen when the star is already on the post-AGB track. There are two different possibilities. First when the hydrogen shell is still burning the pulse is called late thermal pulse. On the other hand when the hydrogen burning shell is already extinguished a very late thermal pulse can occur. Because of the very thin envelope which is left after leaving the AGB both force the star to expand and start the post-AGB evolution again. It is believed that the (very) late thermal pulse is the trigger of the "born again" stars, the PG1159 stars, the Wolf-Rayet central stars, the hydrogen-deficient central stars of planetary nebula and the DO, DB and DC white dwarfs. The origin of the DZ white dwarfs is still under debate, because of diffusion all metals should have sunk to the inner parts of the WD.

For the other low mass hydrogen-deficient stars a binary system is necessary. The more massive star will first evolve to become a red giant. If the system is close enough the giant fills its Roche Lobe and a common envelope is formed. Friction and loss of orbital energy will force the ejection of the common envelope. If the complete hydrogen envelope is ejected a core helium burning He-sdB is left over. For the wider systems stable Roche lobe overflow could transfer the hydrogen rich envelope to the companion and form again a He-sdB binary with a main sequence star. If two common envelopes occur the system can consist of two white dwarfs in such a close system that a merger is possible within a Hubble time. If the merger exceeds the Chandrasekhar mass the star will explode as a supernova Ia. If the newborn star is less massive the star will expand and start again the post-AGB evolution depending on the type of white dwarfs which are involved. The merger of two helium white dwarfs possibly takes the following way (Jeffery 2008b):

$\text{EHe} \rightarrow \text{He-sdB} \rightarrow \text{He-sdO} \rightarrow \text{He-MS} \rightarrow \text{low-mass CO white dwarf}$

The merger of a helium white dwarf and a C/O white dwarf possibly takes the following way (Jeffery 2008b):

$\text{R CrB} \rightarrow \text{EHe} \rightarrow \text{low-gravity sdO} \rightarrow \text{O(He)} \rightarrow \text{high-mass CO white dwarf}$

For binary white dwarfs with high mass ratios no merger will occur but a AM CVn will be formed.

After the general introduction to the evolution of hydrogen-deficient stars the possible evolutionary scenario for extreme helium stars are introduced in more detail. Two different scenarios how to produce an extreme helium star have been discussed over the decades. The late thermal pulse (LTP) model on the one hand and the merger of two white dwarfs on the other. The latter seems to be the more probable one. I will discuss both scenarios and shall argue why the merger scenario is better suited to explain extreme helium stars.

### Formation due to a Late Thermal Pulse

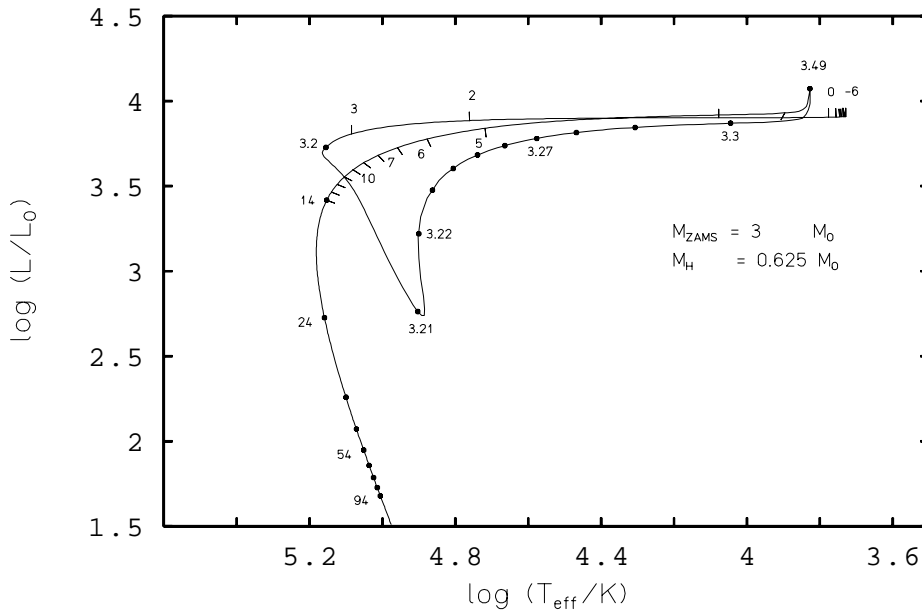


Figure 2.3: Evolution of a post-AGB model with  $M_{\text{ZAMS}} = 3M_{\odot}$  and  $M_{\text{H}} = 0.625M_{\odot}$  suffering from a LTP (Bloeker 1995). Age zero refers to a pulsational period of 50 d. Time marks are in units of  $10^3$  yrs.

From Bloeker (2001)

Helium burning in an AGB star occurs unstable in so-called thermal pulses. The burning shell produces during a flash such an amount of energy that a convective zone is established. This zone mixes He-burning products like carbon and oxygen in the intershell region. Usually the surface abundance is just slightly enriched by processed material. But if the pulse happens when the star is already on the post-AGB sequence the remaining envelope mass is small enough ( $<10^{-4} M_{\odot}$ ) that the pulse has a significant impact on the outer layers and forces the star to become a cool supergiant. This huge expansion of the star cools the hydrogen burning shell in such a way that it disappears and the convection zone from the outer layers passes the hydrogen processed material which enriches the helium and nitrogen abundance at the surface significantly. The bottom of the convection zone reaches also the former intershell region which is enhanced

in carbon and oxygen. Because of the low mass of the envelope the surface is expected to be highly enriched in helium, nitrogen, carbon and oxygen. The models predict a remaining hydrogen abundance of about 2%. The strength of the enrichment of carbon, oxygen and helium depends strongly on the position where the late thermal pulse takes place, how effectively the convective zone brings processed material to the surface and whether overshooting is included or not (Bloeker 2001). When the star reaches again the supergiant phase a stable helium burning shell is established and the star starts the post-AGB evolution again. It seems that stars which suffer the (very) late thermal pulse have much higher carbon and oxygen abundances than observed in extreme helium stars. The way through the Hertzsprung-Russell-diagram for a  $3 M_{\odot}$  star which suffers from a late thermal pulse is illustrated in Fig. 2.3.

### Formation due to a White Dwarf Merger

Webbink (1984) and Iben & Tutukov (1984) introduced the merger scenario in which two white dwarfs in a close binary system merge to produce an extreme helium star. The more massive star in the binary system will first evolve to become a red giant in the initial binary system and fill its Roche Lobe. Unstable mass transfer will lead to a common envelope phase. Friction, loss of orbital energy and therefore a decay of the binary orbit forces the ejection of the common envelope. After that the less massive star will evolve to become a red giant and another common envelope (CE) will be formed which shrinks the orbit even more. Two CE phases are necessary to reduce the orbit significantly that it becomes possible for the system to merge within a Hubble time.

The remaining system consists of a helium white dwarf with about  $0.3 - 0.4 M_{\odot}$  and a carbon/oxygen white dwarf with a mass of about  $0.5 - 0.6 M_{\odot}$ . Because of gravitational wave radiation the orbit of the binary system decays until the helium white dwarf fills its Roche Lobe because the less massive white dwarf has the larger radius. Due to tidal forces the helium white dwarf will be disrupted in about two to three minutes. A debris disk around the CO white dwarf is created. It is assumed that the CO white dwarf accretes around  $10^{-5} M_{\odot} \text{yr}^{-1}$ . After enough helium is accreted the helium ignites and forces the star to expand and become a yellow supergiant. At a pre-assigned final mass, helium accretion is switched off. The helium burning shell around the CO white dwarf core is stable and maintains the star as a supergiant. From that point the helium shell burns outwards leaving a more massive CO core. When the mass of the envelope above the burning shell becomes small the surface temperature increases and the star evolves horizontally bluewards in the Hertzsprung-Russell diagram. During the outward progression of the shell the star contracts. The contraction rate is highly dependent on the hydrogen amount and the mass of the extreme helium star. During its evolution the star will look at one point like the low-gravity He-sdOs and will end as a massive carbon/oxygen white dwarf.

Today it is believed that the merger of two white dwarfs is the most likely scenario to produce an extreme helium star. The late thermal pulse model predicts much higher oxygen and carbon abundances (Herwig et al. 1999). Most parameters for the EHes fit well to the predicted ones from the merger model which is discussed in full detail in Saio & Jeffery (2002). But there are still a lot open questions like is there any nucleosynthesis during the merger or what happens to the angular momentum of the binary system?

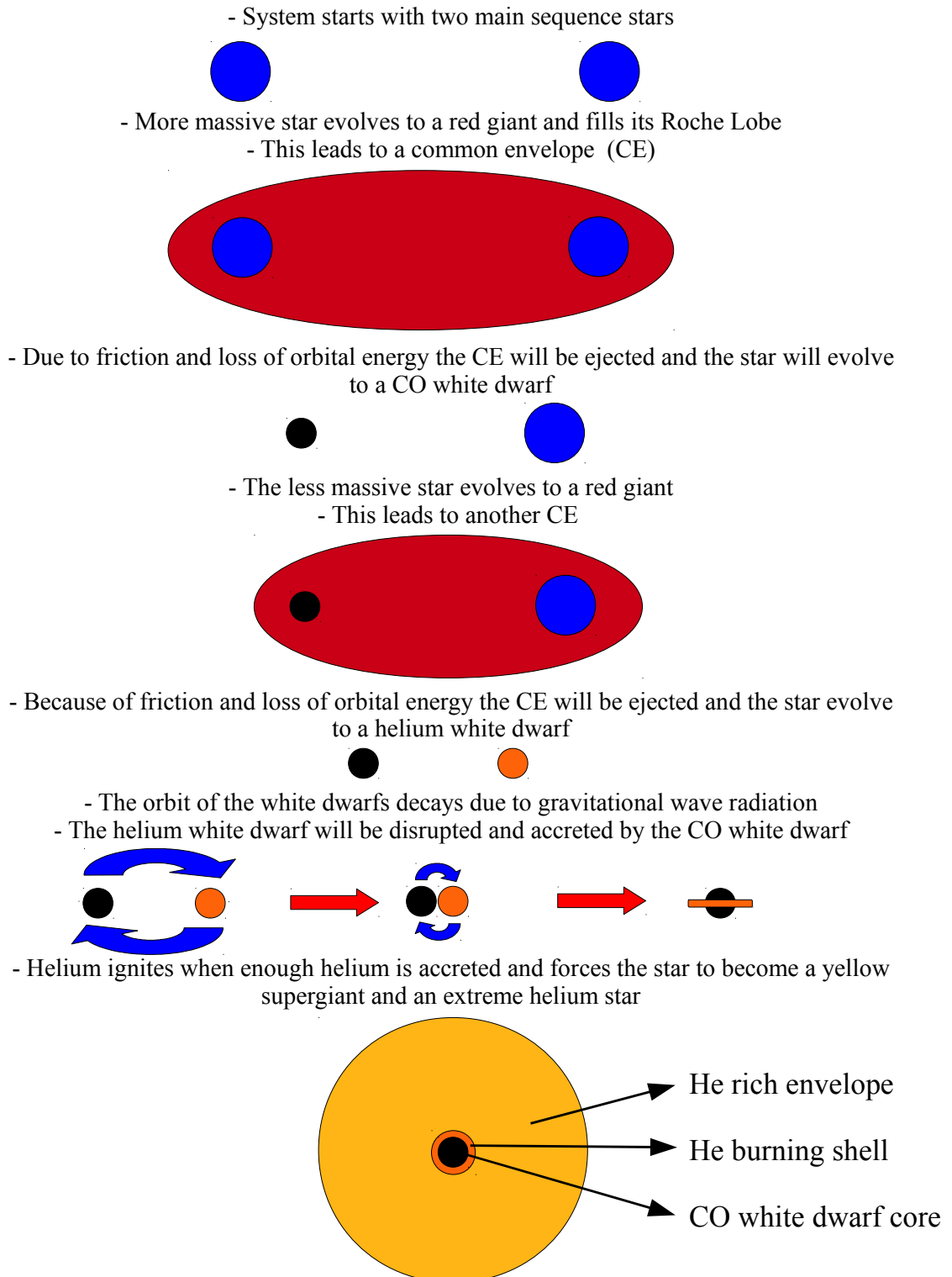


Figure 2.4: Illustration of the formation for an extreme helium star through a merger of a helium and carbon/oxygen white dwarf

## 2.2 Stellar Structure and Atmospheres

Because of their distances, stars remain point sources in almost all cases. What we see is the averaged light of the star which was produced in the center through fusion processes. This light we can observe was emitted in the atmosphere. Our only way to learn something about the temperature, the density, the abundances and the structure of the star is to model these atmospheres. The best parameters of the model are those which reproduce the observed spectrum. In this chapter I will give an introduction to the way to construct a model atmosphere. But before a brief introduction to stellar structure is given.

Stars are spherical symmetric objects and can be described through five equations (Kippenhahn & Weigert 1990):

The continuity equation with the radius  $r$ , the mass within the radius  $M_r$  and the density  $\rho$ :

$$\frac{\partial r}{\partial M_r} = \frac{1}{4\pi r^2 \rho} \quad (2.1)$$

The hydrostatic equation with the pressure  $P$  and the radius  $r$ :

$$\frac{\partial P}{\partial M_r} = -\frac{GM_r}{4\pi r^4} - \frac{1}{4\pi r^2} \frac{\partial^2 r}{\partial t^2} \quad (2.2)$$

The energy conservation equation with the energy  $L_r$  which flows through a sphere with the radius  $r$  per second, the energy  $\epsilon$  which is produced per mass and second, the energy  $\epsilon_\nu$  which is carried by the neutrinos:

$$\frac{\partial L_r}{\partial M_r} = \epsilon - \epsilon_\nu - c_P \frac{\partial T}{\partial t} + \frac{\delta}{\rho} \frac{\partial P}{\partial t} \quad (2.3)$$

The energy transport equation with the temperature  $T$  the opacity  $\kappa$  and the heat capacity  $C_V$  and  $C_P$ :

$$\frac{\partial T}{\partial M_r} = -\frac{3\kappa}{64\pi^2 ac r^4 T^3} \frac{L_r}{r} \quad (\text{radiation in diffusion approximation}) \quad (2.4)$$

or

$$\frac{\partial T}{\partial r} = \left(1 - \frac{C_V}{C_P}\right) \frac{T}{P} \frac{\partial P}{\partial r} \quad (\text{convection}) \quad (2.5)$$

The chemical composition equation with the mass fraction  $X_i$  of the element  $i$ , the mass  $m_i$  of the element  $i$  and the reaction rate  $r_{ji}$  and  $r_{ik}$ :

$$\frac{\partial X_i}{\partial t} = \frac{m_i}{\rho} \left( \sum_j r_{ji} - \sum_k r_{ik} \right) \quad i = 1, \dots, I \quad (2.6)$$

The mass of a spherical shell with the thickness  $dr$  which is at a distance  $r$  from the center (Fig. 2.6) is given by Eq. 2.1. Mass loss is neglected in this equation. The full equation for the mass including mass outflow with the velocity  $v$  is given as

$$dM_r = 4\pi r^2 \rho dr - 4\pi r^2 \rho v dt \quad (2.7)$$

Gravity forces the material of the star to move towards the center which is given by the equation for the force of gravity ( $F_G$ ) with  $G$  as the gravitational constant and  $A$  as the enclosed area.

$$F_G = -G \frac{M_r}{r^2} \rho A dr \quad (2.8)$$

Buoyancy ( $F_P$ ) forces the material to move outwards and is given as

$$F_P = A[P(r + dr) - P(r)] = A \frac{\partial P}{\partial r} dr \quad (2.9)$$

Eq. 2.2 follows when both forces are set equal but for the general case which includes non-equilibrium. For most stars it can be assumed that both forces are in equilibrium which means that the second term on the right side of Eq. 2.2 is zero.

$L_r$  is the energy which flows through a sphere with the radius  $r$  per second. Therefore at the center  $L_r(0) = 0$  and at the surface  $L_r(R) = L$ .  $\epsilon$  is the energy which is produced per mass and second. For the time independent case where stationarity is assumed  $L_r$  can be written as

$$dL_r = \epsilon dM_r \quad (2.10)$$

For the non-stationary case a change of internal energy (first part of the equation) and the exchange of mechanical work (second part of the equation) has to be considered. This leads to

$$\frac{\partial L_r}{\partial M_r} = \epsilon - \frac{\partial u}{\partial t} - P \frac{\partial v}{\partial t} \quad (2.11)$$

Neutrinos are produced during fusion processes. They have almost no interaction with the stellar material and escape unaffected. This leads to Eq. 2.3 for the energy conservation with  $\epsilon_\nu$  as the energy which is carried by the neutrinos.

Three possibilities are known to transport energy: Conduction, convection and radiation. The first is very inefficient because the electrons can move not far enough until they collide with other particles. For most stars energy transport through conduction is negligible. However, for white dwarfs, neutron stars or other compact objects it is important. The mean free paths in these stars are extremely short for photons but can be relatively large for electrons.

A good way of finding out if convection or radiation takes place in the star is the thought experiment from Karl Schwarzschild:

A small bubble moves outwards so fast that there is no energy exchange (adiabatic) but so slow that pressure compensation takes place. If the density in the adiabatic element is smaller than in the surrounding radiative layers the bubble is moving upwards but if the density is higher the bubble is moving back and the layer is stable against convection.

For homogeneous layers convection sets in when  $\nabla_{\text{rad}} > \nabla_{\text{ad}}$  where  $\nabla_{\text{rad}}$  is the radiation gradient and  $\nabla_{\text{ad}}$  is the adiabatic gradient. A high opacity ( $\kappa$ -effect) makes  $\nabla_{\text{rad}}$  high.  $\nabla_{\text{ad}}$  becomes small when the stellar material differs from the ideal gas for example through ionisation (ionisation-effect). Both are responsible that convection dominates in the outermost layers of low-mass stars in particular in the region where hydrogen and helium ionises.  $\nabla_{\text{rad}}$  becomes also high when  $\epsilon$  increases. This leads to convection zones in the core of massive stars where the energy is mainly produced through the CNO-cycle because  $\epsilon \sim T^\gamma$  with  $\gamma \approx 4$  for the

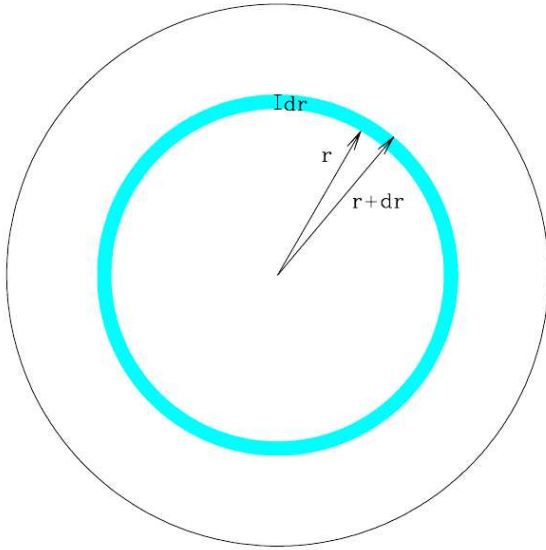


Figure 2.5: Illustration for the continuity equation

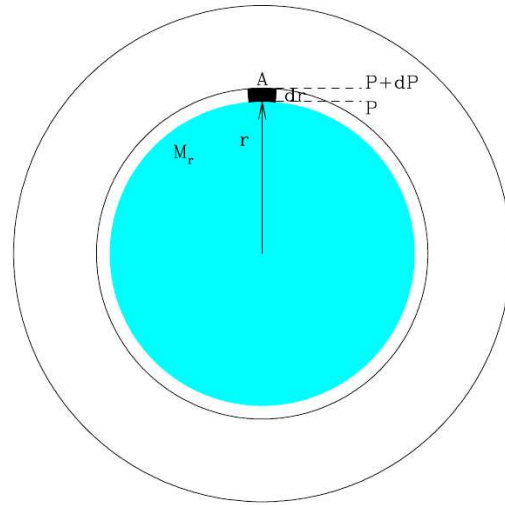


Figure 2.6: Illustration for the hydrostatic equilibrium

pp-chain,  $\gamma \approx 16$  for the CNO-cycle and  $\gamma \approx 30$  for helium burning. The full equations for energy transport by radiation and convection are given by Eq. 2.4 and Eq. 2.5.

The chemical composition has a direct impact on  $\kappa$ ,  $\epsilon$  or  $\mu$ . For a radiative structure the temporal change of the composition is given by Eq. 2.6. In such a structure no direct material exchange is possible but the composition can change through several reactions like the fusion process in the core of the star. The convective regions in a star are always homogeneous ( $\frac{\partial X_i}{\partial M_r} = 0$ ) but the composition of a convective zone can change without any core reactions for example when the border of the convective zone changes.

The stellar atmosphere is just the outermost layer from which we can observe the photons. In general we can use the same equations like I introduced before. Some simplifying assumptions are justified which are mentioned first. However stellar atmospheres are still not easy to compute and there are some complications which we have to deal with. These points are explained after the simplifications.

### Simplifying Assumptions for Stellar Atmospheres

- **Plane-Parallel Geometry** If the height of the atmosphere  $\Delta r$  is negligible compared to the radius of the star  $R$  ( $\Delta r/R \ll 1$ ) plane-parallel geometry can be assumed. This means that the curvature of the atmosphere is hardly noticed by the photons which is correct for almost all stars except some O-stars, M-giants, M-supergiants like Beteigeuze or Wolf-Rayet stars.
- **Homogeneity** Homogeneity means that the chemical composition of the atmosphere is the same at every point.
- **Stationarity** Usually spectra of stars do not show variations over time. If no time dependence exist stationarity is valid

- **Hydrostatic Equilibrium** For stellar atmospheres hydrostatic equilibrium can be assumed which means that due to the second Newtonian law

$$dm \cdot \frac{d}{dt}v(r, t) = \sum_i dF_i = 0 \quad (2.12)$$

is justified. Three different forces ( $F$ ) act in a star:

1. gravitational force:  $dF_{\text{gr}} = -G \frac{M_r \cdot dm}{r^2} = -g(r) \cdot dm$  with  $g(r) = G \frac{M_r}{r^2}$
2. gas pressure:  $dF_{\text{gas}} = -A \frac{dP}{dr} \cdot dr$
3. radiation pressure:  $dF_{\text{phot}} = g_{\text{rad}} \cdot dm$

Using these equations in Eq. 2.12 and inserting

$$dm = A \cdot \rho \cdot dr \quad (2.13)$$

leads to Eq. 2.14. The mass of the atmosphere is negligible compared to the total mass of the star and plane-parallel geometry is assumed. This leads to Eq. 2.15 where  $g$  is the surface gravity and is given by Eq. 2.16 which is a fundamental parameter for the physics in stellar atmospheres.  $g_{\text{rad}}$  is the radiation pressure and important for main sequence stars of more than 40 000 K but also Wolf-Rayet stars. For the case  $g_{\text{rad}} > g$  like in Wolf-Rayet stars or hot supergiants strong stellar winds are established and the assumption of hydrostatic equilibrium fails.

$$\frac{dP}{dr} = -\rho(r)[g(r) - g_{\text{rad}}] \quad (2.14)$$

$$\frac{dP}{dx} = -(g - g_{\text{rad}})\rho(x) \quad (2.15)$$

$$g = -G \frac{M}{R^2} \quad (2.16)$$

- **Radiative Equilibrium** Energy is produced by nuclear processes in the core of the star and is transported outwards and passes also the atmosphere. This energy is absorbed per unit volume summed over frequency and is equal to the energy which is emitted per unit volume summed over frequency (Eq. 2.17). Energy conservation implies that the emitted flux is constant if plane-parallel geometry is assumed.

$$\int_0^\infty j_\nu \rho d\nu = \int_0^\infty \kappa_\nu \rho J_\nu d\nu \quad (2.17)$$

### Complications for Stellar Atmospheres

Even if some simplifying assumption are justified finding a solution for an atmosphere is not an easy task. Some complications are mentioned in the following:

- Radiative transfer in stellar structure is computationally treated in the diffusion approximation because of the photons' small mean free path (Eq. 2.4). For model atmospheres however a detailed solution of the radiative transfer equation is necessary (see Sec. 2.4).

- Hydrostatic equilibrium has to be ensured in each depth point. In calculation codes of model atmospheres this is not an easy task for the outermost layers of the atmosphere. Because of lower temperatures, opacities become higher which leads to an increase of the radiation pressure  $g_{\text{rad}}$ . When  $g_{\text{rad}}$  becomes larger than  $g$  hydrostatic equilibrium fails and the calculation of the model atmosphere aborts. This is not a real physical phenomenon in stellar atmospheres but a computational artefact in model atmosphere codes.
- The atmospheres of supergiants and hot stars are known to experience strong NLTE effects. Therefore NLTE calculations are necessary by solving the full set of equations for the population densities of all atomic levels from the principle of statistical equilibrium (Eq. 2.22). That makes the analysis much more complicated and leads to an increase of the computing time by orders of magnitude. Principles of NLTE calculation are described in the next section.

## 2.3 LTE vs. NLTE

The easiest way to treat a star is that the star is a closed system which leads to thermodynamic equilibrium (TE). In this case the energy distribution is given by the Planck-equation with the frequency  $\nu$ , the Planck constant  $h$ , the light velocity  $c$  and the Boltzmann constant  $k$ .

$$I_\nu d\nu = B_\nu(T) d\nu = \frac{2h\nu^3}{c^2} \frac{1}{e^{\frac{h\nu}{kT}} - 1} d\nu \quad (2.18)$$

The velocity distribution for the thermal movement of particles is given by the Maxwell distribution.

$$f(\vec{v}_{\text{th}}) dv_x dv_y dv_z = \left( \frac{m}{2\pi kT} \right)^{\frac{3}{2}} e^{-\frac{m}{2kT}(v_x^2 + v_y^2 + v_z^2)} dv_x dv_y dv_z \quad (2.19)$$

Atomic levels (u for the upper level, l for the lower level) are populated according to the Boltzmann formula where  $g$  expresses the statistical weight of each level,  $E$  the energy of the level and  $n$  the population density.

$$\frac{n_u}{n_l} = \frac{g_u}{g_l} e^{-\frac{(E_u - E_l)}{kT}} \quad (2.20)$$

The Saha equation with the electron density  $n_e$  and the electron mass  $m_e$  follows if the upper level of the Boltzmann formula is expanded to a two particle system (ion + free electron) which includes the possible ionisation of an atom.

$$\frac{n_u}{n_l} = \frac{1}{n_e} \frac{g_u}{g_l} e^{-\frac{(E_u - E_l)}{kT}} 2 \left( \frac{2\pi m_e kT}{h^2} \right)^{\frac{3}{2}} \quad (2.21)$$

Obviously, stars are not closed systems. Radiation emits from the surface which is due to a temperature gradient in the star and means that stars are never in TE. To improve this, the idea is that every separated volume element is in thermodynamic equilibrium which is called local thermodynamic equilibrium (LTE). The energy distribution is given by the local temperature  $T$ . Boltzmann formula, Maxwell and Saha equation can be solved with this temperature. Notice that the complete radiation field is not just given by the Planck distribution ( $I_\nu(r) \neq B_\nu(T(r))$ ) but as a superposition of  $B_\nu(T(r))$  for the different volume elements. The question is, whether LTE is always justified. Different volume elements can interact with each other through photon emission and absorption. If absorption of photons disturbing the equilibrium LTE is invalid.

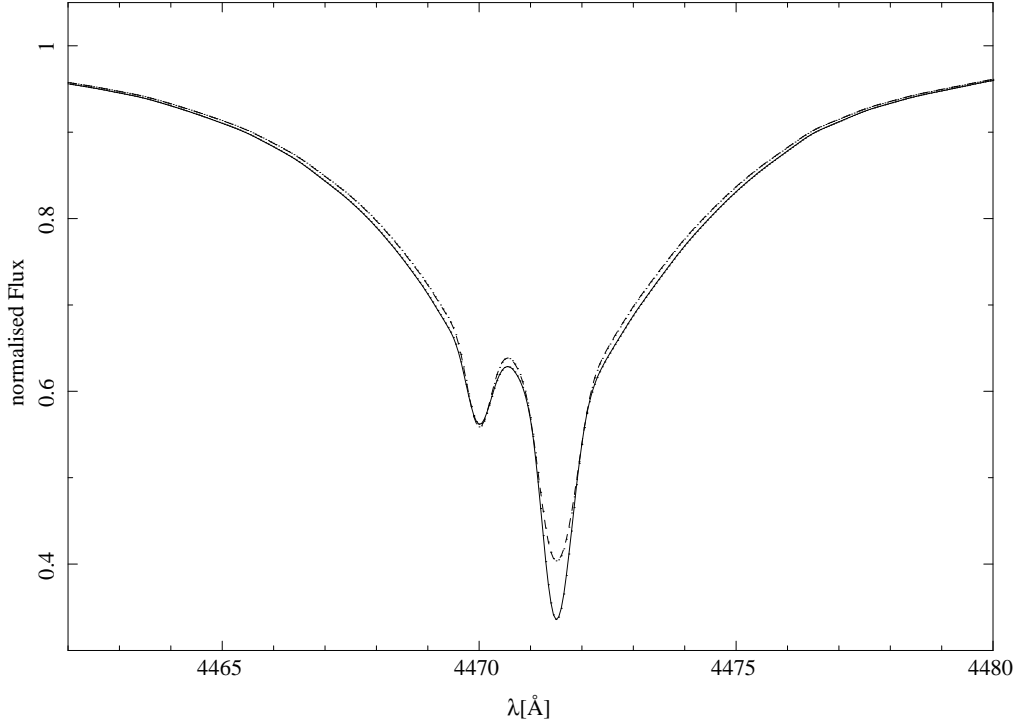


Figure 2.7: Comparison of NLTE (solid line) and LTE (dashed line) model with equal  $T_{\text{eff}} = 16\,800\text{ K}$  and  $\log g = 2.80$  for a helium rich atmosphere. It can be seen that there is an obvious difference between both and a NLTE analysis will increase the accuracy of the parameters significantly

Stellar interiors are well described by LTE. For high temperature and low density LTE becomes problematic. In the atmosphere of supergiants and hot stars with  $T_{\text{eff}} > 30\,000$  the interaction of radiation and matter needs to be considered to calculate the occupation numbers, which means that NLTE calculations are necessary.

The Maxwell distribution is still valid for NLTE. The Boltzmann formula and Saha equation are replaced by  $dn_i/dt = 0$  which means that the populations of the levels do not change over time. This is due to stationarity of the atmosphere. Instead of the Saha equation the rate equation (Eq. 2.22 where  $C_{ij}$  are the collisional rates and  $R_{ij}$  are the radiative rates from level  $i$  to  $j$ ) has to be solved to obtain the occupation numbers for the atoms and ions.

$$n_i \underbrace{\sum_{j \neq i} (R_{ij} + C_{ij})}_{\text{lines}} + \underbrace{n_i (R_{ik} + C_{ik})}_{\text{ionisation}} = \underbrace{\sum_{j \neq i} n_j (R_{ji} + C_{ji})}_{\text{lines}} + \underbrace{n_k (R_{ki} + C_{ki})}_{\text{recombination}} \quad (2.22)$$

The radiation processes depend on the radiation field. The radiation field depends on the opacity and the opacity depends on the occupation numbers. Therefore a lot iteration steps are necessary to find a good solution. The computing time increases by orders of magnitude. NLTE analyses became possible with increasing computer power. Przybilla et al. (2005) could reproduce the helium lines much better for two extreme helium stars by doing a NLTE analysis. Therefore NLTE analyses of extreme helium stars possibly increase the accuracy of the parameters and the abundances significantly. Fig. 2.7 shows the difference in LTE and NLTE for the H $\epsilon$ 4471 line in a helium rich atmosphere.

## 2.4 Radiative Transfer

The fundamental way to describe the radiation field is the specific intensity  $I_\nu(\nu, \vec{n}, \vec{r}, t)$  (Fig. 2.8)

$$I_\nu(\nu, \vec{n}, \vec{r}, t) = \frac{d^4 E}{d\nu dt d\omega d\sigma} \quad (2.23)$$

But before radiation is leaving the star, it interacts with the matter (Fig. 2.10). True absorption, true emission and scattering is possible. Thomson scattering of a photon on an electron or emission of a photon and re-emission of another photon in a different direction and frequency are examples for scattering processes. Photo-ionisation (bound-free), excitation (bound-bound) or excitation followed by ionisation are true absorption processes. The inverse are true emission processes. Bound-bound transitions are responsible for the spectral lines. The energy gap of two levels and therefore the energy of the photon is unique for every element. This means that the position of spectral lines are fingerprints of the elements which is important for a quantitative spectral analysis. Grotrian diagrams are a way to show the transitions which can occur in an atom (Fig. 2.9).

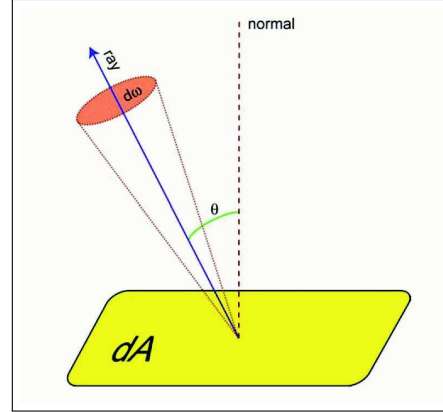


Figure 2.8: Illustration of the way to describe the specific intensity

The decrease of intensity through absorption along the way  $ds$  is given by Eq. 2.24 where  $\kappa_\nu$  is the absorption coefficient (opacity).

$$dI_\nu = -\kappa_\nu I_\nu ds \quad (2.24)$$

$\kappa_\nu$  is in general a complicated function and consists of several kinds of opacity sources like continuum opacity and in the spectral lines the bound-bound opacity. In almost all stars hydrogen is the dominant element for the continuum opacity but as extreme helium stars have almost no hydrogen, helium is the dominant element. But also the influence of the metals increases significantly because the photo-ionisation edges of hydrogen like the Lyman or the Balmer-edge are missing and therefore the flux is much higher in the UV which means that the remaining opacity sources in the UV have much stronger influence.

The optical depth  $\tau$  is also in relation to the opacity.

$$\tau_\nu := \int_0^s \kappa_\nu ds \quad (2.25)$$

The mean free path of the photons is the geometrical way where  $\tau_\nu = 1$  which means that in general photons cover a mean path of  $\Delta\tau_\nu = 1$ . The opacity is higher within a line than within the neighbouring continuum. Therefore the optical depth is larger which leads to the assumption that the photons from the line regions are emitted from sources further out in the atmosphere than the continuum photons. The temperature is increasing towards the center. That means that

with Eq. 2.18 photons from the outer parts of the atmosphere have less flux. In this way the absorption lines in stellar spectra are formed (Fig. 2.11).

Radiation is not just absorbed by the matter but also emitted. The specific intensity for emission is given by Eq. 2.26 with the emission coefficient  $\epsilon_\nu$ . Like the absorption coefficient,  $\epsilon_\nu$  is a complicated function of several parameters like for example temperature or pressure.

$$dI_\nu = \epsilon_\nu ds \quad (2.26)$$

We achieve the full transport equation for any path by combining absorption and emission.

$$\frac{dI_\nu}{ds} = -\kappa_\nu I_\nu + \epsilon_\nu \quad (2.27)$$

Assuming plane-parallel geometry and with the source function in LTE  $S_\nu = \frac{\epsilon_\nu}{\kappa_\nu}$  the transport equation can be written as a linear differential equation of first order.

$$\mu \frac{dI_\nu(\mu, \tau_\nu)}{d\tau_\nu} = I_\nu(\mu, \tau_\nu) - S_\nu(\tau_\nu) \quad (2.28)$$

Solving this differential equation leads to the formal solution of the transport equation.

$$I_\nu(\mu, \tau_1) = \underbrace{I_\nu(\mu, \tau_2)e^{-(\tau_2-\tau_1)/\mu}}_{\substack{\text{emitted intensity at } \tau_2 \\ \text{but alleviated by ab-} \\ \text{orption}}} + \underbrace{\int_{\tau_1}^{\tau_2} S_\nu e^{-(t_\nu-\tau_1)/\mu} \frac{dt_\nu}{\mu}}_{\substack{\text{gain of intensity by emission} \\ \text{and re-emission but also alle-} \\ \text{viated by absorption from } t_\nu \\ \text{to } \tau_\nu}} \quad (2.29)$$

## 2.5 Line Formation

As described above radiation can interact with matter in several ways but just the excitation can produce absorption lines. In the classical view absorption by matter was introduced by H.A. Lorentz. Matter is treated as a damped harmonic oscillator which is periodically excited by the radiation field. The solution of the equation of motion gives the displacement of the oscillator where  $\gamma$  is the damping constant and  $\omega_0$  is the eigenfrequency which is the frequency between two levels.

$$x(t) = \frac{eE_0}{m} \frac{\omega_0^2 - \omega^2 - i\omega\gamma}{(\omega_0^2 - \omega^2)^2 - \gamma^2\omega^2} e^{i\omega t} \quad (2.30)$$

With the knowledge of electrodynamics follows the profile-function. This equation gives the absorbed power for a given frequency.

$$\varphi(\nu) = \frac{\gamma/4\pi^2}{(\nu_0 - \nu)^2 + (\gamma/4\pi)^2} \quad (2.31)$$

The probability for a transition between lower level l and upper level u is expressed by the absorption cross section  $\sigma_{lu}$  and important for the calculation of the bound-bound opacity.

$$\kappa_\nu = n_l \sigma_{lu} \varphi(\nu) \quad (2.32)$$

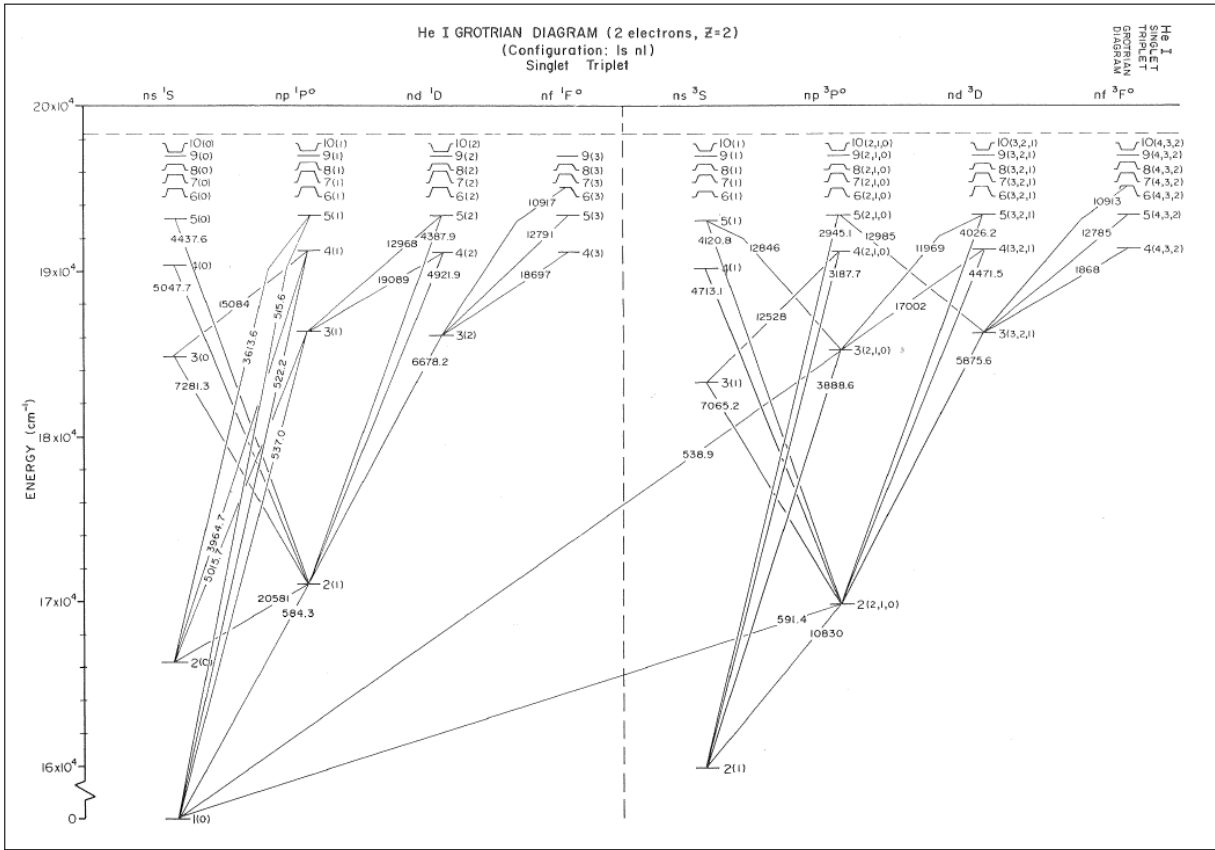


Figure 2.9: Grotrian diagram for neutral helium

In the classical view  $\sigma_{lu}$  is slightly different compared to the quantum-mechanic view. Just a correction factor  $f_{lu}$  has to be included.

$$\sigma_{lu} = \frac{\pi e^2}{mc} f_{lu} \tag{2.33}$$

$f_{lu}$  is the oscillator strength and essential for an accurate spectroscopic analysis. However, for a lot transitions it is not easy to derive. Laboratory measurements, quantum-mechanic calculations or empirical determinations from the solar spectrum are the ways to obtain values. For allowed transitions  $f_{lu}$  lies in the range of  $10^{-4}$  to 1. For the forbidden transitions the values are much smaller and typically in a range of less than  $10^{-10}$ . The extreme helium stars show every helium line (allowed and forbidden) due to their high helium abundance. Therefore they are also a good testbed for the atomic physics of helium.

Spectral line profiles contain information about the physics in the plasma but also about elemental abundances. To analyse the profiles good knowledge of the physics in the plasma which affects the lines is necessary and sometimes not easy to constrain. Transition probabilities, effective temperatures, abundances or broadening effects have influence on the strength and the shape of the line. I will give an overview of the different line broadening mechanisms in the following paragraph:

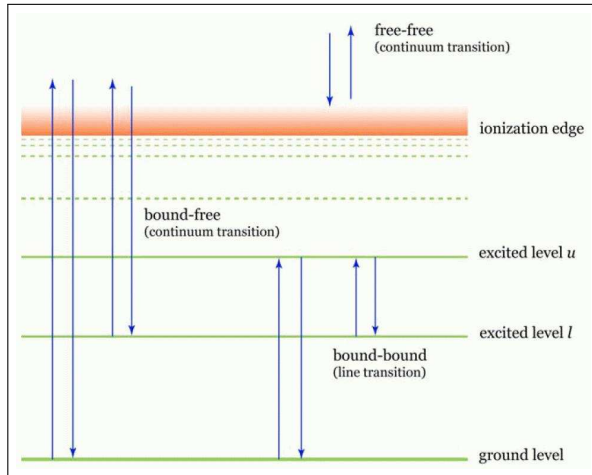


Figure 2.10: Illustration of different types of interaction between matter and radiation

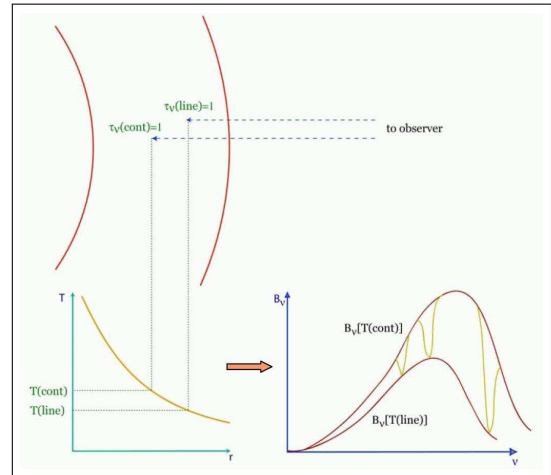


Figure 2.11: Illustration of the formation of absorption lines

- Natural line width** Every energy level (except the ground state) has a finite lifetime  $\tau$  which is in orders of about  $10^{-8}$  s. Due to the Heisenberg uncertainty principle  $\Delta E \cdot \tau \geq \hbar$  and the finite lifetime the energy levels are not any sharp which leads to a broadening of the spectral line. The profile of the line is given by the profile function (Eq. 2.31) which is a so called Lorentz profile.
- Collisional or pressure broadening** This broadening effect is caused by interaction with other particles and therefore proportional to their number density and the pressure. This interaction forces a modification of the energy levels for example through the Stark-effect. Depending on the nature of the disturbance the strength of modification is given by Eq. 2.34 where  $r$  is the distance to the interacting particle and  $n$  is given by the nature of the disturbance.

$$\Delta E(t) = h\Delta\nu = C/r^n(t) \quad (2.34)$$

Two basic properties must be distinguished. First when the duration of the disturbance is shorter than the lifetime of the energy level (Impact Approximation) and on the other hand when the duration of the disturbance is longer (Quasistatic Approximation).

For the Impact Approximation the broadening is in general due to a shortening of the lifetime of the energy level. The strongest impact has the linear Stark effect where  $n = 2$ . This effect is important in hot stars where high particle densities, free electrons and ions dominate the matter.  $n$  is equal three for self-pressure broadening. Two neutral atoms from the same element disturb each other. This is important in cool stars. The Balmer-series in the Sun is an example for this broadening effect. In hot stars the collision of metal ions with electrons cause the quadratic Stark-effect ( $n = 4$ ) and is responsible for the broadening of metal lines in hot stars but also for the helium wings in extreme helium stars. The smallest effect has the van der Waals broadening ( $n = 6$ ) where two atoms from different elements disturb each other. This is important for spectral lines in cool stars like the Na lines in the Sun where sodium is disturbed by hydrogen.

The duration of the disturbance could be longer than the lifetime of the energy level for slow ions or far away electrons. In this case the interaction is constant during the emission or absorption and the emitted photon depends on the nature of the disturbance. The calculation for the complete field where interaction between particles is included is quite complicated. The easiest way to calculate the modification is the Nearest-Neighbour-Approximation. In this case just the closest particle is considered.

- **Thermal broadening** The matter in the atmosphere is not static but moves with the velocity  $\vec{v}$  which is given by the Maxwell distribution (Eq. 2.19). This causes a Doppler-effect where the observed frequency is shifted compared to the rest wavelength. An atom with the velocity  $\vec{v}$  emits at the frequency  $\nu$  whereas the receiver achieves the frequency  $\nu'$  with  $v$  being the velocity component in direction to the receiver.

$$\nu' = \nu - \nu \frac{v \cos \beta}{c} \quad (2.35)$$

With the Maxwell distribution for this component

$$P(v)dv = \frac{1}{\sqrt{\pi}v_0} e^{-(v/v_0)^2} dv \quad \text{with} \quad v_0 = \sqrt{2kT/m} \quad (2.36)$$

and the approximation  $v \ll c$  follows

$$\varphi(\nu' - \nu_0) = \varphi\left(\nu - \nu_0 - \nu_0 \frac{v}{c}\right) \quad (2.37)$$

where  $\nu_0$  is the center of the line. The modified line profile can be calculated using a convolution.

$$\varphi^{\text{new}}(\nu - \nu_0) = \int_{-\infty}^{\infty} \varphi\left(\nu - \nu_0 - \nu_0 \frac{v}{c}\right) P(v)dv \quad (2.38)$$

$$\Rightarrow \varphi^{\text{new}}(\nu - \nu_0) = \frac{1}{\sqrt{\pi}} \int_{-\infty}^{\infty} \varphi\left(\nu - \nu_0 - \underbrace{\nu_0 \frac{v}{c}}_{\Delta\nu_D: \text{Doppler width}} \frac{v}{v_0}\right) e^{-(v/v_0)^2} \frac{dv}{v_0} \quad (2.39)$$

Two approximations can be done to solve this equation and receive the line profile. In first when the line profile is dominated by Doppler broadening  $\varphi(\nu - \nu_0)$  is approximately a delta function. The resulting profile is a Gauss-function.

$$\varphi^{\text{new}}(\nu - \nu_0) = \frac{1}{\sqrt{\pi}\Delta\nu_D} e^{-\left(\frac{\nu - \nu_0}{\Delta\nu_D}\right)^2} \quad (2.40)$$

On the other hand when the line is dominated by the Lorentz-function a superposition of Gauss and Lorentz function which is called Voigt-profile is the resulting line profile (Fig. 2.12)

$$\varphi_{\text{Voigt}} = \varphi_{\text{Gauss}} \otimes \varphi_{\text{Lorentz}} \quad (2.41)$$

The core of the line can be calculated by Doppler broadening whereas the wings of the spectral line are dominated by the Lorentz-function. The full solution for the Voigt profile is given by the following equation:

$$\varphi^{\text{new}}(\nu - \nu_0) = \frac{1}{\sqrt{\pi}\Delta\nu_D} H\left(a, \frac{\nu - \nu_0}{\Delta\nu_D}\right) \quad (2.42)$$

where  $H\left(a, \frac{\nu-\nu_0}{\Delta\nu_D}\right)$  is approximately

$$e^{-\left(\frac{\nu-\nu_0}{\Delta\nu_D}\right)^2} \quad \text{for the line core (Doppler broadening)} \quad (2.43)$$

$$\frac{a}{\sqrt{\pi} \left(\frac{\nu-\nu_0}{\Delta\nu_D}\right)^2} \quad \text{for the line wings (Lorentz – profile)} \quad (2.44)$$

In general  $a$  is much smaller than one. For  $a = 1$  the profile is completely given by the Lorentz-profile.

- **Rotational broadening** The rotation of stars leads to relative Doppler shifts of the light which is emitted from different parts of the stellar surface. The equivalent widths stay unaffected just the line shape is affected by the frequency redistribution of the photons. The projection of the velocity vector onto line of sight corresponds to the observed rotational velocity. Stars can have rotational velocities from a few  $\text{kms}^{-1}$  up to several hundred  $\text{kms}^{-1}$ .
- **Broadening by microturbulence** Turbulent flows with a scale height which is much smaller than the optical path length cause a broadening in the lines which is called microturbulent velocity. In the easiest way this velocity  $\xi$  leads to a modification of the Gauss-profile. The correct value for a stellar atmosphere is empirically determined as described in the next section (Sec. 2.6).

$$\Delta\nu_D = \frac{\nu_0}{c} \sqrt{v_0^2 + \xi^2} \quad (2.45)$$

- **Broadening by macroturbulence** Macroturbulence occurs when the size of the turbulent elements is large compared to the unit optical depth. Corresponding to different Doppler shifts of different macroturbulence cells the lines are smeared and well described by the radial-tangential model for macroturbulence.

The spectral lines in an extreme helium star like BD+10 2179 are also broadened in different ways. The strong broad helium lines are broadened by both collisional and Doppler broadening. These lines are superposition of Lorentz- (for the wings) and Gauss-profiles (for the cores). Therefore they are Voigt-profiles. The metal lines in general are reproduced by Gauss-profiles due to Doppler broadening. Because of the high carbon abundance some abnormally broad carbon lines can be seen.

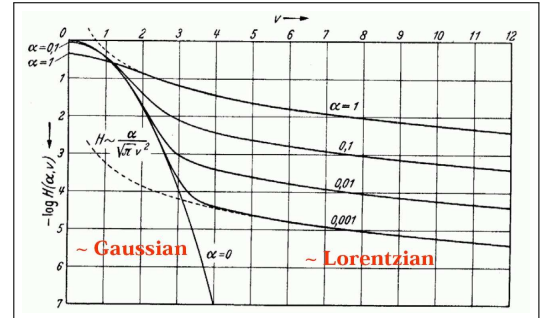


Figure 2.12: Superposition of Lorentz and Gauss-profile

## 2.6 Deriving Spectroscopic Parameters

The challenge of a quantitative spectral analysis is to find the parameters for the model which reproduce the observation best. This is not an easy task. In general a solution in multi-dimensional parameter space spanned by  $T_{\text{eff}}$ ,  $\log g$ ,  $\xi$ ,  $X_{\text{H}}$ ,  $X_{\text{He}}$  and metallicity needs to be found. The first parameters which will be determined are the effective temperature and  $\log g$ . The wings of the broad helium lines are sensitive to  $\log g$  and temperature whereas the cores are sensitive only to the temperature. The gradient of the wings is an indicator for the temperature stratification

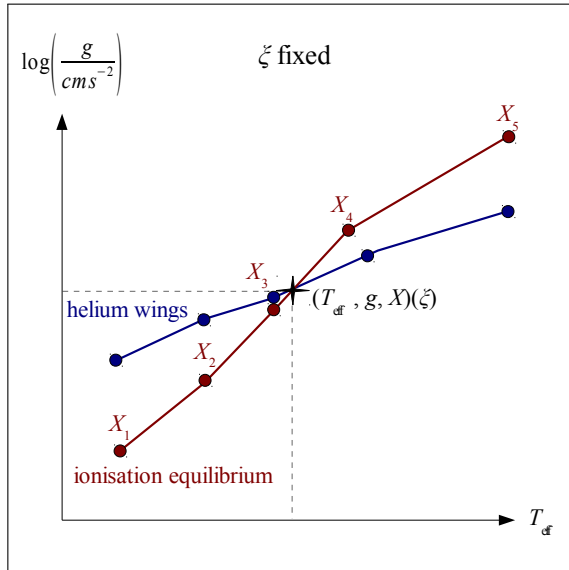


Figure 2.13: Determination of effective temperature and  $\log g$  using the helium wings and an ionisation equilibrium

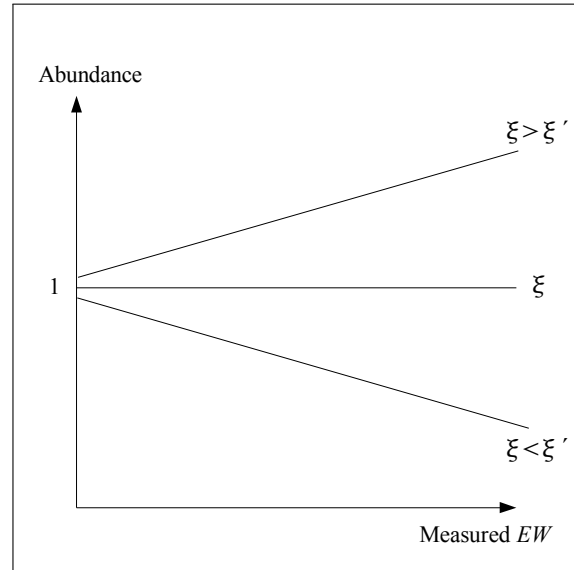


Figure 2.14: Determination of the microturbulence velocity using the equivalent widths of spectral lines for one element

which is related to the metallicity and the microturbulent velocity. The metal lines are an important indicator for the effective temperature and the rotational velocity. For extreme helium stars some more parameters like the abundances of carbon, nitrogen, oxygen or neon need to be included in the parameter space which makes the analysis more complicated. The parameters can not be determined independently because they affect each other. In the following I will give an introduction how we can determine spectroscopic parameters in the case of extreme helium stars.

The first step is to find a good starting point. For "normal" stars solar abundances are in general good. But this is not the case for extreme helium stars. With a lot of experience and knowledge about stellar spectra good starting values can be found. The existing ionisation stages give an idea for the effective temperature whereas the width of the helium wings are an indicator for  $\log g$ . A composition of about 99% helium, 1% carbon, 0.1% hydrogen and half of solar metallicity are in general good initial values.

The first parameters which result from the comparison with models are the effective temperature and  $\log g$ . For that case strong helium lines and ionisation equilibria are needed. For temperatures above the maximum of the helium line strength the higher the effective temperatures, the more helium atoms are ionised, therefore the neutral lines become weaker. This can be compensated by increasing  $\log g$  (Fig. 2.15). For different effective temperatures different  $\log g$  values fit the profile of the strong helium lines best. Therefore the profiles of the helium lines are not enough to fix both parameters. A second correlation between  $\log g$  and  $T_{\text{eff}}$  is needed. This can be an ionisation equilibrium which means that spectral lines of different ionisation stages have to indicate the same abundance. If the temperature is too low, too many atoms are in the lower ionisation stage of the synthetic model and too few are in the upper one (Fig. 2.16). Therefore

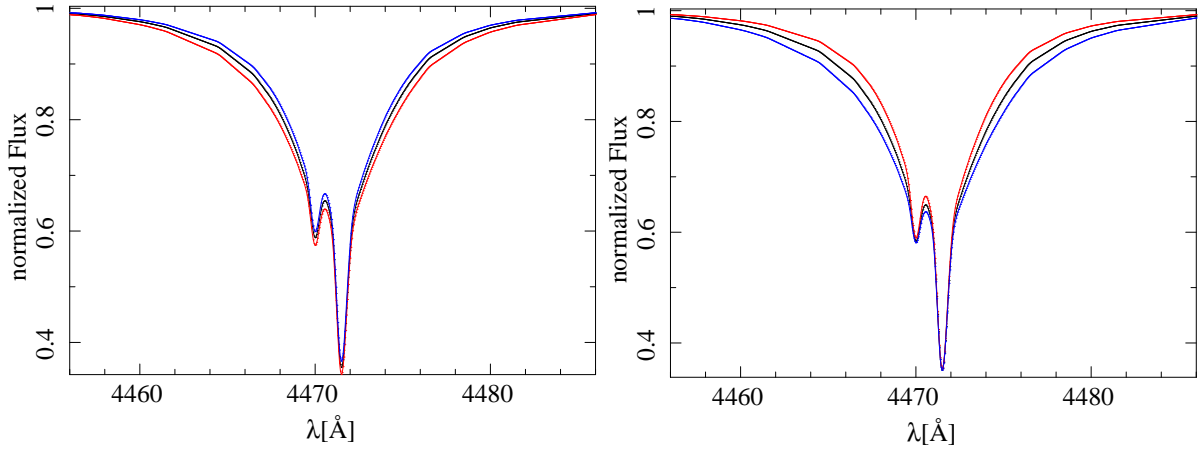
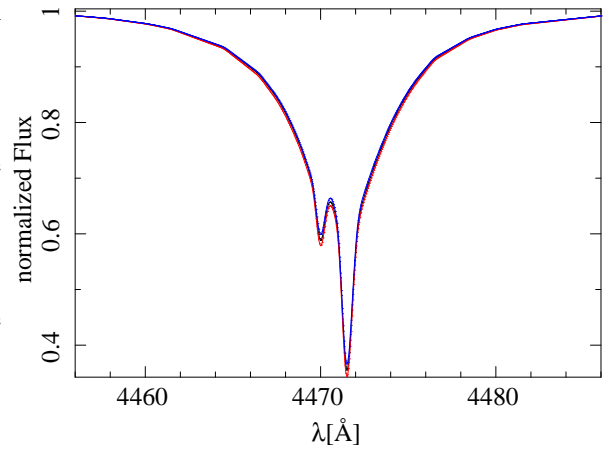


Figure 2.15: gravity and temperature effect on the helium lines; **upper left panel:** blue/red lines indicate and increase/decrease of the temperature ( $\pm 600\text{K}$ ) with respect to the black line with  $T_{\text{eff}} = 17\,000\text{ K}$  and  $\log g = 2.80$ , **upper right panel:** blue/red lines indicate and increase/decrease of the gravity ( $\pm 0.2$ ) with respect to the black line with  $T_{\text{eff}} = 16\,800$  and  $\log g = 2.80$ , **right down panel:** blue line ( $T_{\text{eff}} = 16\,400\text{ K}$ ,  $\log g = 2.65$ ), red line ( $T_{\text{eff}} = 17\,600\text{ K}$ ,  $\log g = 2.85$ ) and black line ( $T_{\text{eff}} = 17\,000\text{ K}$ ,  $\log g = 2.75$ ) illustrates the  $T_{\text{eff}}$ - $\log g$  degeneracy of the helium wings



the computed spectral lines are too strong for the lower ionisation stage and too weak for the upper. This means that for different  $\log g$  values different effective temperatures are determined where the lines for each ionisation stage fits the observed one. For this measurement weak lines are the best ones because they are independent of microturbulence. The requirement is that the spectrum shows different ionisation stages for the same element. The interception point of both correlations is the obtained  $T_{\text{eff}}$  and  $\log g$  value (Fig. 2.13).

The next step is to determine the microturbulent velocity with fixed  $T_{\text{eff}}$  and  $\log g$ . A way is to measure the equivalent width (EW) of different lines for an element and calculate the abundances. The microturbulence has a much stronger influence on strong lines than for weak ones. This means that the abundance is much higher for strong lines than for the weak lines if the microturbulent velocity is underestimated. The right velocity is found when the abundance is the same for the strong and the weak lines (Fig. 2.14).

The parameters are fixed now. The last step is to obtain the right abundances all other elements. This could be done by finding the best agreement between the model and the observation for

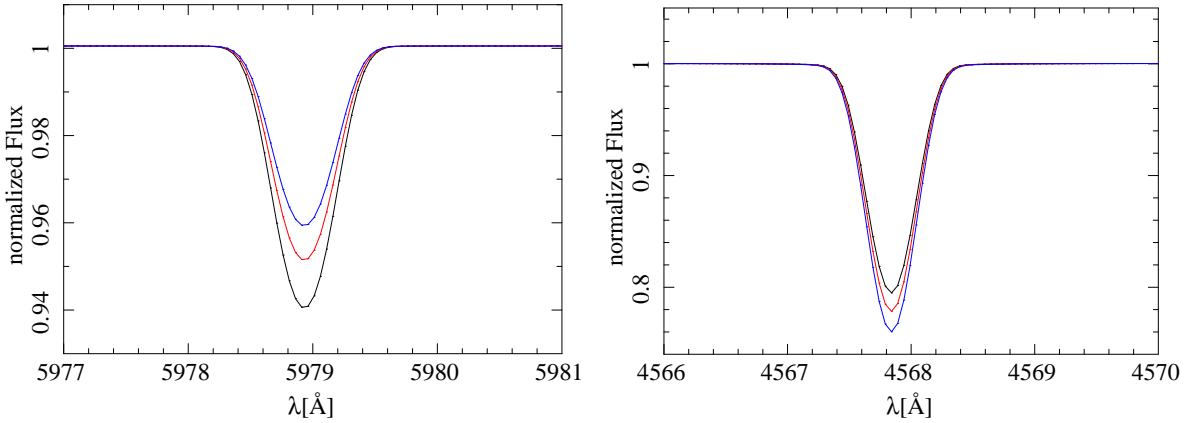


Figure 2.16: Temperature effect on the silicon lines; black ( $T_{\text{eff}} = 17\,500\text{ K}$ ,  $\log g = 3.00$ ), red ( $T_{\text{eff}} = 18\,000\text{ K}$ ,  $\log g = 3.00$ ) and blue line ( $T_{\text{eff}} = 18\,500\text{ K}$ ,  $\log g = 3.00$ ) illustrates the change of the profiles for SiII (left hand) and SiIII (right hand)

every line of each element.

Because most parameters are correlated more iterations are necessary to obtain the right value for each parameter which could be hard work especially for stars like BD+10°2179 with a lot more free parameters.

## 2.7 Computing Model Atmospheres: ATLAS12 vs. STERNE

STERNE and ATLAS12 are codes which compute model atmospheres in LTE including plane parallel geometry, homogeneity, hydrostatic and radiative equilibrium. Different equations (see Sec. 2.2) are necessary to obtain a model atmosphere. These are the same for STERNE and ATLAS. The main differences are the input data like the opacity but also the way of solving these equations. The way how the radiation transport and the temperature correction is solved in ATLAS as it is described in Kurucz (1970) in full detail.

- The starting point is either the gray approximation or an already computed model atmosphere. From that point the hydrostatic equation (Eq. 2.15) including the ideal gas law is solved and the pressure and electron gradient is obtained.
- The population density is calculated using the Saha-Boltzmann equation
- With all the obtained values and the opacity which is taken from different sources for STERNE and ATLAS the radiation field is calculated using the radiation transport equation. There are different possibilities to solve this equation. The first which was used in an old STERNE version is solving an integral using the Avrett - Loeser method (Avrett & Loeser 1966). Whereas the current STERNE version solves the differential equation for the radiation transport (Eq. 2.28) using the Feautrier Scheme.
- The next step is the temperature correction which is computed using Lucy-Unsöld procedure (Lucy 1964) for STERNE. The basic assumption is that the obtained radiation field needs to

satisfy the energy conservation

$$F(\tau) = \frac{\sigma(\tau)}{\pi} T_{\text{eff}}^4 \quad (2.46)$$

For every iteration a correction factor to the flux is added. When the variation of the total flux throughout the atmosphere becomes small enough the iteration stops and the new model atmosphere is finished.

From that point the structure of the atmosphere stays fixed. Having a well converged atmosphere the next steps differs if a LTE or a NLTE analysis will be done.

## 2.8 Calculating Synthetic Spectra in LTE and NLTE: DETAIL + SURFACE/SPECTRUM

The program DETAIL is used to compute the occupation numbers in NLTE by solving the rate equation (Eq. 2.22) and the radiation transfer equation. The results are the occupation numbers in NLTE and the radiation field but in a relatively rough grid. This means that the radiation field needs just to be computed in a more detailed frequency grid and the resulting spectrum can be obtained by integrating the formal solution of the transport equation (Eq. 2.29) over a full hemisphere. The other point is that detailed line broadening is included.

$$F_{\nu}(0) = 2\pi \int_0^1 \left( I_{\nu}(\mu, \tau_1) e^{-(\tau_1)/\mu} + \int_0^{\tau_1} S_{\nu} e^{-(t_{\nu}-\tau_1)/\mu} \frac{dt_{\nu}}{\mu} \right) d\mu \quad (2.47)$$

To obtain a normalised spectrum the continuum flux ( $F_{\nu}^{\text{cont}}(0)$ ) has to be calculated and the final normalised spectrum is given by dividing the flux by the continuum flux.

$$F_{\nu}^{\text{norm}} = \frac{F_{\nu}(0)}{F_{\nu}^{\text{cont}}(0)} \quad (2.48)$$

This calculation can be done with codes like SURFACE and SPECTRUM. If DETAIL is omitted a full LTE analysis is done. The computing time in this case decreases significantly.

Finally follow a few words about the opacity calculations which are really important especially for extreme helium stars. In old versions of STERNE and ATLAS opacity distribution functions (ODFs) are used to calculate the opacity. In this case the opacity data are tabulated in different tables for scaled abundances with respect to the solar abundance. This gives a wrong solution in the case of strange abundances like in extreme helium stars. The recent version uses so called opacity sampling (OS). In this case the spectrum is divided in several frequency points where the opacity is calculated separately for each frequency point using LTE statistics. STERNE uses Opacity Project data, which covers only a relatively limited number of elements. Among the iron elements only Fe is included. ATLAS12 treats most elements. Therefore many more metal lines are included. The huge advantage of OS is that the possible abundance input is variable which is necessary for accurate solutions for extreme helium stars.



## 3 Comparison between ATLAS12 and STERNE

Stars with chemical compositions like BD+10°2179 put high requirements on programs which compute synthetic models. Therefore these stars are good testbeds for a comparison between different model atmosphere codes. In this chapter a comparison between ATLAS12 and STERNE including NLTE calculations with DETAIL was done for a chemical composition like in the Sun and in BD+10°2179.

Because of different normalisations for the abundances a small error could not be avoided. STERNE uses particle fractions normalised over all elements whereas ATLAS12 normalises over hydrogen and helium with respect to  $n_{\text{He}} + n_{\text{H}} = 1$ . For the chosen abundances the error should be in the range of about 1 - 2 %. ATLAS12 includes metal lines of almost all elements whereas STERNE includes data from the Opacity Project which provides accurate atomic data for a limited number of elements. In the first step a model with  $T_{\text{eff}} = 16\,800\text{ K}$ ,  $\log g = 2.80$  and solar composition was compared. In the second step a helium-rich atmosphere with the same  $T_{\text{eff}}$  and  $\log g$  but  $n_{\text{He}} = 0.9995$ ,  $n_{\text{H}} = 0.0005$ ,  $n_{\text{C}} = 0.01$  and a tenth of solar metallicity which is close to the LTE results of BD+10°2179 was chosen.

STERNE and ATLAS12 calculate different fluxes (astronomical flux  $F$  and Eddington flux  $H$ ). In order to compare the two programs we need to convert the fluxes into each other. STERNE calculates the astronomical flux  $F_{\lambda}$  [ $\text{erg cm}^{-2}\text{s}^{-1}\text{\AA}^{-1}$ ]. In the ATLAS12 output file the Eddington flux  $H_{\lambda}$  [ $\text{erg cm}^{-2}\text{s}^{-1}\text{nm}^{-1}$ ] and  $H_{\nu}$  [ $\text{erg cm}^{-2}\text{s}^{-1}\nu^{-1}$ ] is given. The ATLAS12 flux was converted to  $F_{\lambda}$  using the relationship:

$$F_{\lambda} = 4H_{\lambda} \quad (3.1)$$

DETAIL contains just the Eddington flux  $H_{\nu}$ . For the comparison with the LTE flux of STERNE a relation between  $F_{\lambda}$  and  $H_{\nu}$  is necessary:

$$F_{\lambda} = 4\frac{c}{\lambda^2}H_{\nu} \quad (3.2)$$

### 3.1 Solar Composition

Before the comparison for the helium rich atmosphere is discussed in full detail a much less challenging comparison using a solar composition was done. Behara & Jeffery (2006) did the same using ATLAS9 and STERNE and found a good match for the flux distribution. We can confirm this result using ATLAS12 and STERNE (Sect. 3.1.2).

#### 3.1.1 Temperature and Density Stratification

For the comparison of ATLAS12 and STERNE for solar abundances models with  $T_{\text{eff}} = 16\,800\text{ K}$ ,  $\log g = 2.80$  and solar composition were computed. To reproduce the structure of the atmosphere a comparison of the temperature and density stratification is necessary. This was not an easy task because a suitable height scale is necessary. In general the Rosseland mean opacity  $\tau$  is taken as the height scale. The ATLAS12 output file comprised  $\tau$  over the full wavelength

range whereas STERNE gives the monochromatic opacity at  $4\,000\text{ \AA}$  ( $\tau_{4000}$ ). The solution is that the input file for SPECTRUM contains the mass scale. Using a conversion tool, this file is converted to the DETAIL input file. The same is done for the ATLAS12 atmosphere which contains the mass scale, too. Therefore it is possible to compare temperature and density stratification with the DETAIL input file using the mass scale as the height scale. Density and temperature stratification matches each other well (Fig. 3.1).

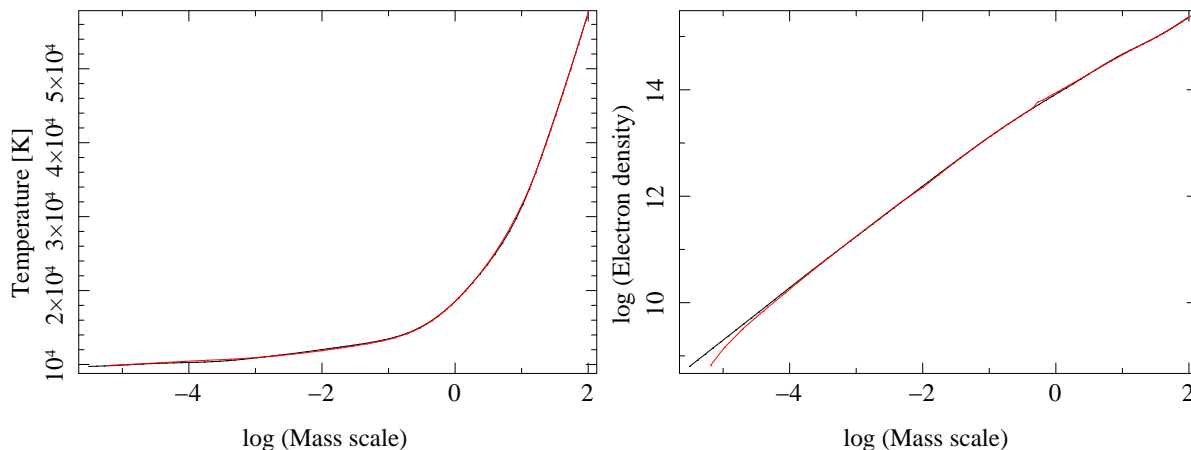


Figure 3.1: Temperature and Density stratification for STERNE(red) and ATLAS12(black) using an atmosphere with solar composition. In the **left hand panel** the temperature profile. In the **right hand panel** the electron density profile

### 3.1.2 Flux Distribution

Because of the good match of the density and temperature stratification it is not surprising that the flux distribution in general fits well (Fig. 3.2). Only a few differences should be listed.

- The flux of the ATLAS12 model is slightly above the STERNE model redwards of the helium edge (at  $504\text{ \AA}$ ), whereas bluewards of the helium edge the STERNE flux is lower than the ATLAS12 flux.
- The other point is that especially in the UV much more lines are considered by ATLAS12. One example is the helium resonance line at  $584.3\text{ \AA}$  which is missing in the STERNE model (Fig. 3.2).

### 3.1.3 Hydrogen and Helium Line Profiles

To check the differences in the synthetic spectra LTE line profiles were calculated using the codes SPECTRUM for the STERNE atmosphere and SURFACE for the ATLAS12 atmosphere. The line profiles match each other well. Just one point is mentionable:

- The most remarkable issue for the profiles is that the forbidden component of the helium line  $4\,471\text{ \AA}$  does not agree well (see Fig. 3.3), a problem caused by uncertainties in the collisional broadening of the forbidden component. The line depth and the wings of the four lines agree pretty well.

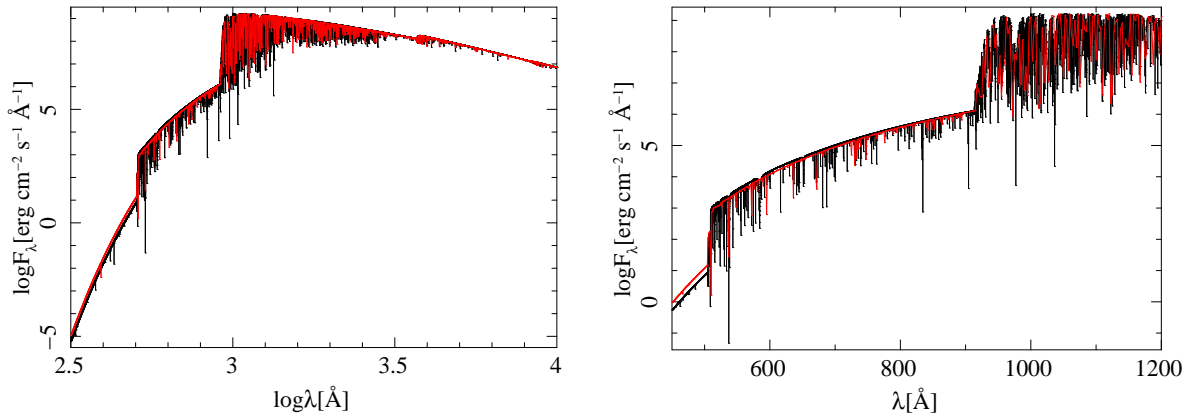


Figure 3.2: Flux distribution from STERNE (red) and ATLAS12 (black) for solar composition. In the **left hand panel** the range between 316 and 10 000 Å. In the **right hand panel** the range between 450 and 1 200 Å

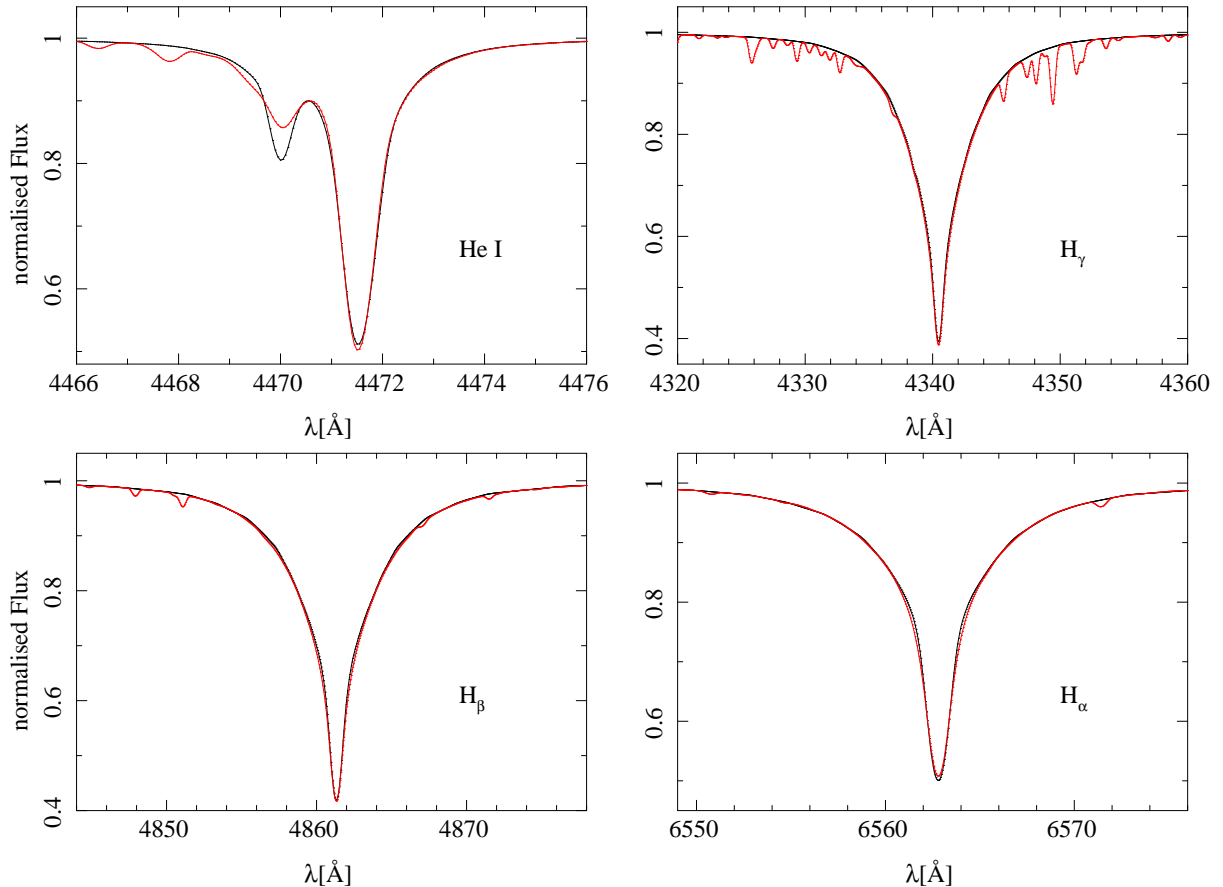


Figure 3.3: Computed line profiles using ATLAS and SURFACE (black) and STERNE and SPECTRUM (red) for a model with solar composition with  $T_{\text{eff}} = 16800$  K and  $\log g = 2.80$ . Note that the SPECTRUM profiles include metal line blends, while the SURFACE profiles do not

## 3.2 Helium-Rich Atmosphere in LTE

We found that the flux distribution,  $T$ - $\rho$ -stratification and H, He line profiles of ATLAS12 and STERNE match each other well for solar composition. The next step is to change the composition to typical helium star abundances and see whether the comparison is still in agreement. The comparison in this case turns out to be not that easy and strong discrepancies were found in the first attempt. ATLAS12 and STERNE compute temperature and density stratification. The comparison of the  $T$ - $\rho$ -stratification is done in Sec. 3.2.1. The flux distributions of ATLAS12 and STERNE are compared in Sec. 3.2.2. Furthermore, LTE line profiles were computed using ATLAS12/SURFACE and STERNE/SPECTRUM. The LTE line profiles are discussed in Sec. 3.2.3. DETAIL computes the occupation numbers in NLTE using the  $T$ - $\rho$ -stratification from ATLAS12 or STERNE. The output of DETAIL are the NLTE occupation numbers and the NLTE flux distribution including these numbers. Note that the different input models (ATLAS12 or STERNE) lead to differences in the solution. This problem and difficulties of building an accurate model atom are described in Sec. 3.3. SURFACE includes detailed line broadening and computes the normalised spectrum on a fine grid using the computed occupation numbers. Depending if the input occupation numbers are in LTE (ATLAS12 or STERNE) or in NLTE (DETAIL) the line-profiles are computed in LTE or NLTE. Comparison of these line profiles are done in Sec. 3.3.5.

### 3.2.1 Temperature and Density Stratification in LTE

Like for the solar composition we compared the temperature and density stratification. Both agree well. The small discrepancy in the temperature gradient in the line forming region (Fig. 3.4) is due to fewer lines and therefore less opacity in STERNE. This effect is not so strong for solar composition because the Lyman edge suppresses the UV flux very strongly in contrast to extreme helium stars where the EUV flux stays high because the Lyman edge is small.

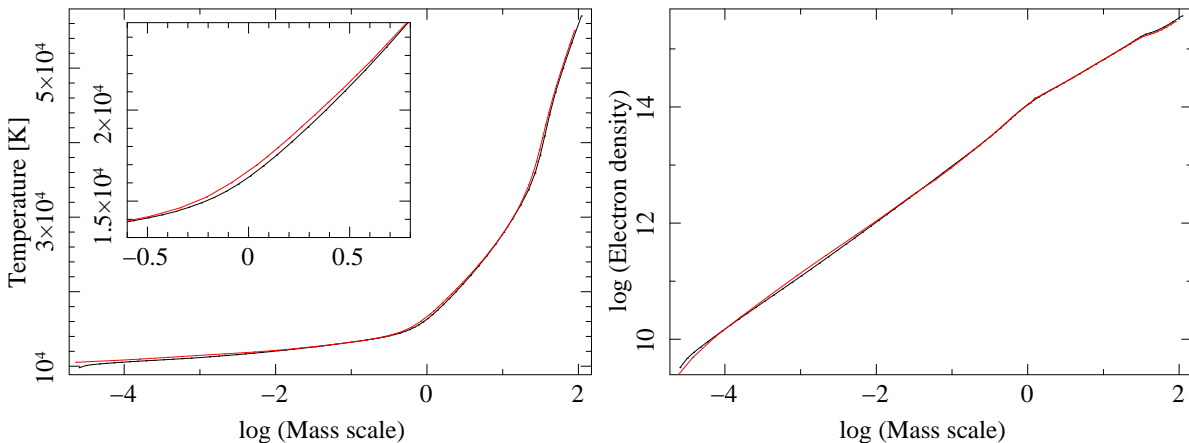


Figure 3.4: Temperature and density stratification for STERNE (red) and ATLAS12 (black) using a helium rich atmosphere. In the **left hand panel** the temperature gradient. In the **right hand panel** the electron density gradient

### 3.2.2 Flux Distribution for ATLAS12 and STERNE

Unlike for solar composition the flux distributions match each other not so well and a couple of remarkable differences become apparent in the STERNE and ATLAS12 flux distributions mainly in the EUV (Fig. 3.5, 3.6).

- The STERNE flux is slightly above the ATLAS12 flux for the complete UV range (Fig. 3.5).
- Many lines are not included in the STERNE model like e.g. the strong HeI resonance line at 584 Å together with the whole series (Fig. 3.5). The broadening of the HeI resonance lines is inappropriate.
- The ATLAS12 model shows a broad and strong line at 651.3 Å which is one of the transitions in the quartet spin system of the CII atom. The upper level for this transition lies close to the ionisation edge. Observations for this transition are impossible due to interstellar extinction. The line is not included in the source of the STERNE opacities and therefore not present in the STERNE model (Fig. 3.5). We found that this line has huge wings (several 100 Å) due to an erroneous line-broadening parameter in ATLAS12. A correction of the line-broadening parameter (difficult, because it is encoded in binary format) or excluding the line of the ATLAS12 model would probably increase the agreement between ATLAS12 and STERNE significantly.
- An ionisation edge at 440 Å is present in the STERNE model but not in ATLAS12. Whereas, an ionisation edge at 482 Å is present in the ATLAS12 model but not in STERNE (Fig. 3.5).
- The optical range fits well together (Fig. 3.6).

Most of the discrepancies are in a range where the flux has no big influence on the helium and hydrogen lines in the optical range. This becomes clear by comparing profiles of some helium and hydrogen lines which is demonstrated in the next chapter.

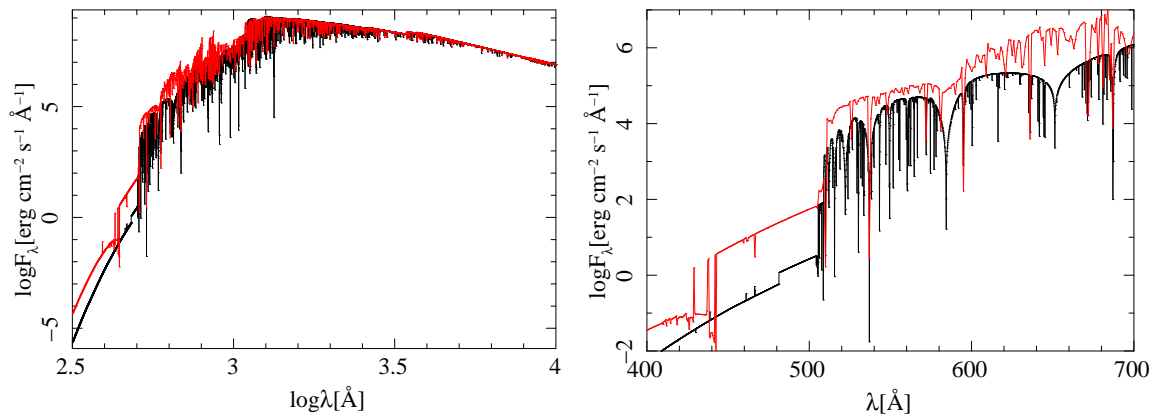


Figure 3.5: Flux distribution from STERNE (red) and ATLAS12 (black). In the **right hand panel** the range between 400 and 700 Å. In the **left hand panel** the range between 316 and 10 000 Å

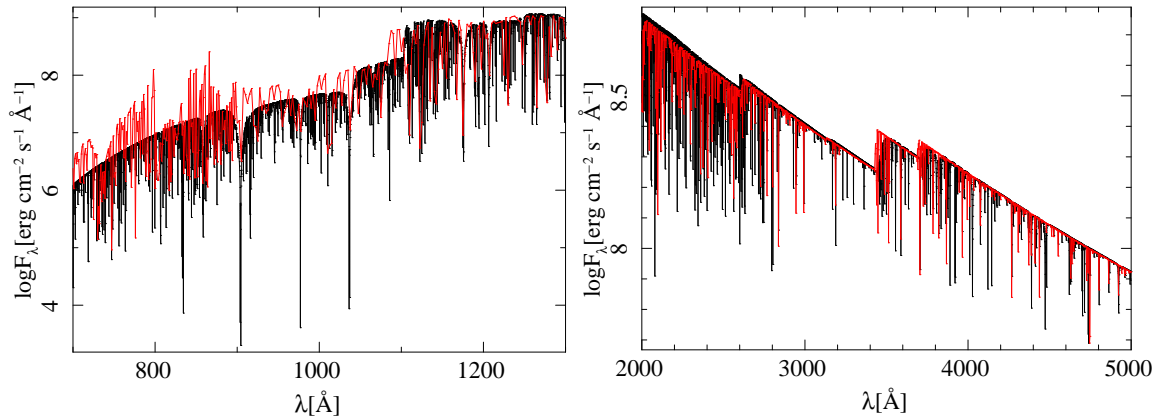


Figure 3.6: Flux distribution from STERNE (red) and ATLAS12 (black). In the **left hand panel** the range between 700 and 1 300 Å. In the **right hand panel** the range between 2 000 and 5 000 Å

### 3.2.3 Helium, Hydrogen and Silicon Line Profiles

Some helium, hydrogen and silicon lines were taken to check the agreement between STERNE and ATLAS12. The STERNE model with the above mentioned composition was taken and a synthetic spectrum was computed using the program SPECTRUM. For the ATLAS12 model SURFACE was taken to compute the synthetic spectrum with hydrogen and helium in LTE. The result is shown in Figure 3.7. In contrast to the flux distributions the line profiles fit well together for both helium and hydrogen. The small discrepancy could be due to different broadening theories of STERNE and ATLAS12. The small difference in the line depth can be explained by the different standardisations of the abundances. The differences in the flux distributions do not affect the line formation of helium. The reason is that the ionisation edge of neutral helium is further in the UV, where the flux is low and the differences are not that strong.

This is not the case for the silicon lines. The most probable reason is that the sources of atomic data are different leading to different line profiles.

After the tests for the LTE flux distributions from ATLAS12 and STERNE the next step is to include NLTE DETAIL calculations and see whether the flux distribution and the line profiles change significantly. These comparisons are discussed in the next section.

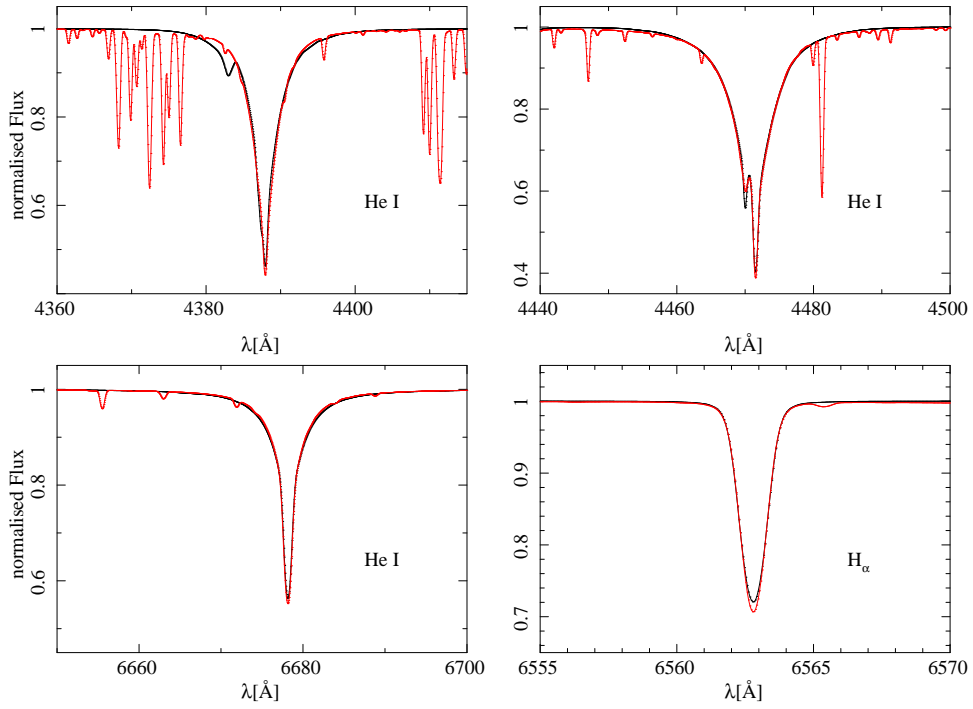


Figure 3.7: Computed helium and hydrogen line profiles using ATLAS and SURFACE(black) or STERNE and SPECTRUM(red) for a helium rich model with  $T_{\text{eff}} = 16\,800$  K and  $\log g = 2.80$ . Note that the SPECTRUM profiles include metal line blends, while the SURFACE profiles do not

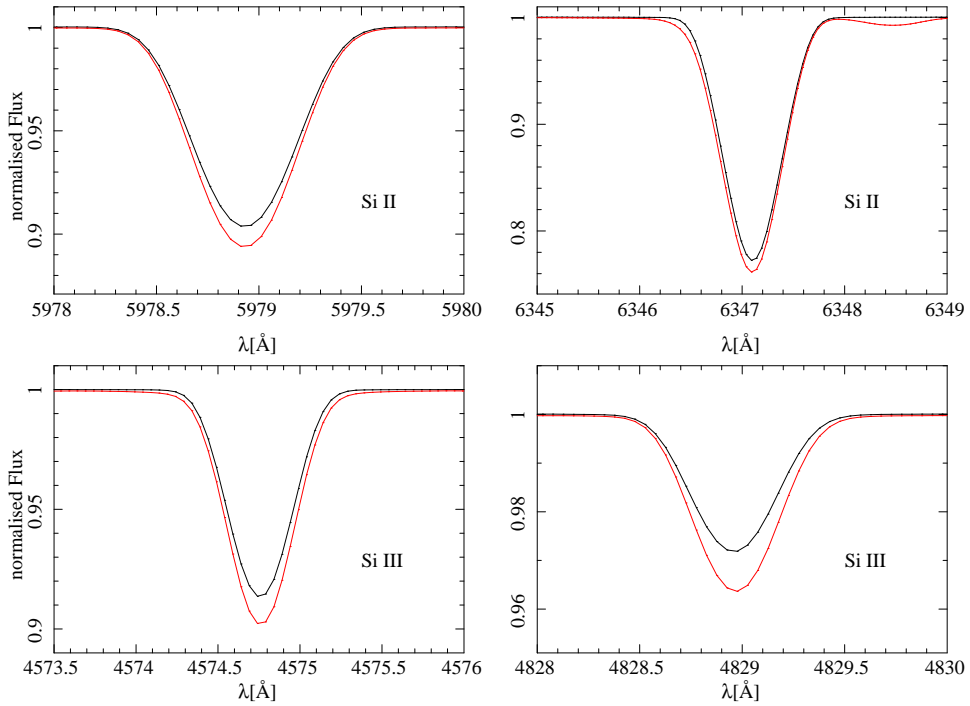


Figure 3.8: Computed silicon line profiles using ATLAS and SURFACE(black) and STERNE and SPECTRUM(red) for a helium rich model with  $T_{\text{eff}} = 16\,800$  K and  $\log g = 2.80$

## 3.3 Helium-Rich Atmosphere in NLTE

### 3.3.1 Flux Distribution from ATLAS12 and STERNE

The structure from the ATLAS12 and STERNE models are the input for the NLTE calculation which was done using the code DETAIL. For the first estimate of the NLTE calculation a standard model atom which treats hydrogen, helium and silicon in NLTE was taken. Effective temperature,  $\log g$  and abundances are hold at the same value like in the tests before. We found a totally wrong solution for the NLTE flux from STERNE and ATLAS12 (Fig. 3.9 left hand panel). The helium wings in the UV were not calculated far enough and the bound-free opacities of carbon were missing. This is no problem for usual main sequence stars but is important for extreme helium stars. Therefore we needed to construct a new model atom including the main opacity sources like hydrogen, helium, carbon, nitrogen and oxygen. That was not an easy task. Due to interstellar absorption of neutral hydrogen the important EUV part was never observed in helium stars. Therefore no observational experiences can be included.

Taking the new model atom which contains the bound-free opacities for carbon, we found that the NLTE flux from STERNE and ATLAS12 matches each other well (Fig. 3.9 right hand panel). The only thing is that the STERNE flux is slightly above the ATLAS12 flux. The small discrepancy is due to small differences in the temperature stratification. Comparing the NLTE flux with the LTE flux from ATLAS12 and STERNE we found some even larger differences. For ATLAS12 the range below the C II line at 651.3 Å is hardly below the NLTE flux (Fig. 3.10 left hand panel). The LTE flux from STERNE is much more different compared to the NLTE flux from STERNE (Fig. 3.10 right hand panel). Due to that significant discrepancies we had a closer look at the mentioned C II line and found that the red wing is that large that it dominates the opacity in the whole UV. Whereas the blue wing could not put the flux down which is quite strange. Including this line in STERNE would force the flux distribution closer to the ATLAS12 solution whereas excluding this line in ATLAS would bring the ATLAS12 solution closer to STERNE. No observational data could be checked. The question was, what is correct? We found that calculation of the line broadening in ATLAS12 and DETAIL was wrong.

The upper energy level of this line lies close to the ionisation edge. Therefore the energy difference ( $E_{\text{up}} - E_{\text{ion}}$ ) between the ionisation edge and the upper level is extremely small. The wings of the C II line are broadened by Stark broadening. The damping constant and as a consequence the strength of this broadening mechanism is proportional to  $E_{\text{up}} - E_{\text{ion}}$  which leads to this huge wings. Due to selection rules the upper energy level will not ionise to the ionisation edge but to an excited state of C III which leads to a greater value of  $E_{\text{up}} - E_{\text{ion}}$  and therefore to a significant lower value for the broadening.

This leads to the assumption that the ATLAS12 flux distribution is incorrect with a wrong treatment of the line broadening of the C II line at 651.3 Å. The correction for ATLAS is not that easy but we could correct the treatment of the line profile in DETAIL. Taking a new model atom which computes the main opacity sources like H, He, C I,II,III, N I,II, O I,II and Si II,III in NLTE leads to a much better agreement between the NLTE and LTE flux from STERNE. The huge discrepancy between the NLTE and LTE flux from ATLAS12 is due to the wrong treatment of the C II line. The other elements are treated in LTE. These comparisons are described in full detail in the next sections.

The next two subsections describe the comparison between the LTE and the NLTE fluxes from STERNE and ATLAS12. Whereas the subsection thereafter describes the comparison between the NLTE fluxes from STERNE and ATLAS12.

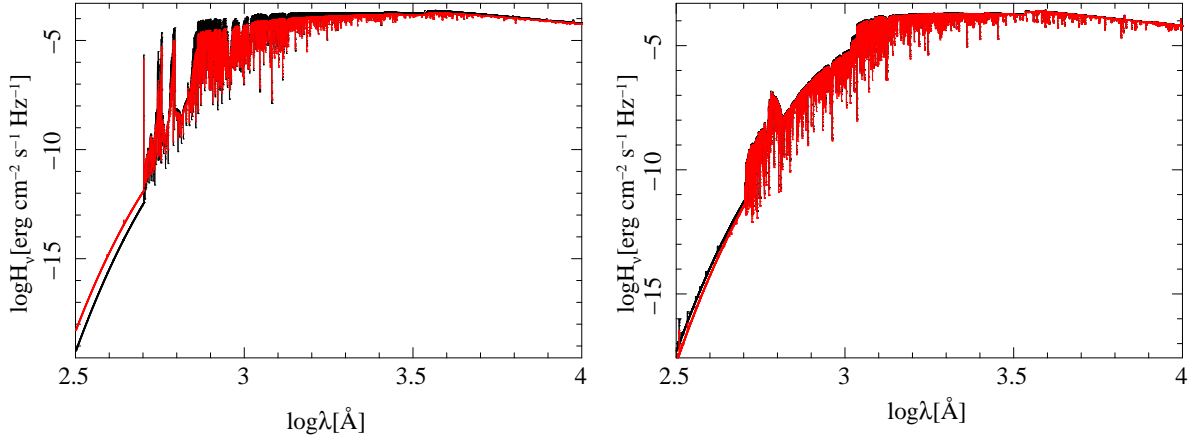


Figure 3.9: NLTE flux distribution from STERNE (black) and ATLAS12 (red) model atmospheres. In the **left hand panel** the range between 316 and 10000 Å using the model, where carbon b-f opacities are missing. In the **right hand panel** the same range using the model atom with the erroneous Stark broadening of the CII line at 651.3 Å

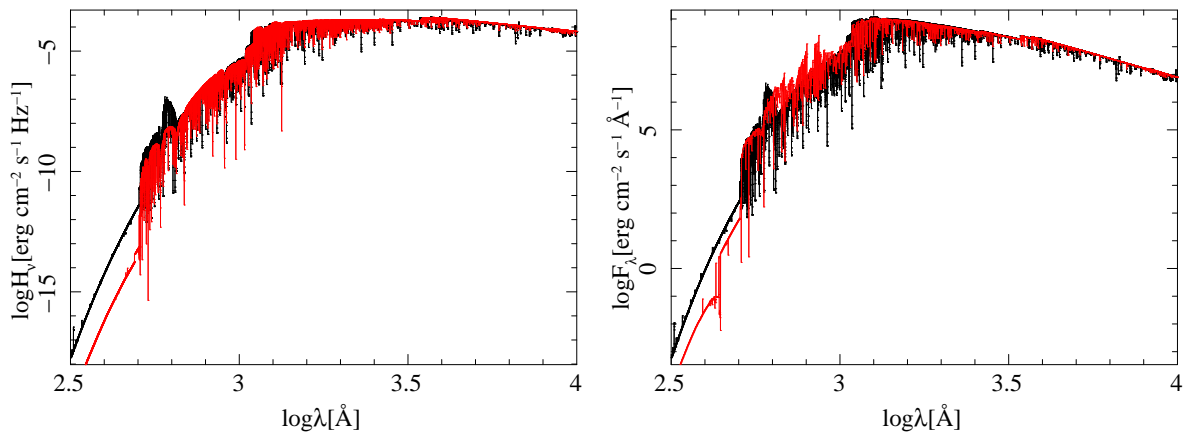


Figure 3.10: In the **left hand panel** the flux distribution in LTE (red) and NLTE (black) from the ATLAS12 structure using the model atom with the erroneous Stark broadening. In the **right hand panel** the flux distribution in LTE (red) and NLTE (black) from the STERNE structure using the model atom with the erroneous Stark broadening.

### 3.3.2 Comparison of the LTE and NLTE Flux from ATLAS12

The comparison of the LTE and NLTE flux from ATLAS12 are separated in two ranges above and below the ionisation edge of C I at around 1 100 Å.

The fluxes match each other well above the ionisation edge (Fig. 3.12). This is not the case below the ionisation edge (Fig. 3.11). The UV differs completely. The disagreement is due to the broad and wrong wing of the C II line at 651.3 Å which is corrected in DETAIL but not in ATLAS12. This leads to much more opacity for the whole UV range and therefore to a much lower flux.

The comparison of the NLTE and LTE flux from STERNE looks much nicer. We found no huge differences.

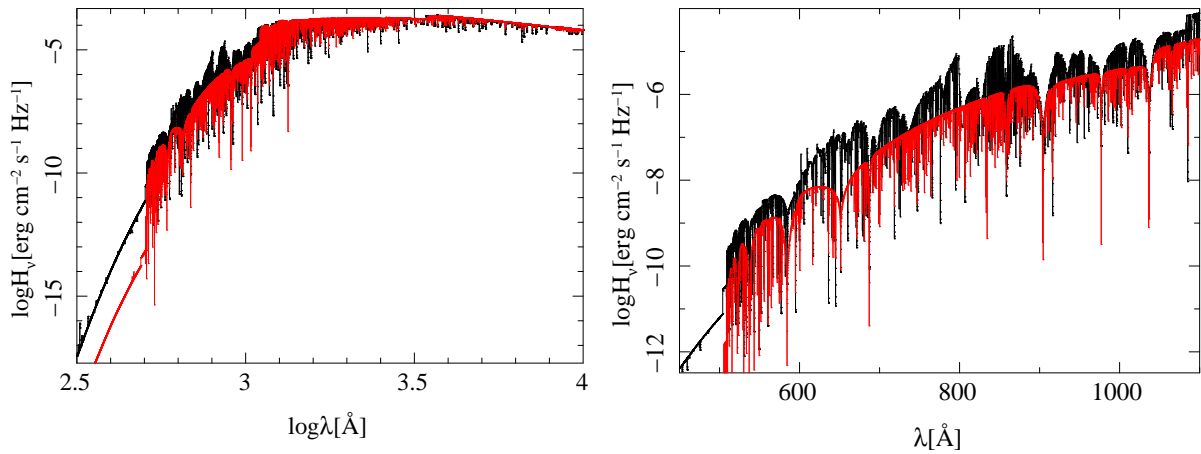


Figure 3.11: LTE(red) and NLTE(black) flux distribution from ATLAS12(red). In the **left hand panel** the range between 316 and 10 000 Å. In the **right hand panel** the range between 450 and 1 100 Å

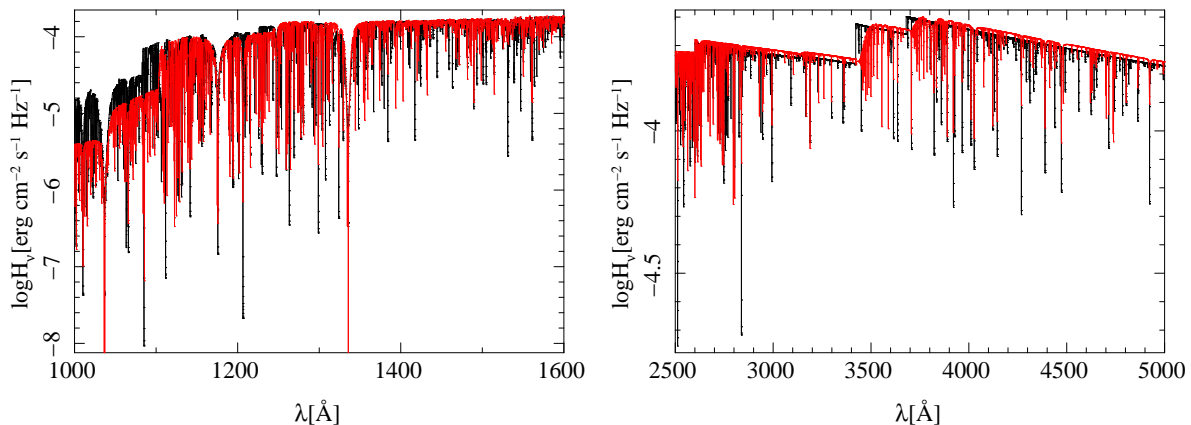


Figure 3.12: LTE(red) and NLTE(black) flux distribution from ATLAS12(red). In the **left hand panel** the range between 1 000 and 1 600 Å. In the **right hand panel** the range between 2 500 and 5 000 Å

### 3.3.3 Comparison of the LTE and NLTE Flux from STERNE

Most analyses of extreme helium stars are done using STERNE models. Therefore it is interesting to see whether the change of the flux distribution using DETAIL is that strong that it could change parameters significantly. We found that the differences are small (Fig 3.13,3.14). Just two things need to be mentioned:

- The STERNE model includes much less lines than DETAIL because more elements are included in the DETAIL computations.
- In the range around 800 and 1 100 Å the LTE flux is slightly above the NLTE flux which could be a real NLTE effect due to a discrepancy in the ionisation edge of C I at around 1 100 Å.

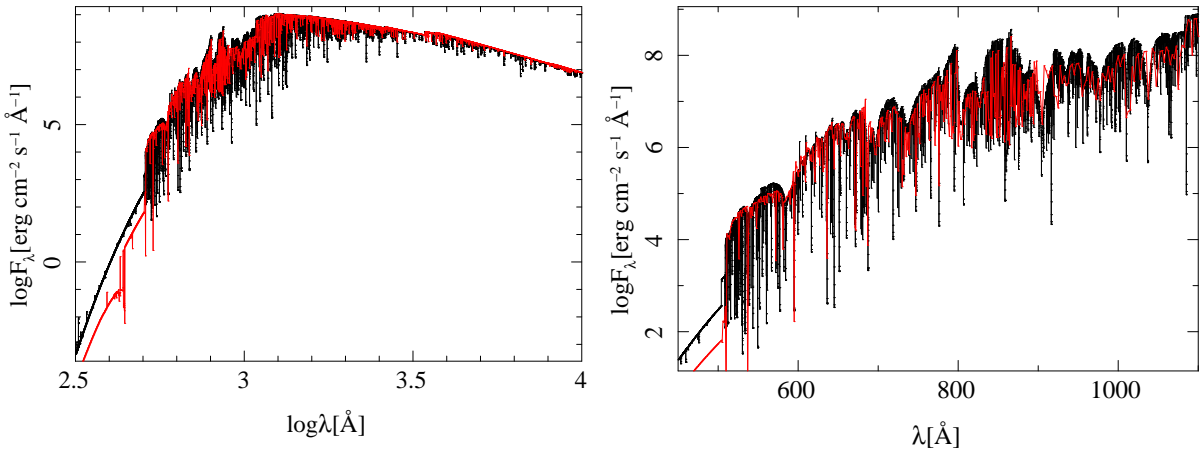


Figure 3.13: LTE(red) and NLTE(black) flux distribution from STERNE(red). In the **left hand panel** the range between 316 and 10 000 Å. In the **right hand panel** the range between 450 and 1 100 Å

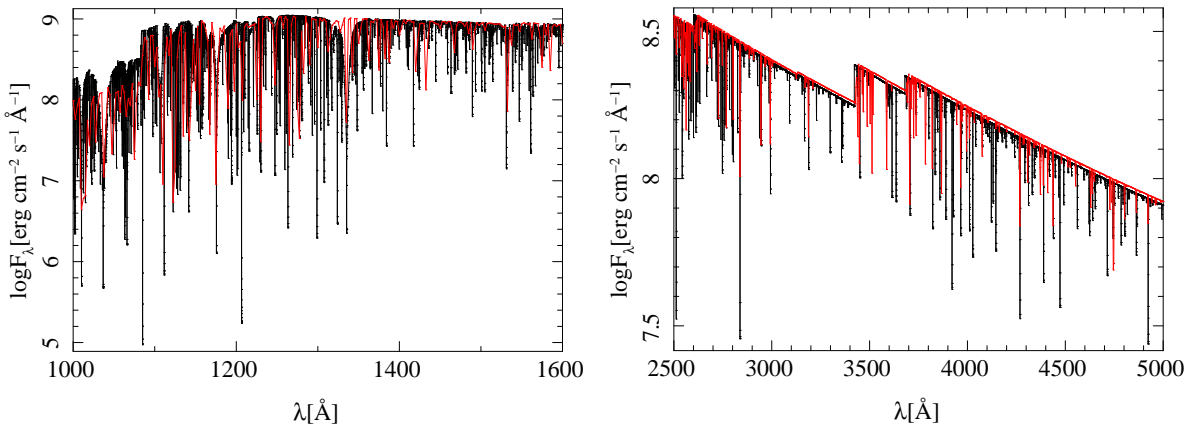


Figure 3.14: LTE(red) and NLTE(black) flux distribution from STERNE(red). In the **left hand panel** the range between 1 000 and 1 600 Å. In the **right hand panel** the range between 2 500 and 5 000 Å

### 3.3.4 Comparison of the NLTE Flux from STERNE and ATLAS12

The comparison of the NLTE flux distribution from STERNE and ATLAS12 is good. The only issue which needs to be mentioned is that the ionisation edge of carbon is slightly lower in the STERNE flux. This fact is due to small differences in the temperature and pressure stratification. Interesting is that the huge differences in the LTE flux distributions and the wrong treatment of the CII line have no significant impact on the NLTE flux distribution (Fig. 3.15, 3.16).

The comparison of the NLTE fluxes shows that there is no significant discrepancy using STERNE or ATLAS12 structures. The question is how do the LTE and NLTE flux distributions fit together. Huge differences could lead to significant changes in the results for stellar parameters but also for abundances.

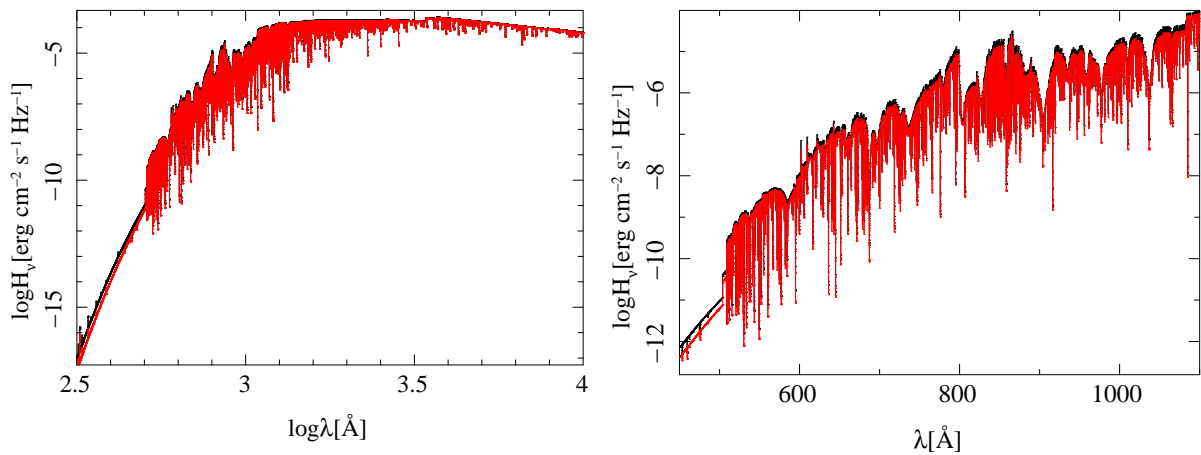


Figure 3.15: NLTE flux distribution from STERNE (black) and ATLAS12 (red). In the **left hand panel** the range between 316 and 10 000 Å. In the **right hand panel** the range between 450 and 1 100 Å

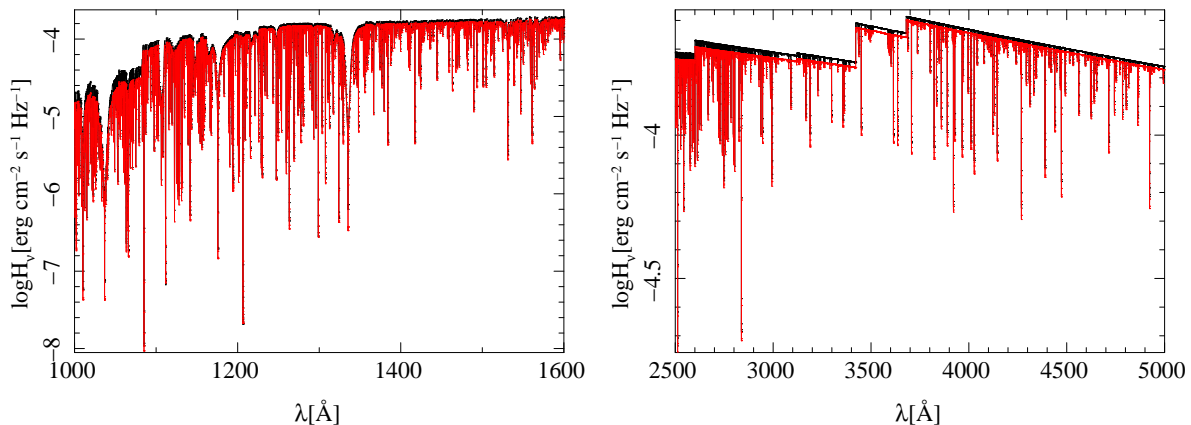


Figure 3.16: NLTE flux distribution from STERNE (black) and ATLAS12 (red). In the **left hand panel** the range between 1 000 and 1 600 Å. In the **right hand panel** the range between 2 500 and 5 000 Å

The LTE and NLTE fluxes from STERNE are in good agreement but the final line profiles could

be strongly different for the ions which are computed in NLTE due to the fact that the occupation numbers which are responsible for the strength of the line are computed in NLTE. In the next section the comparison of line profiles is explained in full detail.

### 3.3.5 Line Profiles computed in LTE and NLTE

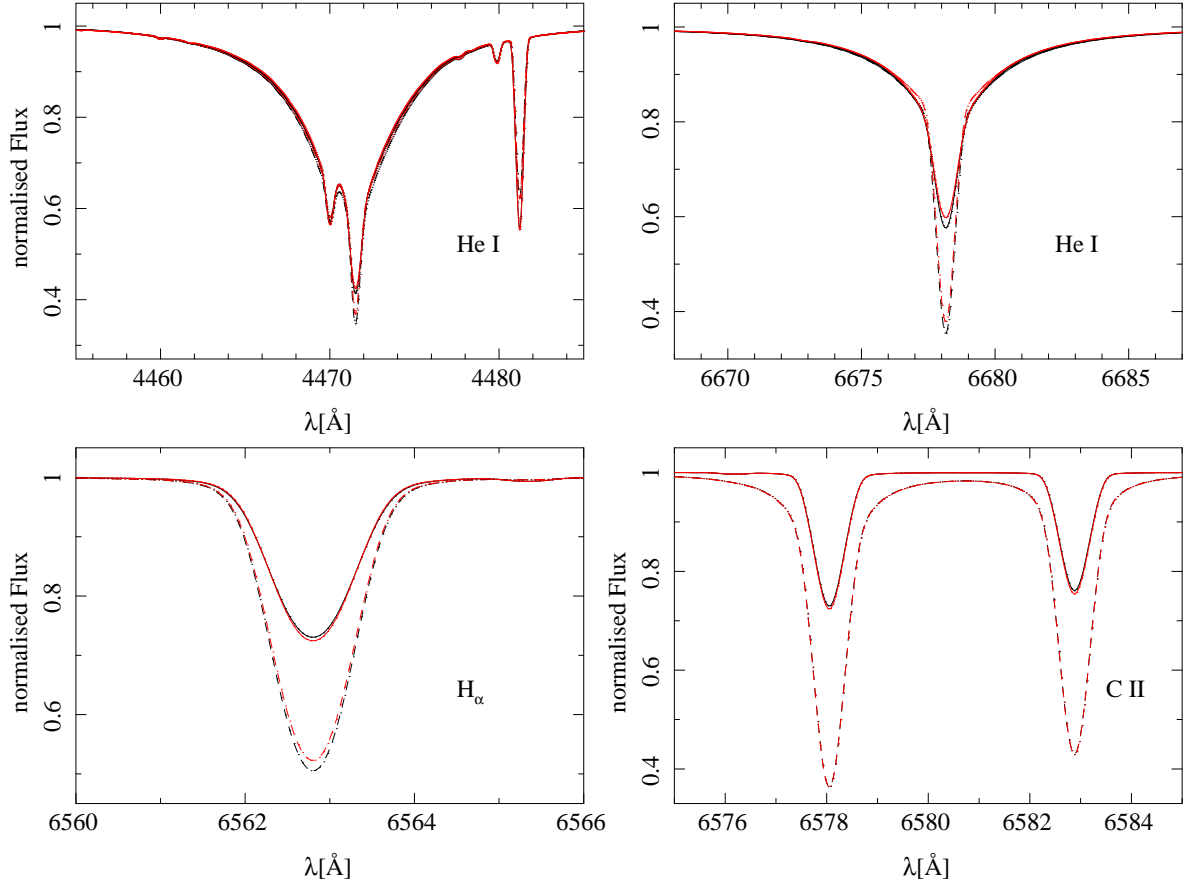


Figure 3.17: Computed helium and hydrogen line profiles using ATLAS/SURFACE (black) and STERNE/SURFACE (red) for a helium rich model with  $T_{\text{eff}} = 16\,800$  K and  $\log g = 2.80$  in LTE (solid line) and NLTE (dashed)

For a comparison of the line profiles SURFACE was taken to compute synthetic spectra from STERNE and ATLAS12. Including/excluding the DETAIL calculation leads to NLTE/LTE line profiles. We focussed on two issues. First, how big are the NLTE effects, and second, how well match the profiles taking ATLAS12 or STERNE models.

Looking at the NLTE effects (Fig. 3.17) reveals huge effects especially for the hydrogen lines and the red helium lines. In NLTE  $H_{\alpha}$  appears to be twice as strong as in LTE. This could lead to a significant change of the hydrogen abundance. But not just hydrogen and helium are affected, also the other metals are governed by NLTE effects. The strong C II doublet close to  $H_{\alpha}$  is one example for a significant change in the line profile (Fig. 3.17). This strong effects could have an huge impact on abundance results for extreme helium stars.

The line profiles (LTE and NLTE) for helium, hydrogen and carbon are very similar from STERNE and ATLAS12 despite of the problem of the EUV CII line discussed above. This leads to the conclusion that the EUV CII line wings have no significant impact. Hence, the results of a quantitative spectroscopic analysis should not show significant differences when using ATLAS12 instead of STERNE models. In the following chapter the quantitative LTE analysis of BD+10°2179 using STERNE models is described in full detail.

## 4 Quantitative Spectral Analysis of BD+10°2179

Table 4.1: Basic properties of BD+10°2179

RA (2000)	$10^h 38^m 17.30^s$	(Høg et al. 2000)
DEC (2000)	$+10^\circ 19' 26.7''$	(Høg et al. 2000)
$v_{\text{rad}}$	$155 \text{ km s}^{-1}$	(Klemola 1961)
$m_v$	9.93	(Landolt 1973)

The star BD+10°2179 was discovered as an extreme helium star by Klemola (1961). His analysis had to be coarse due to the lack of appropriate model atmospheres. The first fine analysis was done by Hunger & KlingleSmith (1969). They found a mass fraction of 0.45 for helium, 0.0001 for hydrogen and as the most surprising result a mass fraction of 0.55 for carbon. Heber (1983) reanalysed BD+10°2179 using line blanketed LTE model atmospheres and found that the carbon abundance is not that high but just 0.01 by number fraction whereas the helium abundance is much higher at 0.989 by number fraction. He found  $T_{\text{eff}} = 16\,800 \pm 600 \text{ K}$  and  $\log g = 2.55 \pm 0.2$  for the stellar parameters. The latest analysis of BD+10°2179 was done by Pandey et al. (2006) using STERNE model atmospheres. They found  $T_{\text{eff}} = 16\,900 \text{ K}$  and  $\log g = 2.55 \pm 0.2$  from the UV spectra but  $T_{\text{eff}} = 16\,400 \text{ K}$  and  $\log g = 2.35 \pm 0.2$  from the optical. The helium and carbon abundance is similar to the study of Heber (1983), but some of the other elements are discrepant. Why is it useful to reanalyse BD+10°2179 again? There are several reasons:

- The absence of hydrogen leads to a significantly increased relevance of all other opacity sources. During the last years new calculations increased the number of opacity data. Much more line and continuum opacities became available. Behara & Jeffery (2006) included in the recent STERNE version opacities for all ions which are available in the Opacity Project database and an opacity-sampling procedure. The analysis shows a huge difference in the UV-flux distribution due to larger number of opacities treated in the model. The change of effective temperature is up to 2 000 K for some stars.
- Przybilla et al. (2005, 2006) were the first to consider NLTE effects for two higher-gravity extreme helium stars. They used ATLAS12 LTE model atmospheres. Line formation is treated in NLTE for HeI and several metal lines. Treating more elements in NLTE could increase the accuracy of abundances of different elements and could shed light on the anomalous abundances of some elements, not yet understood at all.
- A new analysis could help to understand the differences between the analysis of Heber (1983) and Pandey et al. (2006). Several abundances show high differences up to 0.7 dex (for example Al, Mg and S).
- The last point is that a FEROS spectrum and UVES spectra are available covering a range from 3 000 to 10 000 Å. This observational material is far superior to all previous studies and makes it possible to analyse for the first time the red and the near infrared part of the spectrum. Important abundances for elements like neon and new ionisation equilibria (Ni/II, OI/II) are measurable now.

## 4.1 LTE Analysis of BD+10° 2179

### 4.1.1 Basic Measurements

The analysis of BD+10°2179 is based on a high resolution FEROS spectrum (3 650 - 9 200 Å) and three high resolution UVES spectra (3 050 - 3 850 Å, 6 700 - 8 550 Å, 8 650 - 10 250 Å). But before stellar parameters or abundances could be derived an accurate line identification was necessary using the tables of Moore (1945, 1970) and the NIST-database<sup>1</sup>. Most of the lines could be identified but there are still some unidentified lines (even strong ones, Tab. A.3). Two reasons are plausible. They can be due to a high overabundance of an element. The spectra show a lot of CII lines, many of which are unseen in normal stars. Hence higher excitation lines of carbon might exist which are not discovered by laboratory experiments yet. The atomic data for all transitions are given in a linelist which is complete for most of the important elements in the range from 3 800 Å to 5 200 Å. For shorter and longer wavelength the linelist was filled up with data from the VALD database<sup>2</sup>.

For the analysis a grid of models with 99 % He and 1 % C and a metallicity of 0.1 solar metallicity was calculated (Behara & Jeffery 2006,opacity-sampled). CII/III, SII/III and NI/II were used as ionisation equilibria. Note that the lines used are given in Tab. A.6 and marked with (\*). Together with the wings of the four broad helium lines (4026 Å, 4471 Å, 4921 Å, 4388 Å) stellar parameters were derived. 22 NII and 17 CII lines were taken to derive the microturbulence (Fig. B.5, B.6). The final result was  $T_{\text{eff}} = 17\,000 \pm 500$  K,  $\log g = 2.85 \pm 0.2$  and  $v_{\text{turb}} = 10 \pm 1.5$  km s<sup>-1</sup>. Compared to previous analyses (Heber 1983; Pandey et al. 2006)  $\log g$  seems quite high.

Before abundances can be derived the projected rotational velocity needs to be fixed using the DIPSO program package. Ten unblended metal lines were selected and the best fit from the model with different  $v \sin i$  (Tab. 4.2) resulted in  $v \sin i = 17 \pm 2$  km s<sup>-1</sup>. The last step was

Table 4.2: Measured  $v \sin i$  values

X	Wavelength [Å]	$v \sin i$ [km s <sup>-1</sup> ]
CII	6731.07	18
CII	6787.22	17
CII	6791.47	17
CII	6798.11	16
CII	6800.68	17
CII	6812.29	19
NII	5676.020	17
NII	5679.560	18
NII	5686.210	17
NII	5931.790	17

to measure abundances with the model  $T_{\text{eff}} = 17\,000$  K,  $\log g = 3.0$ ,  $v \sin i = 17$  km s<sup>-1</sup> and

<sup>1</sup>[http://physics.nist.gov/PhysRefData/lines\\_form.html](http://physics.nist.gov/PhysRefData/lines_form.html)

<sup>2</sup><http://ams.astro.univie.ac.at/~vald/>

$v_{\text{turb}} = 10 \text{ km s}^{-1}$  by using the computer code SFIT. The results are given in Tab. 4.3. But these results are coarse because of several limitations of SFIT:

Table 4.3: Adopted Abundances of BD+10°2179

X	Solar <sup>a</sup>	Pandey <sup>b</sup>	UVES	FEROS	UVES	UVES
			(3050-3850)Å	(3650- 9200)Å	(6700-8550)Å	(8650-10250)Å
H	12	8.3	8.354	8.645	-	-
He	10.93	11.54	11.532	-	-	-
C	8.43	9.4	9.599	9.402	9.531	-
N	7.83	7.9	7.923	8.007	-	-
O	8.69	7.5	7.508	7.740	-	-
Ne	7.93	-	-	8.449	8.458	-
Mg	7.60	7.2	7.238	-	-	-
Al	6.45	5.7	5.718	5.785	-	-
Si	7.51	6.8	6.908	6.555	-	-
P	5.41	5.3	5.304	5.069	-	-
S	7.12	6.5	6.556	6.463	-	-
Ar	6.40	6.1	6.135	6.334	-	-
Ti	4.95	3.9	3.909	-	-	-
Cr	5.64	4.1	4.107	-	-	-
Fe	7.50	6.2	6.389	6.315	-	-
Ni	6.22	5.1	5.117	-	-	-

<sup>a</sup> Recommended solar abundances from Tab. 1 of Asplund et al. (2009)

<sup>b</sup> From Pandey et al. (2006)

- The FEROS spectrum has about 200 000 data points but to save computing time SFIT uses just 20 000. SFIT resampled the spectrum to 20 000 data points and measured the abundance which leads to undersampling and to an unreliable result. The UVES spectra have the same problem with 60 000 and 120 000 data points.
- The next important fact are the atomic data. No broadening data for the helium lines in the infrared and in the blue ( $< 3850 \text{ \AA}$ ) are available. The linelist is complete for the range from  $3800 \text{ \AA}$  to  $5200 \text{ \AA}$  but for shorter and longer wavelengths it needs to be filled up with data from the VALD database<sup>1</sup> which is not reliable for some lines. Therefore a quality check of the linelist using line-by-line measurements for aluminium and phosphorus was done (Sec. 4.1.2).
- The last point are the NLTE effects which could lead to a significant change in the abundance. E.g. the hydrogen abundance changes by about 0.3 dex if  $H_{\alpha}$  is considered or not.

#### 4.1.2 Phosphorus and Aluminium - a Quality Check

To check the quality of the linelist and the synthetic spectra, the phosphorus and aluminium abundances were reanalysed carefully. It seems that the synthetic spectra are too strong for

<sup>1</sup><http://ams.astro.univie.ac.at/~vald/>

some lines, but for other lines the fit is very good. Every Al and P line in the range 3 700 - 6 800 Å was picked out and checked by visual inspection (Tab. A.4). Pandey et al. (2006) obtained an Al abundance of 5.7 and a P abundance of 5.3. SFIT was run with a starting value of 3.0 for both. The result was  $3.04 \pm 66.18$  for Al and  $3.05 \pm 46.80$  for P which means it did not converge. Some of the lines were rejected (AlII 3 900.675, AlII 6 226.195, AlII 6 231.621, AlII 6 231.750, AlIII 5 722.730, AlIII 5 163.859, AlIII 5 163.910, PII 5 425.880, PII 6 034.039 and PII 6 301.933) for the reasons which are given in Tab. A.4 and SFIT was run with start values 5.0 for Al and 4.5 for P. The result was  $5.26 \pm 0.06$  for Al and  $4.13 \pm 0.50$  for P which is even with a small error also wrong. The start values were changed to Pandey's expected abundances and  $5.78 \pm 0.03$  for Al and  $5.45 \pm 0.04$  for P was obtained. The original SFIT measurement with every line considered in the linelist yielded a value of 5.79 for Al and 5.07 for P. This means the Al abundance does not change significantly but the P abundance increases by about 0.4 dex. The fit for aluminium is not bad for most of the lines but for phosphorus the fit is still not very good.

The best phosphorus lines in the range 3 700 - 6 800 Å were chosen and the abundance was measured separately for every line using SFIT (Tab. A.5). Just the most trustable lines were taken (PII 6 043.084, PIII 4 059.312, PIII 4 080.089, PIII 4 222.198) and the abundance was measured from these lines. We obtained a value of 5.42 which still seems too high.

The next step was to take just the range of 3 700 - 4 500 Å to have less data points and a higher resolution in the fit. For this case the abundance was measured using three lines (PIII 4 059.312, PIII 4 080.089, PIII 4 222.198). The other lines were rejected from the linelist. The result is 5.27.

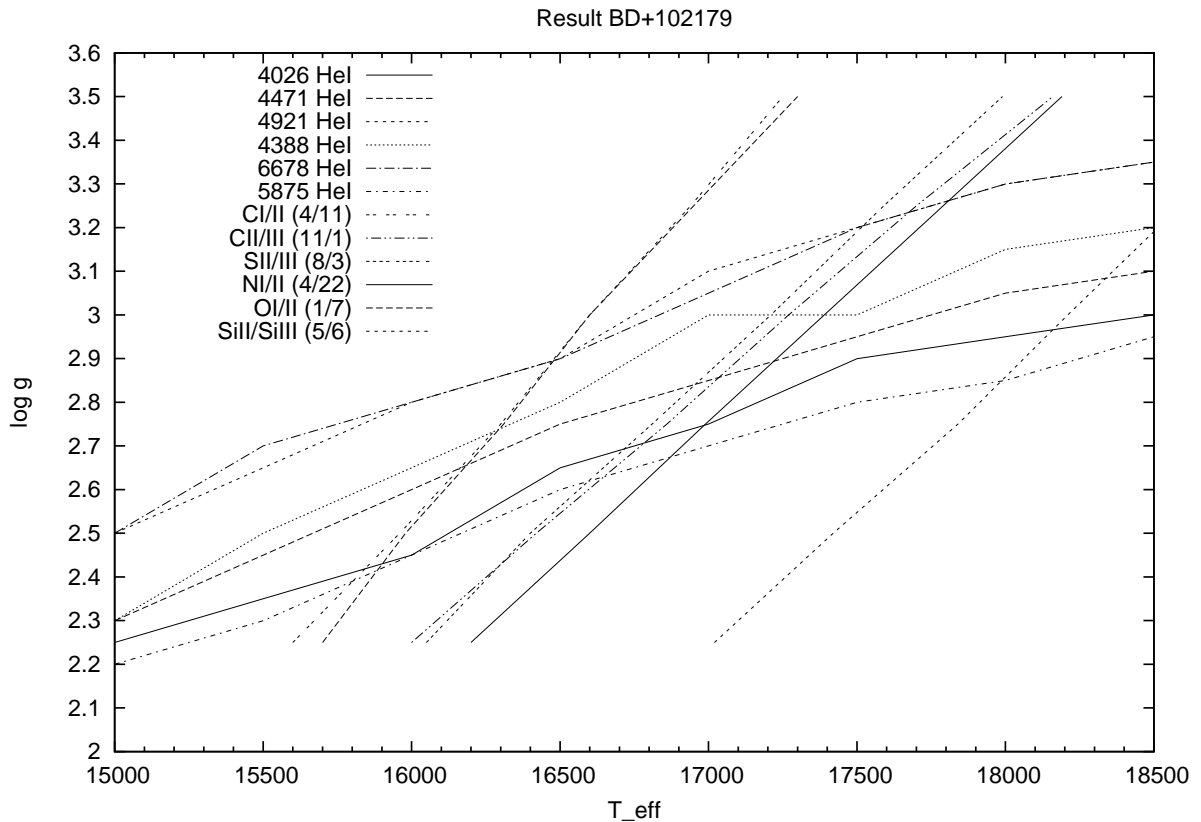
For the last test the original linelist with every phosphorus line was taken and the abundance was measured again in the range of 3 700 - 4 500 Å. We obtained an abundance of 5.31 which seems to be a good value.

The conclusion of these tests and the line-by-line analysis is, that it is not useful to fill the linelist up with every line which exists and to measure abundances for the whole range. One reason is that SFIT considered just 20 000 data points. The FEROS spectrum includes about 200 000 data points. The resolution for the fit decreases by a factor of ten. The other reason is, that every line with erroneous values (e.g. PII 6 301.933 with large differences for the  $\log gf$  value) or every bad line (e.g. disturbed by a cosmic particle) distorts the result.

It is much better to cut a small part of the spectrum and take a few lines with good atomic data. This includes a preselection which should be done carefully. In the case of the phosphorus lines the preselection and the cut of the spectrum leads to an increase in abundance of 0.3 and a much improved line profile fit.

### 4.1.3 Full LTE Analysis of BD+10° 2179

The surface gravity was found to be higher than in previous analyses therefore the stellar parameters  $T_{\text{eff}}$  and  $\log g$  were determined again. To verify the quality of the obtained  $T_{\text{eff}}$  and  $\log g$  some of the measured equivalent widths were checked again (Fig. A.6). Atomic data for the used lines was compared with the NIST-database and the KURUCZ-database and two more Helium lines (6 678 Å, 5 875 Å) were included to the analysis. Atomic data and equivalent width fit well to the first measurement. Therefore it is not surprising that the obtained value of

Figure 4.1: ( $T_{\text{eff}}$ ,  $\log g$ )-plane for BD+10° 2179

$T_{\text{eff}} = 17\,000$  K and  $\log g = 2.8$  does not change significantly (Fig. 4.1).

The most trustable ionisation equilibria are SII/III, NI/II, CII/III because reliable atomic data are available. They are well in agreement with each other. The SiII/III equilibrium gives values which are too high. This could probably be explained by NLTE effects. The equilibrium of CI/II and OI/II is too low. For OI/II only one OI (7 771.941 Å) line can be used. An error in this line leads to a significant change in the obtained values for  $T_{\text{eff}}$ . The four CI lines show a high spread up to 0.5 dex in the abundance which makes these lines not trustable (Fig. B.1, B.2, Tab. A.1).

Synthetic helium line profiles for different  $T_{\text{eff}}$  and  $\log g$  were calculated using the SPECTRUM program. The  $\log g$  for each  $T_{\text{eff}}$  was found by visual inspection. The best agreement between observation and synthetic spectrum was found for the HeI line 4 471 Å. The synthetic profiles for the other helium lines seem in some cases slightly asymmetric (Fig B.3, B.4, Tab. A.2).

To increase the quality of the fit the spectra were cut in several chunks (400 Å for FEROS and UVES (6 700 - 8 550 Å) and 100 Å for UVES (3 050 - 3 850 Å)) to reduce the number of data points to less than 20 000. Unusable lines (e.g. unidentified lines, lines with incomplete or non-existent atomic data) were excluded. For some lines, where no reasonable solution could be found, atomic data were compared with the NIST- and the KURUCZ-database and atomic parameter like  $\log gf$  values were improved. The quality of the fit increases in most cases. Especially for a few CII lines there is still no acceptable match. These lines were also ex-

cluded. Each part was checked for the existent lines. The abundances for the non-detectable elements were fixed to Pandey's value (Pandey et al. 2006). The third UVES spectrum (8 650 - 10 250 Å) was not used for this analysis because it is crowded by telluric lines. The result for the abundance measurement is given in Tab. 4.5. The atmosphere of BD+10° 2179 shows three significant features.

- Hydrogen is strongly underabundant (about 1/1 000 % solar) but not totally absent whereas helium is extremely overabundant.
- The enrichment of nitrogen and carbon is an indicator that the atmosphere contains CNO and triple  $\alpha$  processed material.
- The normal abundance of oxygen and the high overabundance of neon can just be explained by  $\alpha$ -captures.

Table 4.4: Stellar parameters of the LTE analysis of BD+10° 2179

Stellar parameter	Heber <sup>a</sup>	Pandey <sup>b</sup>	this work
$T_{\text{eff}}$ [K]	16 800 ± 600	16 400 ± 500	17 000 ± 500
$\log(g[\text{cm s}^{-2}])$	2.55 ± 0.2	2.35 ± 0.2	2.80 ± 0.2
$v_{\text{rot}}$ [km s <sup>-1</sup> ]	20 ± 20	20 ± 2	17 ± 2
$\xi$ [km s <sup>-1</sup> ]	7.5 ± 1.5	6.5	10 ± 1.5

Table 4.5: Derived abundances of the LTE analysis of BD+10° 2179. Note that solar abundances for the element  $X$  are given with respect to  $\log(X/H) + 12$  and the other abundances  $\epsilon$  are given with respect to  $\log \sum \mu_X \epsilon(X) = 12.15$ , where  $\mu_X$  is the atomic weight of element  $X$

X	Solar <sup>a</sup>	Heber <sup>b</sup>	Pandey <sup>c</sup>	This work
H	12	8.5	8.3	9.45 (H $_{\alpha}$ ); 8.73 (H $_{\beta}$ ); 8.48 (< H $_{\beta}$ )
He	10.93	11.53	11.54	was fixed to 11.54
C	8.43	9.54	9.4	9.30 (FEROS); 9.24 (UVES <sub>blue</sub> Å); 9.60 (UVES <sub>red</sub> )
N	7.83	8.11	7.9	8.06 (NII); 8.28 (NI FEROS); 8.46 (NI UVES <sub>red</sub> )
O	8.69	8.1	7.5	7.62 (OII); 7.83 (OI FEROS); 8.01 (OI UVES <sub>red</sub> )
Ne	7.93	-	-	8.47 (FEROS); 8.58 (UVES <sub>red</sub> )
Mg	7.60	8.02	7.2	7.08 (FEROS and UVES <sub>red</sub> ); 6.64 (MgII 4481 Å)
Al	6.45	6.25	5.7	5.78 (FEROS); 5.52 (UVES <sub>blue</sub> )
Si	7.51	7.32	6.8	6.93 (SiIII); 6.36 (SiII)
P	5.41	5.5	5.3	5.30 (FEROS)
S	7.12	7.12	6.5	6.54 (FEROS and UVES <sub>blue</sub> )
Ar	6.40	6.4	6.1	6.30 (FEROS)
Ca	6.34	< 5.9	5.2	4.95 (FEROS)
Fe	7.50	6.49	6.2	6.43 (FEROS and UVES <sub>blue</sub> )

<sup>a</sup> Recommended solar abundances from Tab. 1 of Asplund et al. (2009)

<sup>a</sup> From Heber (1983)

<sup>b</sup> From Pandey et al. (2006)

Solar and obtained abundances can not be compared directly because different normalisations are used. Solar abundances for the element  $X$  are given with respect to  $\log(X/H) + 12$  whereas our abundances are given with respect to  $\log \sum \mu_X \epsilon(X) = 12.15$  for all elements, where  $\mu_X$  is the atomic weight of element  $X$ . However, quantitative statements can be made.

*Iron* - Iron should be unaffected by H and He burning and the nuclear reactions involved. Therefore it was taken as the indicator for the initial metallicity. The low abundance indicates that BD+10°2179 is metal poor. The initial abundance should therefore be below solar.

*Hydrogen* - Hydrogen is highly depleted. The abundance in the atmosphere is less than 1% by number fraction. The decreasing values along the Balmer series is due to decreasing NLTE effects which are strongest for  $H_\alpha$ .

*Carbon* - Carbon is the most abundant element after helium. It is highly enriched. This leads to the conjecture that the atmosphere is highly affected by the triple  $\alpha$ -process.

*Nitrogen* - Nitrogen is overabundant for NII and slightly more for NI. The enrichment can be explained by the CNO-process. In this process nitrogen will be enhanced by the factor whereas oxygen and carbon are depleted. NI is measured by some weak lines (Moore linelist Nr. 1 and 2) which are highly sensitive to small changes in the parameters and sensitive to NLTE effects.

*Oxygen* - Oxygen is below solar and probably unaffected. There are two different processes which could affect the oxygen abundance. OI is measured by the weak triplet at  $\sim 7770 \text{ \AA}$  which is highly sensitive to small changes in the parameters like the NI lines. As  $\alpha$ -elements like neon in BD+10°2179 are enhanced, oxygen should also be enriched by  $\alpha$ -capture on carbon which can happen during the AGB-phase of the progenitor or during the merger. To explain the unaffected low abundance oxygen needs to be depleted which could occur during the CNO-cycle but only if the central temperature of the progenitor is high enough to maintain the NO-bicycle. To explain the obtained unaffected abundance both processes need to cancel each other out which needs a special fine tuning.

*Neon, Magnesium* - Neon is strongly overabundant whereas magnesium is unaffected or slightly overabundant depending on the initial metallicity. Both enrichments could be explained by subsequent  $\alpha$ -captures on oxygen.

*Argon, Aluminium, Silicon, Sulphur and Calcium* - These elements show a wide spread from almost solar for argon and strongly below solar for calcium whereas Al, S and SiIII fit well together. The high discrepancy between SiII and SiIII (0.55 dex) is not surprising because the ionisation equilibrium for silicon requires a much higher  $T_{\text{eff}}$  and  $\log g$ . Notable is that phosphorus is about solar whereas a value below solar due to poor metallicity is expected. Up to now there is no explanation for such a high abundance.

The quality of the fit for the full spectrum could be increased considerably compared to the first analyses. For most elements the abundances fit well to older analyses but there are still some problems which need to be solved. Probably the NLTE analysis will shed light on these problems.

## 4.2 Quantitative NLTE Analysis of BD+10°2179

BD+10°2179 is a supergiant and therefore NLTE effects are supposed to be quite strong at least for some spectral lines. Indeed our calculations show strong effects (see Sec. 3.3.5) but we need to mention that this is not the case for every line. The spectral lines in the red part are supposed

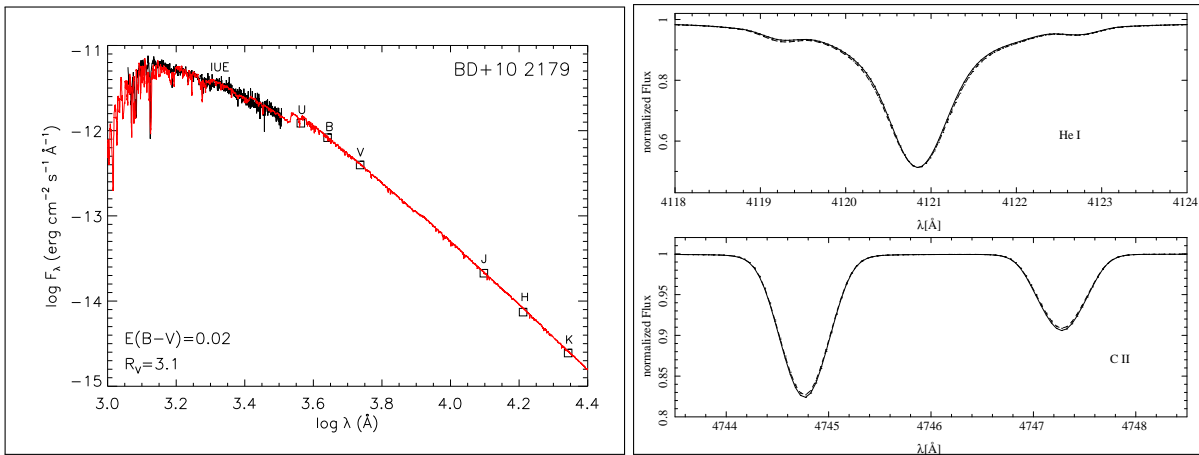


Figure 4.2: **Left hand panel:** Spectral energy distribution as a further indicator for  $T_{\text{eff}}$  and  $\log g$ . Observations (black line and open squares) are over plotted by a synthetic spectrum (red) computed with DETAIL for  $T_{\text{eff}} = 17\,700$  K and  $\log g = 2.95$ . **Right hand panel:** Two examples of spectral lines (He I and C II which show no NLTE effects)

to be more affected due to stimulated emission whereas lines in the blue part should on average not be affected so strongly (Fig. 4.2). In this chapter the NLTE analysis of BD+10°2179 is presented which proceed in the same way as the LTE analyses described in the previous section. That is ionisation equilibria combined with helium lines. We were able to reproduce spectral lines like  $H_{\alpha}$  (Fig. 4.7) much better and found a significantly higher effective temperature and  $\log g$ .

Sec. 3.3.5 showed that the line profiles calculated with STERNE/SURFACE and ATLAS12/SURFACE are consistent. We choose ATLAS12 models for the analysis. The affected UV-flux (see Sec. 3.3) has no impact for most elements as the radiation field is calculated correctly with DETAIL. We concentrated on the FEROS spectrum for the analysis because all significant lines are available in the range which is covered by the spectrum. Only the Ni multiplet  $2s^2 2p^2 2(3P)3s - 2s^2 2p^2 2(3P)3p$  (8 650 - 8 747 Å) was taken from the UVES spectrum. The strong enhancement of carbon and nitrogen and the FEROS and UVES spectra which contains the red part, lead to the opportunity that using C I/II/III, Ni/II and O I/II as much as four ionisation equilibria are available. Note that some Ni lines are blended (Fig. 4.3) and in the wing of a broad helium which is not considered in the model atom. Therefore the Ni/II equilibrium has to be taken with a grain of salt. We found  $T_{\text{eff}} = 17\,700$  K and  $\log g = 2.95$  which is the best mean for all four equilibria. The parameter were determined iteratively. The LTE solution  $T_{\text{eff}} = 17\,000$  K and  $\log g = 2.80$  was the starting point. Because O I, C I was much too strong and C III much too weak for the starting point effective temperature and gravity were increased until the model and the observation was in satisfactory agreement for the equilibria and the helium wings. Taking just C II/III the best  $T_{\text{eff}}$  would be slightly cooler whereas taking just O I/II the best  $T_{\text{eff}}$  would be slightly hotter. Examples are plotted in Fig. 4.3. The helium wings and the redundant information from four ionisation equilibria (C I/II/III, Ni/II and O I/II) make the parameter determination quite reliable. To check the accuracy, the spectral energy distribution was computed and compared with observation. We have found good agreement and thus could strengthen the result from the ionisation equilibria (Fig. 4.2).

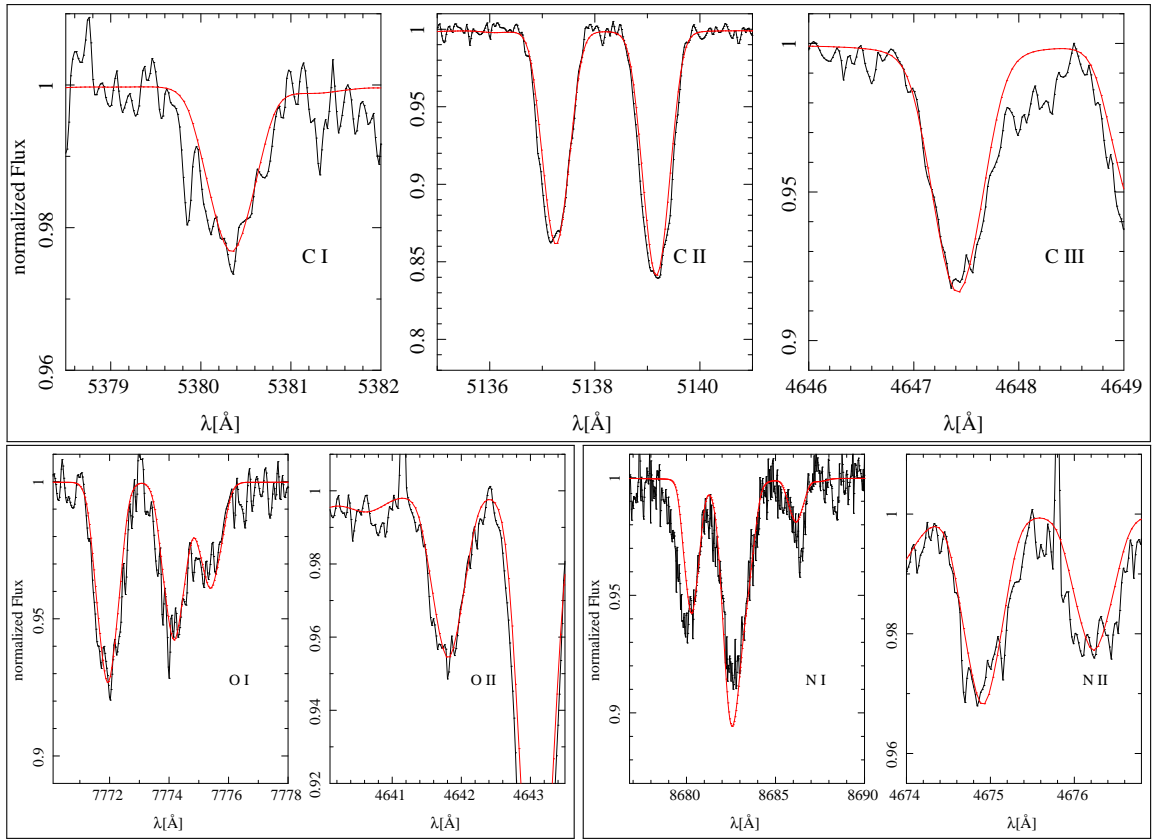


Figure 4.3: ionisation equilibrium of BD+10°2179. Note that for N I just the 8 686.15 Å is unblended. The red part of 8 680.28 Å has a Ne I blend and the 8 683.40 Å has strong C II blend

Due to the high carbon abundance one has not just the advantage of having spectral lines of three different ions (neutral and singly/doubly ionised) at hand. Also many spectral lines of C II of different strength, from faint lines to strongly broadened ones, are available. That makes C II ideal to determine the microturbulence. Synthetic spectra for  $T_{\text{eff}} = 17\,700\text{ K}$ ,  $\log g = 2.95$  and different microturbulent velocities ( $\xi = 2, 4, 6$  and  $8$ ) were computed. We found  $\xi = 2$  to match both the weak and the strong lines best (Fig. 4.4).

To obtain an excellent match between the FEROS observation and the SURFACE synthetic spectrum rotation and macroturbulent broadening ( $\zeta$ ) had to be included. We found the best agreement for  $v_{\text{rot}} = 20\text{ km s}^{-1}$  and  $\zeta = 15\text{ km s}^{-1}$ . Significant Rotation was found also in previous analyses but this is the first time that the macroturbulence was discovered as a necessity to match the synthetic spectrum to the observation. The macroturbulent motion could be due to a convection zone that could develop at the boundary of He II/III transition zone. It depends, however, on the depth where the convection occurs and whether overshooting is involved. BD+10°2179 is one of only a few extreme helium stars where no pulsation has been detected. Aerts et al. (2009) showed that in hot massive stars non-radial pulsations of high order are the explanation of macroturbulence. We may suppose that such pulsations are also the reason for macroturbulence in the atmosphere of BD+10°2179. They need to be of small amplitude because they are not detected in optical light curves.

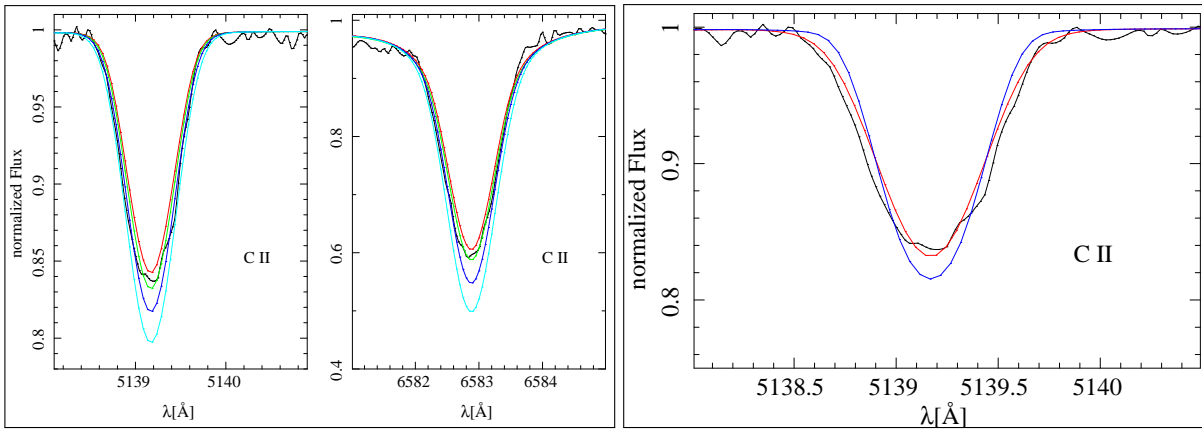


Figure 4.4: **Left hand panel:** Comparison of the observation with computed line profiles of different microturbulent velocities 0 (red), 2 (green), 4 (blue) and 6 (cyan) plotted for two examples. The obtained microturbulence  $\xi = 2$  was obtained by visual inspection of 24 C II lines. **Right hand panel:** Comparison of the observation with computed line profiles including macro-turbulence and rotation (red) or only rotation (blue). Note that the values  $v_{\text{rot}} = 20 \text{ km s}^{-1}$  and  $\zeta = 15 \text{ km s}^{-1}$  were obtained simultaneously by visual inspection of several lines of different elements

The obtained parameters and the abundances for some elements are summarised in Tab. 4.6. For the comparison with the Sun, mass fractions were calculated (Tab. 4.7). The iron abundance is still about a factor of ten below solar. Therefore BD+10°2179 is a metal poor star. Helium is strongly enriched and with 95.6 % (by mass) clearly the most abundant element. The second most abundant element is carbon which turns to be even higher than derived in the LTE analysis with an enhancement with a factor of more than 100. The neon abundance decreases by 0.5 dex compared to LTE but is still like nitrogen almost solar but due to the low metallicity we conclude an overabundance with a factor of about 10 for both. Aluminium shows almost no NLTE effects and is slightly enriched (factor of 2.8). Magnesium shows small NLTE effects. Compared to the LTE analysis the abundance decreases but a small overabundance (factor of 2.5) is still there. This enhancement is predicted for Population II stars. Oxygen seems to be almost unaffected or slightly depleted (factor of 2). The abundances were measured from several lines of each element. We are able to match almost all synthetic profiles to the observation perfectly. Some selected ranges of the FEROS spectrum with the synthetic spectrum are plotted in Figure 4.5, 4.6 and 4.7. Other elements are supposed to be unaffected and set to a tenth of the solar abundance due to the low metallicity of BD+10°2179.

The NLTE analysis turns out to change the parameters compared to previous works by Heber (1983) and Pandey et al. (2006) significantly, implying an increase of effective temperature of about 1 000 K and about 0.5 dex in  $\log g$ . The wings of the helium lines show no differences between LTE and NLTE. This leads to the assumption that the change in ionisation equilibria are responsible for the different  $T_{\text{eff}}$  and  $\log g$ .

A complete error analysis still needs to be done and is essential for a correct interpretation of the abundance pattern in terms of nucleosynthesis models.

Table 4.6: Stellar parameters and elemental abundances of the NLTE analysis of BD+10°2179. Abundances  $\epsilon$  with respect to  $\log \sum \mu_X \epsilon(X) = 12.15$ , where  $\mu_X$  is the atomic weight of element  $X$

Stellar parameter	this work	Heber <sup>a</sup>	Pandey <sup>b</sup>
$T_{\text{eff}}$ [K]	17 700	16 800 $\pm$ 600	16 400 $\pm$ 500
$\log(g[\text{cms}^{-2}])$	2.95	2.55 $\pm$ 0.2	2.35 $\pm$ 0.2
$v_{\text{rot}}$ [ $\text{kms}^{-1}$ ]	20	20 $\pm$ 20	20 $\pm$ 2
$\xi$ [ $\text{kms}^{-1}$ ]	2	7.5 $\pm$ 1.5	6.5
$\zeta$ [ $\text{kms}^{-1}$ ]	15	-	-
X	Abundance		
Hydrogen	8.42	8.5	8.3
Helium	11.54	11.53	11.54
Carbon	9.69	9.54	9.4
Nitrogen	7.98	8.11	7.9
Oxygen	7.50	8.1	7.5
Neon	8.05	-	-
Magnesium	7.05	8.02	7.2
Aluminium	5.95	6.25	5.7
Iron	6.55	6.49	6.2

<sup>a</sup> From Heber (1983)

<sup>b</sup> From Pandey et al. (2006)

Table 4.7: Derived mass fractions of the NLTE analysis of BD+10°2179

X	Solar <sup>a</sup>	This work	[X/Fe]
H	$73.8 \cdot 10^{-2}$	$1.83 \cdot 10^{-4}$	-2.64
He	$24.9 \cdot 10^{-2}$	$95.6 \cdot 10^{-2}$	1.56
C	$2.37 \cdot 10^{-3}$	$4.05 \cdot 10^{-2}$	2.21
N	$6.93 \cdot 10^{-4}$	$9.21 \cdot 10^{-4}$	1.10
O	$5.73 \cdot 10^{-3}$	$3.49 \cdot 10^{-4}$	-0.24
Ne	$1.26 \cdot 10^{-3}$	$1.56 \cdot 10^{-3}$	1.07
Mg	$7.08 \cdot 10^{-4}$	$1.86 \cdot 10^{-4}$	0.40
Al	$5.56 \cdot 10^{-5}$	$1.66 \cdot 10^{-5}$	0.45
Fe	$1.29 \cdot 10^{-3}$	$1.36 \cdot 10^{-4}$	-

<sup>a</sup> Recommended solar abundances from Tab. 1 of Asplund et al. (2009)

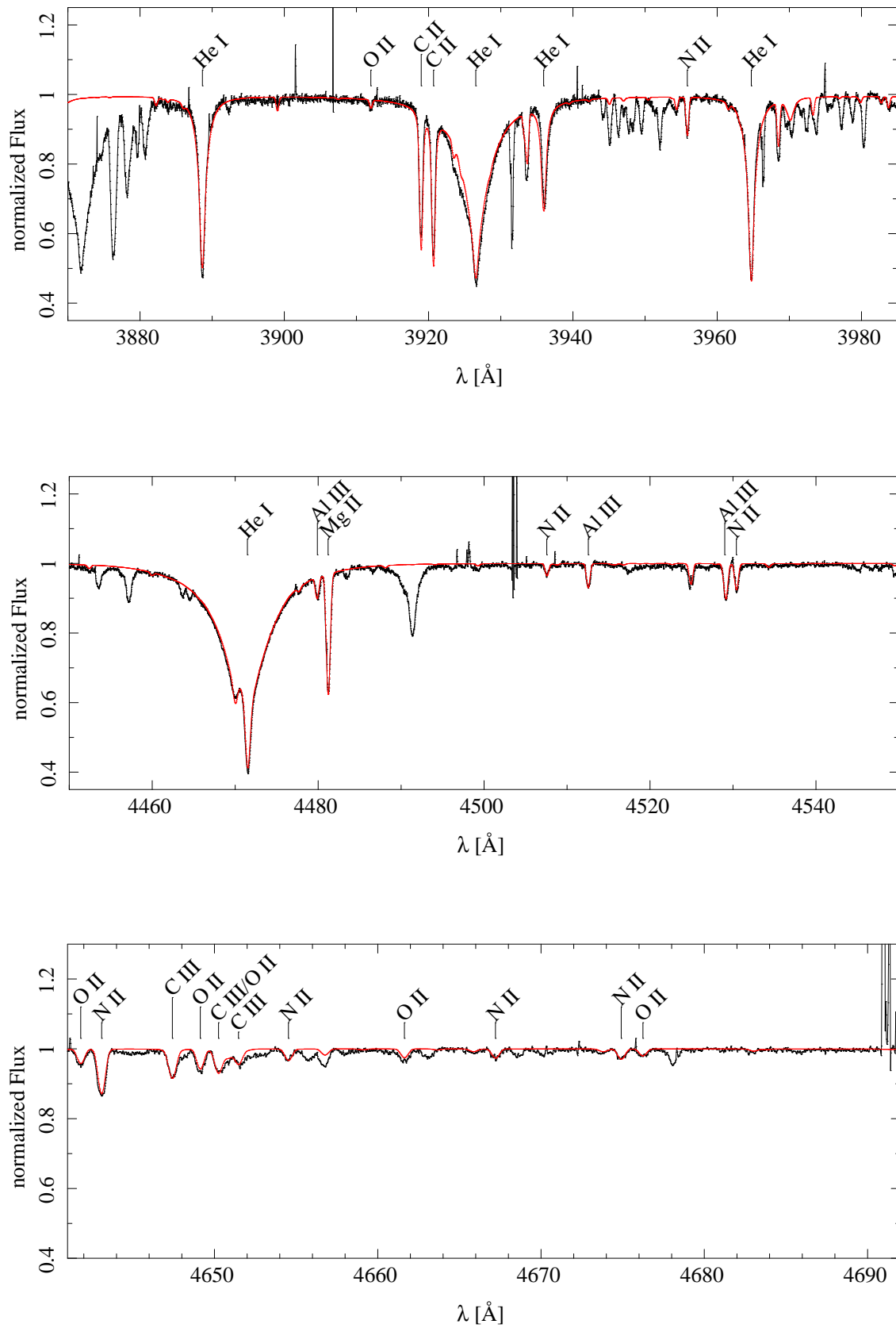


Figure 4.5: Comparison of observation (black) with final synthetic spectrum (red)

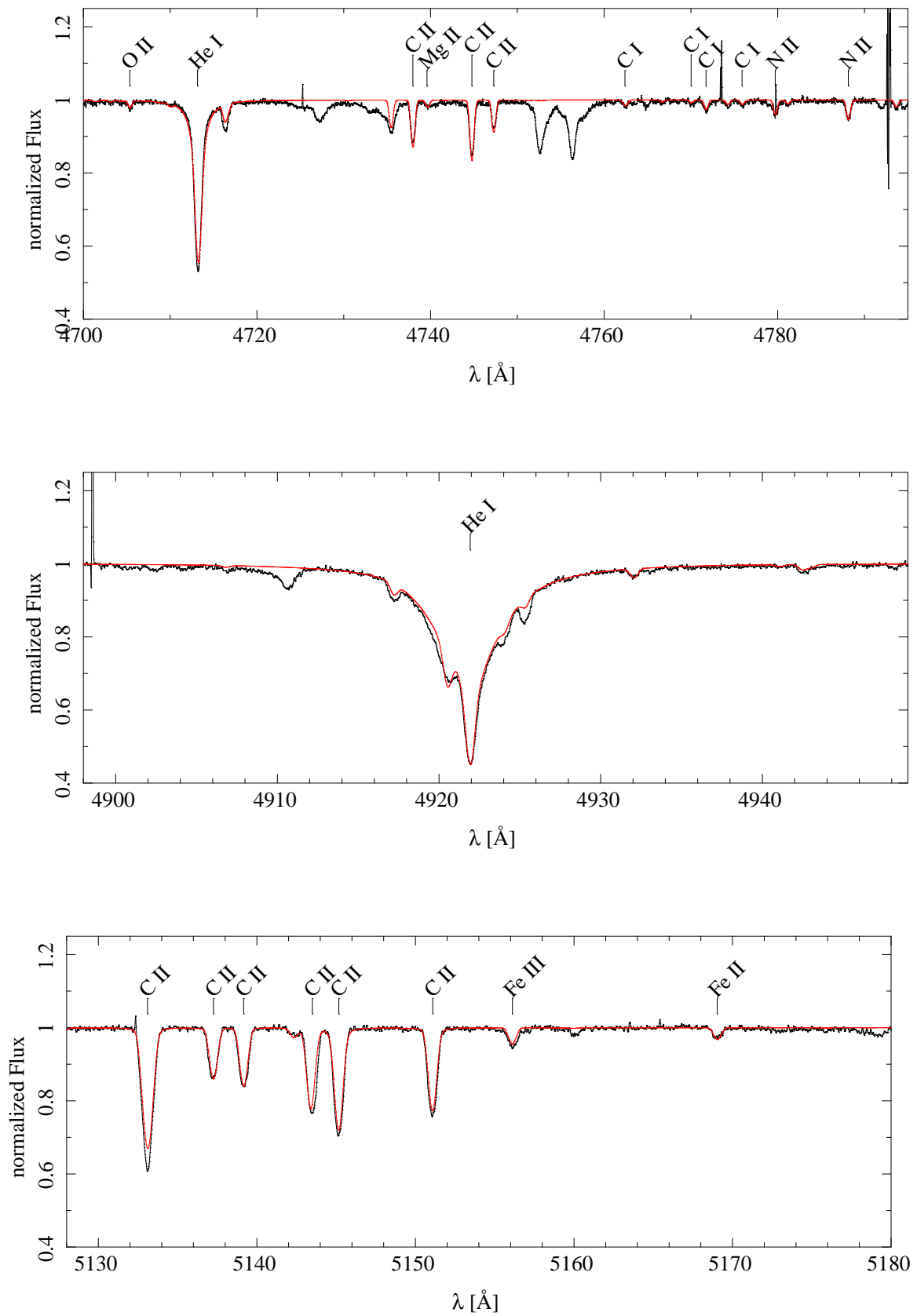


Figure 4.6: Comparison of observation (black) with final synthetic spectrum (red)

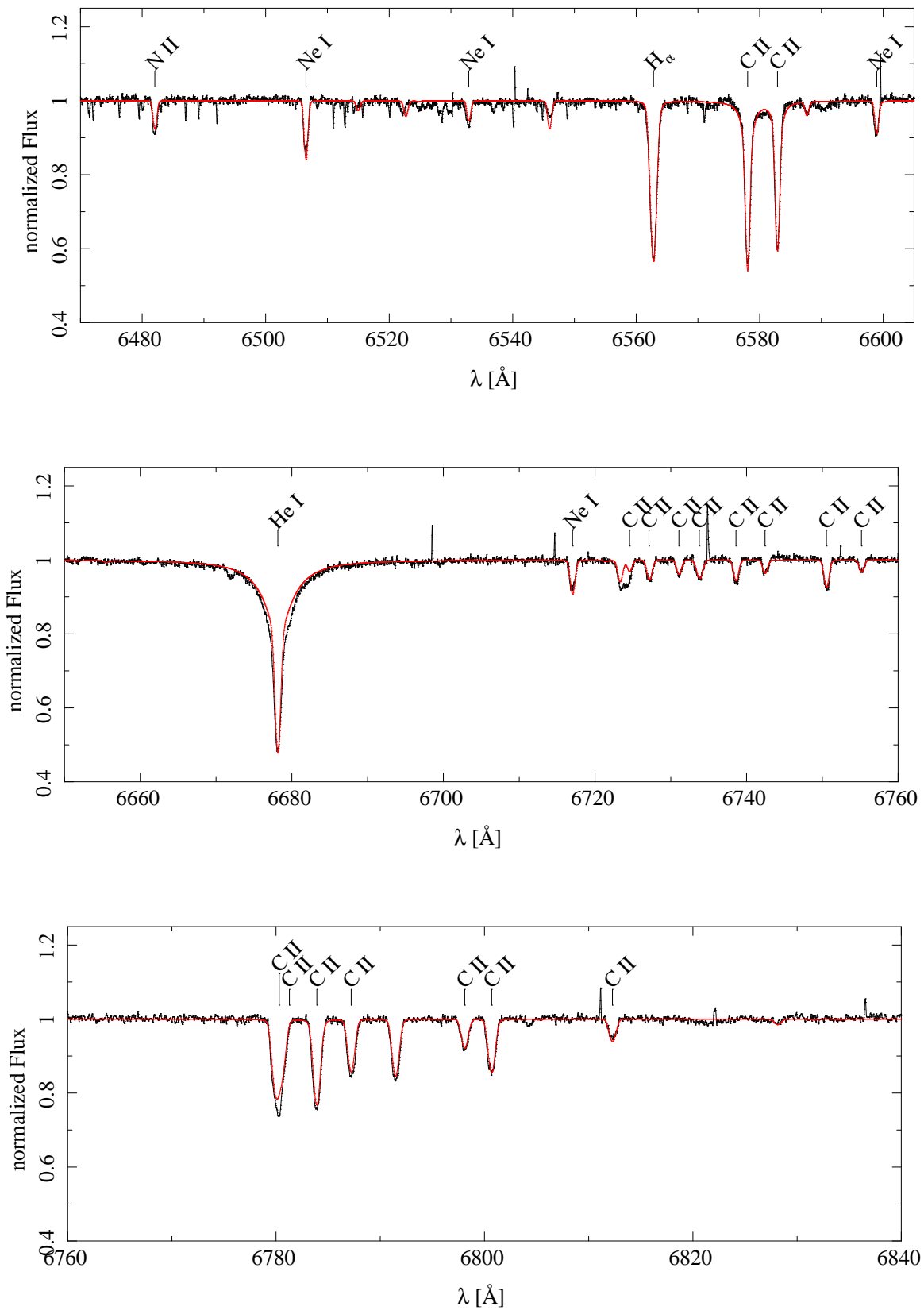


Figure 4.7: Comparison of observation (black) with final synthetic spectrum (red): Note that H $\alpha$  can now be matched perfectly

## 5 Summary and Outlook

Extreme helium stars are a rare class of low-mass supergiants with highly non-solar compositions. Just 17 are known and no one is known to be in a binary system. The origin of these objects has been discussed over the decades and is today supposed to be the merger of a close binary system consisting of a helium and a carbon/oxygen white dwarf. The atmosphere shows a deficit of hydrogen, which is almost completely replaced by helium, carbon and other products of nucleosynthesis processes. Because of the extremely low hydrogen abundance (about 1/1 000 solar) the spectral energy distribution is very different from that of normal stars, in particular in the ultraviolet. The Lyman edge is small and the EUV-flux much higher compared to solar composition models. The missing Lyman edge and the non-solar composition leads to dominance of all other opacity sources and the need for a opacity-sampling procedure to account for the vast number of absorption lines (metal line blanketing). Behara & Jeffery (2006) included opacities for all ions which are available in the Opacity Project database in the recent STERNE version using an opacity-sampling procedure. They found a change in effective temperature up to 2 000 K. Extreme helium stars are supergiants and supposed to show NLTE effects. Przybilla et al. (2005) found NLTE effects for two higher-gravity extreme helium stars and a significant change of  $T_{\text{eff}}$  and  $\log g$ . The prototype of the extreme helium stars, BD+10°2179, was analysed by Heber (1983) and Pandey et al. (2006) before. Their results are discrepant for some elements.

Hence there is a need for the next step, that is to account for both the metal line blanketing and the NLTE effects. Therefore BD+10°2179 was used as a testbed to carry out a NLTE analysis using metal line blanketed LTE model atmospheres computed with the ATLAS12 program. The ATLAS12 code is the most recent version of the ATLAS package including opacity sampling which is necessary for highly non-solar compositions. The other code is STERNE which is optimised to compute model atmospheres for A- and B-type stars with highly non-solar compositions and provides the benchmark. Before the spectroscopic analysis was carried out using ATLAS12 models a detailed comparison of both codes was mandatory since ATLAS12 has never before been applied to such unusual conditions.

The extreme helium stars are He- and C-rich stars. Stars with compositions like BD+10°2179 put high requirements on programs which compute synthetic models. For the first time a detailed comparison of such codes was done. We found that the ATLAS12 flux distribution is incorrect due to a wrong treatment of the line broadening of the CII line at 651.3 Å which is way too strong, so it dominates the whole EUV range. For "normal" compositions this line does not matter because of two reasons. The Lyman edge suppresses the UV flux to much lower values and this line is weak because carbon abundance is low. Comparing computed line profiles of optical lines with STERNE and ATLAS12 it can be seen that for most elements the flaw is insignificant.

STERNE models were computed to carry out a LTE analysis using high resolution FEROS and UVES spectra making it possible to analyse the red part of the spectrum (NeI, Ni and OI) for the first time. The resulting abundances differ not much from those of Pandey et al. (2006) who also used STERNE models. Only the value of  $\log g$  is quite high compared to previous analyses. We could also verify that phosphorus is strongly enriched, which is a long standing puzzle. Some inconsistencies still remain like for example the wide spread of the heavy element abundances, the high overabundance of phosphorus or the poor match for some lines, e.g.  $H_{\alpha}$ .

Are these deficits due to NLTE effects?

For the first time a NLTE analysis of BD+10°2179 was carried out taking the  $T$ - $\rho$ -stratification from ATLAS12 and NLTE occupation numbers computed with DETAIL. The complete synthetic spectrum including detailed broadening was computed using the program SURFACE. Compared to previous analyses the effective temperature increases by about 1 000 K and  $\log g$  by about 0.5 dex which is caused by a shift of the ionisation equilibria. The HeI line profiles remain unchanged mostly. The spectral energy distribution confirmed this result. A detailed inspection of the line profile fits forced us to introduce another non-thermal broadening mechanism – macroturbulent motion – in addition to microturbulence and rotation. We are now able to reproduce  $H_\alpha$  perfectly. Some of the notorious lines can now be matched perfectly. But for the analysis an accurate error analysis is essential which still remains to be done.

This thesis presented major improvements in the modelling of complex atmospheres of extreme helium stars. The metal line blanketing was treated in more detail than before and for the first time NLTE effects for 14 ions have been accounted for. These models were applied to new optical spectra of unprecedented high quality for a fine abundance analysis.

In the course of this work model atoms were generated which include atomic data of several important elements, but more are needed for other interesting elements like phosphorus. Other extreme helium stars await a NLTE analysis – excellent optical spectra have already been obtained. Extreme helium stars are supposed to be mergers of two white dwarfs. New NLTE abundances will probably help to verify or dismiss the merger model. To this end the numerical simulations modelling the merger process need to be improved including nuclear burning in more detail.

# A Tables

Table A.1: Measured  $T_{\text{eff}}$  values for different  $\log g$  by using ionization equilibrium for the LTE analysis

$\log g$	$T_{\text{eff}}(\text{C I/II})$ [K]	$T_{\text{eff}}(\text{C II/III})$ [K]	$T_{\text{eff}}(\text{O I/II})$ [K]
2.25	15600 $\pm$ 200	16000 $\pm$ 200	15700 $\pm$ 200
2.5	15960 $\pm$ 200	16420 $\pm$ 200	15980 $\pm$ 200
2.75	16300 $\pm$ 200	16860 $\pm$ 200	16310 $\pm$ 200
3.0	16600 $\pm$ 200	17270 $\pm$ 200	16600 $\pm$ 200
3.25	16940 $\pm$ 200	17700 $\pm$ 200	16950 $\pm$ 200
3.5	17250 $\pm$ 200	18160 $\pm$ 200	17300 $\pm$ 200

$\log g$	$T_{\text{eff}}(\text{Si III/III})$ [K]	$T_{\text{eff}}(\text{Si II/III})$ [K]	$T_{\text{eff}}(\text{Ni II})$ [K]
2.25	17020 $\pm$ 200	16050 $\pm$ 200	16200 $\pm$ 200
2.5	17420 $\pm$ 200	16400 $\pm$ 200	16600 $\pm$ 200
2.75	17840 $\pm$ 200	16810 $\pm$ 200	16990 $\pm$ 200
3.0	18210 $\pm$ 200	17240 $\pm$ 200	17390 $\pm$ 200
3.25	18590 $\pm$ 200	17590 $\pm$ 200	17790 $\pm$ 200
3.5	18990 $\pm$ 200	17990 $\pm$ 200	18190 $\pm$ 200

Table A.2:  $\log g$  values for different  $T_{\text{eff}}$  by comparing the calculated He profiles with the observed for the LTE analysis

$T_{\text{eff}}$ [K]	$\log g(4026)$	$\log g(4388)$	$\log g(4471)$	$\log g(4921)$	$\log g(6678)$	$\log g(5875)$
15000	2.25 $\pm$ 0.1	2.3 $\pm$ 0.1	2.3 $\pm$ 0.1	2.5 $\pm$ 0.2	2.5 $\pm$ 0.2	2.2 $\pm$ 0.1
15500	2.35 $\pm$ 0.1	2.5 $\pm$ 0.1	2.45 $\pm$ 0.1	2.65 $\pm$ 0.2	2.7 $\pm$ 0.2	2.3 $\pm$ 0.1
16000	2.45 $\pm$ 0.1	2.65 $\pm$ 0.1	2.6 $\pm$ 0.1	2.8 $\pm$ 0.2	2.8 $\pm$ 0.2	2.45 $\pm$ 0.1
16500	2.65 $\pm$ 0.1	2.8 $\pm$ 0.1	2.75 $\pm$ 0.1	2.9 $\pm$ 0.2	2.9 $\pm$ 0.2	2.6 $\pm$ 0.1
17000	2.75 $\pm$ 0.1	3.0 $\pm$ 0.1	2.85 $\pm$ 0.1	3.1 $\pm$ 0.2	3.05 $\pm$ 0.2	2.7 $\pm$ 0.1
17500	2.9 $\pm$ 0.1	3.0 $\pm$ 0.1	2.95 $\pm$ 0.1	3.2 $\pm$ 0.2	3.2 $\pm$ 0.2	2.8 $\pm$ 0.1
18000	2.95 $\pm$ 0.1	3.15 $\pm$ 0.1	3.05 $\pm$ 0.1	3.3 $\pm$ 0.2	3.3 $\pm$ 0.2	2.85 $\pm$ 0.1
18500	3.0 $\pm$ 0.1	3.2 $\pm$ 0.1	3.1 $\pm$ 0.1	3.35 $\pm$ 0.2	3.35 $\pm$ 0.2	2.95 $\pm$ 0.1

Table A.3: Unidentified lines

3240.3	
3245.6	CrII ?
3246.3	
3285.7	CrII ?
3286.4	FeII ?
3382.05	
3387.3	FeII ?
3556.6	
3567.2	
3568.55	
3595.0	
3596.05	
3617.0	
3638.3	
4053.3	Cr II ?
4058.3	
4065.4	
4068.5	
4123.85	
4131.7	very strong
4156.2	
4197.0	
4208.05	
4211.35	
4256.1	
4259.55	
4292.45	very strong
4306.0	
4307.25	both lines should be CII but lines shifted of about 0.3 A
4329.9	very strong
4383.15	
4453.5	
4457.15	
4464.45	
4491.3	very strong
4752.6	very strong
4756.3	very strong
5370.9	
5374.8	
5442.2	Fe II ?
5443.7	Fe II ?
5788.7	
5790.3	

with a estimated error for every line of about +/- 0.1 A

Table A.4: Comments to the different lines

line	comment
AlII 3900.675	fit is much too strong ( $\log gf_{\text{lines.woolf.d}} = -1.270$ , $\log gf_{\text{NIST}} = -2.26$ )
AlII 6226.195	
AlII 6231.621	
AlII 6231.750	lines are not in the Spectrum but in the fit
AlII 4663.050	
AlII 5593.300	
AlII 6243.073	
AlII 6243.203	
AlII 6243.367	fit too strong
AlIII 4149.900	
AlIII 4150.140	
AlIII 4479.890	
AlIII 4479.970	fit is good
AlIII 5722.730	line in sepctrum is asymmetric
AlIII 4512.540	
AlIII 4528.910	
AlIII 4529.200	fit too strong
AlIII 5696.604	fit is good but line in spectrum is asymmetric (unidentified blend?)
AlIII 5163.859	lines are not in the Spectrum but in the fit
AlIII 5163.910	(noise of the spectrum?)
PII 5425.880	continuum is too low
PII 6034.039	(very broad line or bad normalization)
PII 6024.178	fit is good
PII 6043.084	fit is too weak
PII 6301.933	fit is much too strong ( $\log gf_{\text{vald}} = 1.544$ , $\log gf_{\text{KAERI AMODS Database}} = -2.46$ )
PIII 4059.312	
PIII 4080.089	fit is good
PIII 4222.198	
PIII 4246.720	fit is too weak

Table A.5: Phosphorus abundance for every line

line	abundance	comment
P <sub>II</sub> 6024.178	5.094	cosmic is in the line
P <sub>II</sub> 6043.084	5.337	
P <sub>III</sub> 4059.312	5.282	fit is good, line is in wing of unidentified line
P <sub>III</sub> 4080.089	5.153	
P <sub>III</sub> 4222.198	5.362	
P <sub>III</sub> 4246.720	5.457	core of the fit is too deep
P <sub>II</sub> 5425.880	unused	continuum is too low
P <sub>II</sub> 6034.039	unused	(very broad line or bad normalization)
P <sub>II</sub> 6301.933	unused	wrong log gf value

Table A.6: Equivalent width measured with hand by using Dipso

CI	CII	CIII
4762.41 $9 \pm 3$	3167.931 $43 \pm 6$	4647.420 $51 \pm 4$ (*)
4771.747 $21 \pm 4$ (*)	3920.693 $236 \pm 19$	9715.096 $20 \pm 4$
4775.897 $16 \pm 3$ (*)	4295.912 $58 \pm 5$	
4932.050 $11 \pm 2$ (*)	4306.330 $46 \pm 5$ (*)	
5052.167 $24 \pm 3$ (*)	4307.590 $67 \pm 9$	
5380.336 $17 \pm 3$	4313.100 $81 \pm 6$ (*)	
6587.771 $22 \pm 3$	4317.260 $108 \pm 9$	
9078.278 $63 \pm 5$	4318.600 $78 \pm 6$ (*)	
	4321.647 $45 \pm 4$	
	4323.102 $36 \pm 3$	
	4413.260 $29 \pm 3$ (*)	
	4737.97 $67 \pm 5$	
	4744.77 $86 \pm 7$	
	4747.279 $43 \pm 3$ (*)	
	4867.066 $38 \pm 4$	
	4953.857 $100 \pm 8$	
	4964.736 $174 \pm 12$	
	5032.128 $214 \pm 15$	
	5125.20 $44 \pm 4$	
	5137.26 $90 \pm 7$	
	5139.17 $114 \pm 9$	
	5151.09 $161 \pm 13$	
	5535.35 $81 \pm 6$	
	5537.61 $62 \pm 5$	
	5640.55 $212 \pm 17$	
	5891.59 $153 \pm 12$	
	6098.51 $66 \pm 5$	
	6102.56 $34 \pm 3$	
	6578.100 $455 \pm 15$	
	6582.900 $347 \pm 13$	
	6727.19 $45 \pm 4$	
	6731.072 $37 \pm 3$ (*)	
	6738.610 $60 \pm 5$ (*)	
	6750.537 $71 \pm 6$ (*)	
	6755.16 $25 \pm 2$	
	6783.90 $226 \pm 18$	
	6787.22 $136 \pm 11$	
	6791.466 $150 \pm 12$ (*)	
	6798.104 $75 \pm 6$ (*)	
	6800.683 $135 \pm 10$ (*)	
	6812.280 $48 \pm 4$ (*)	

SiII	SiIII
3853.657 40 ± 3	3241.67 17 ± 2
3862.592 83 ± 3 (*)	3791.41 42 ± 3 (*)
4128.053 176 ± 2	3796.11 72 ± 4 (*)
5056.020	4338.52 12 ± 2
5056.353 83 ± 4	4552.654 143 ± 5
5957.612 18 ± 2 (*)	4567.872 101 ± 4 (*)
5978.970 36 ± 4 (*)	4574.777 66 ± 3 (*)
6347.091 130 ± 6 (*)	4813.290 17 ± 2 (*)
6371.359 91 ± 4 (*)	4819.740 42 ± 3
	4828.923 26 ± 3 (*)
	5739.762 59 ± 3
SII	SIII
4153.100 53 ± 4 (*)	3662.010 14 ± 3
4162.700 52 ± 4	3717.780 21 ± 3
4189.710 21 ± 3	4253.590 40 ± 3 (*)
4282.630 18 ± 3 (*)	4332.710 14 ± 3 (*)
4483.420 17 ± 3	4361.530 19 ± 3 (*)
4815.520 69 ± 5 (*)	
4991.940 40 ± 3 (*)	
5103.300 33 ± 2	
5428.655 56 ± 4 (*)	
5432.797 85 ± 5 (*)	
5473.614 55 ± 4 (*)	
5509.705 57 ± 5 (*)	
5606.110 50 ± 4	
FeII	FeIII
3227.742 23 ± 3	4164.790 14 ± 3
4549.474 18 ± 3	4395.780 12 ± 3
5018.450 12 ± 3	
5169.033 19 ± 3	
OI	OII
7771.941 93 ± 5 (*)	4085.114 10 ± 3 (*)
	4349.426 29 ± 4 (*)
	4414.901 28 ± 4
	4590.972 19 ± 3 (*)
	4596.176 9 ± 3 (*)
	4641.817 27 ± 4 (*)
	4649.143 37 ± 4 (*)
	4661.633 25 ± 4 (*)

---

NI	NII
8680.286 65 ± 5 (*)	3408.130 9 ± 2
8686.154 33 ± 5	3437.150 31 ± 2
8703.250 17 ± 4 (*)	3842.180 27 ± 3 (*)
8711.707 20 ± 5 (*)	3955.850 55 ± 4 (*)
8718.835 16 ± 5 (*)	3995.000 135 ± 4
	4035.080 42 ± 3
	4041.310 59 ± 3
	4043.530 37 ± 2
	4095.900 15 ± 2
	4171.590 23 ± 2
	4176.160 33 ± 3
	4227.740 46 ± 3 (*)
	4236.980 57 ± 3
	4442.050 17 ± 2
	4447.030 68 ± 3
	4507.560 16 ± 2
	4601.480 83 ± 6 (*)
	4607.160 72 ± 4 (*)
	4613.870 58 ± 3 (*)
	4643.090 83 ± 3 (*)
	4654.530 15 ± 3 (*)
	4667.210 18 ± 3 (*)
	4674.910 17 ± 3 (*)
	4788.130 33 ± 3 (*)
	4793.650 9 ± 2 (*)
	4810.310 22 ± 3
	5002.700 36 ± 4 (*)
	5005.140 86 ± 4
	5025.670 25 ± 3 (*)
	5666.640 102 ± 5 (*)
	5676.020 73 ± 3 (*)
	5679.560 136 ± 5 (*)
	5686.210 61 ± 3 (*)
	5710.760 65 ± 4 (*)
	5730.670 14 ± 3
	5931.790 34 ± 2 (*)
	5941.670 55 ± 3 (*)
	6610.580 41 ± 4 (*)

---



# B Figures

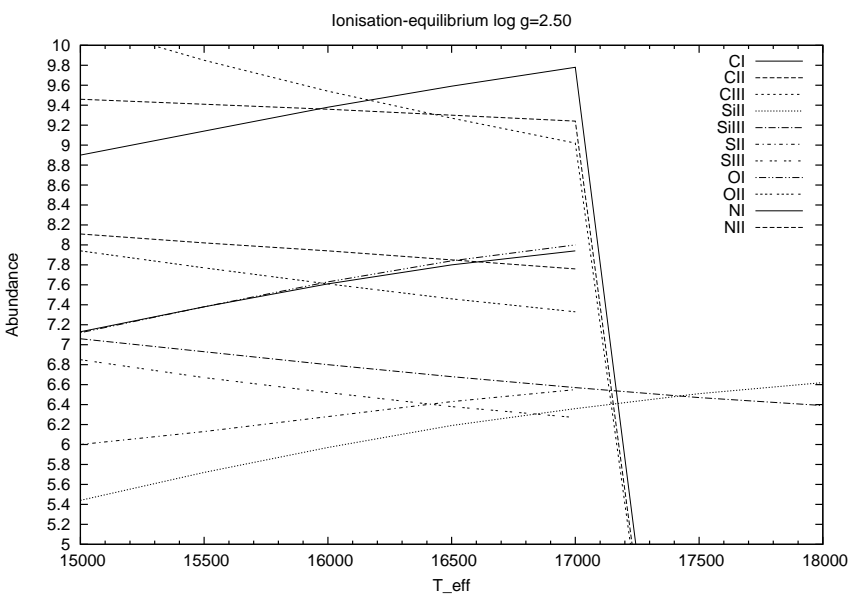
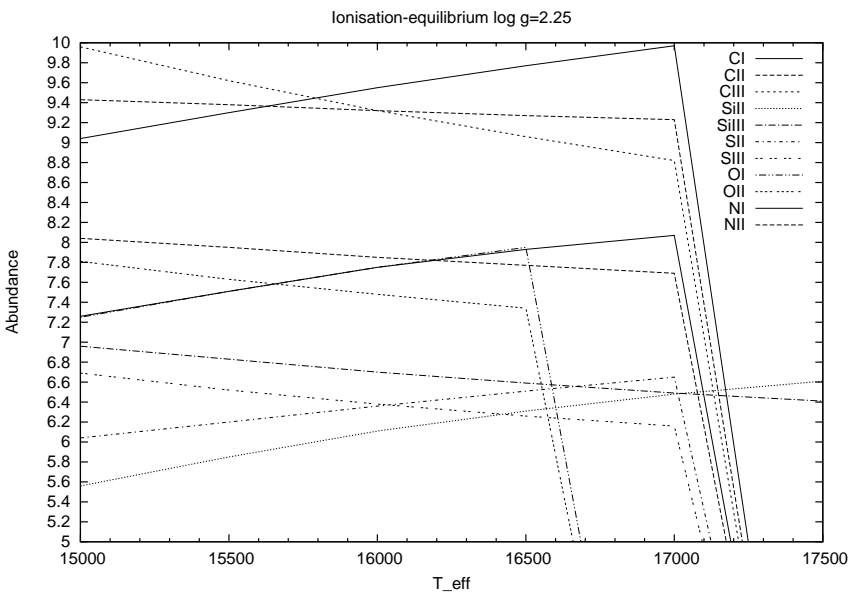


Figure B.1: Ionisation equilibrium for  $\log g = 2.25$  (left) and  $\log g = 2.50$  (right). Note that the edges are artificial and no real effect

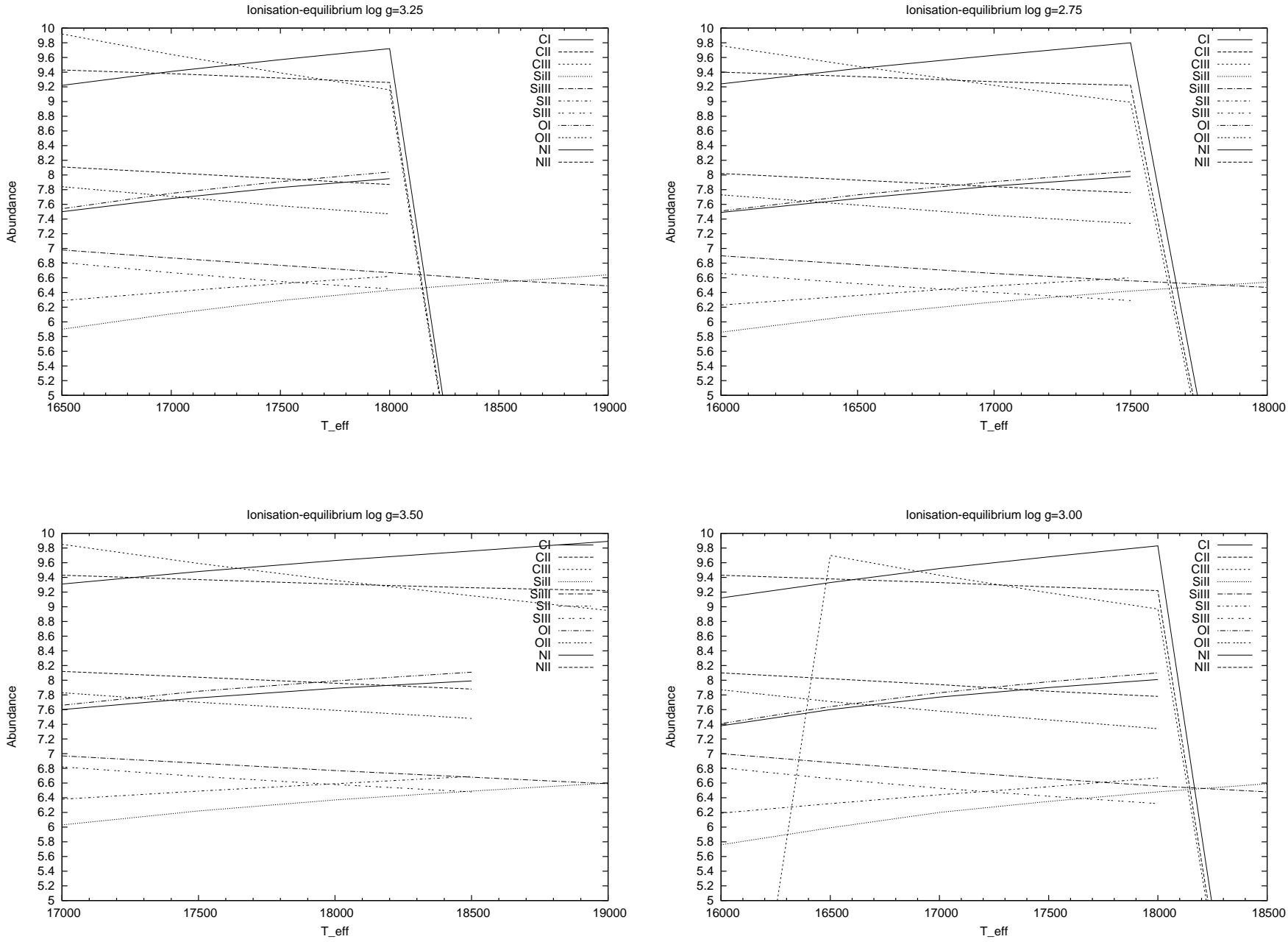


Figure B.2: Ionisation equilibrium for  $\log g = 2.75$  (left top),  $\log g = 3.00$  (right top),  $\log g = 3.25$  (left bottom) and  $\log g = 3.50$  (right bottom). Note that the edges are artificial and no real effect

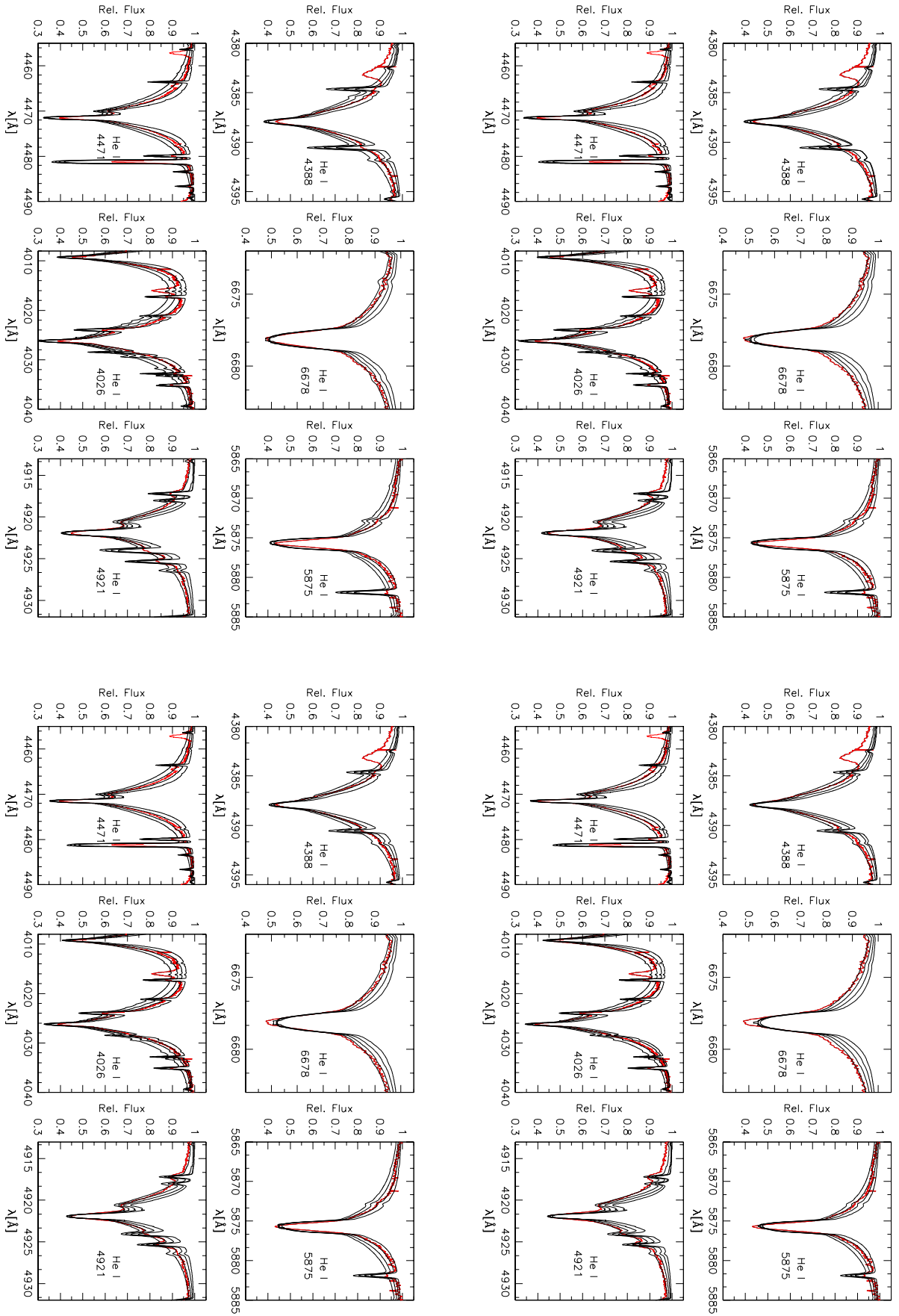


Figure B.3: He-Profile with synthetic spectra in 0.25 steps starting with  $\log g = 2.0$  for  $T_{\text{eff}} = 15\,000$  K (left top),  $\log g = 2.0$  for  $T_{\text{eff}} = 15\,500$  K (right top),  $\log g = 2.25$  for  $T_{\text{eff}} = 16\,000$  K (left bottom) and  $\log g = 2.25$  for  $T_{\text{eff}} = 16\,500$  K (right bottom)

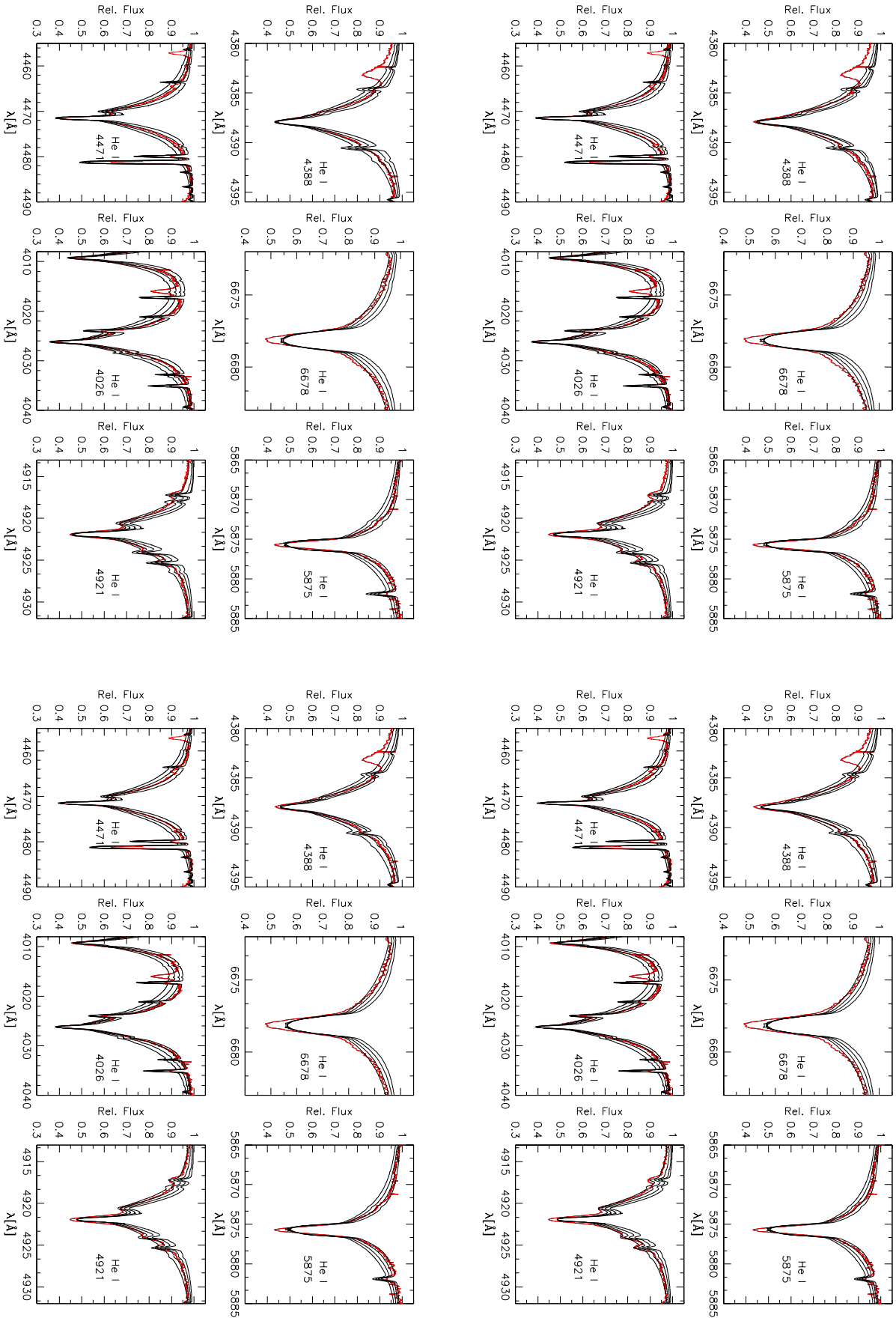


Figure B.4: He-Profile with synthetic spectra in 0.25 steps starting with  $\log g = 2.5$  for  $T_{\text{eff}} = 17000$  K (left top),  $\log g = 2.5$  for  $T_{\text{eff}} = 17500$  K (right top),  $\log g = 2.75$  for  $T_{\text{eff}} = 18000$  K (left bottom) and  $\log g = 2.5$  for  $T_{\text{eff}} = 18500$  K (right bottom).

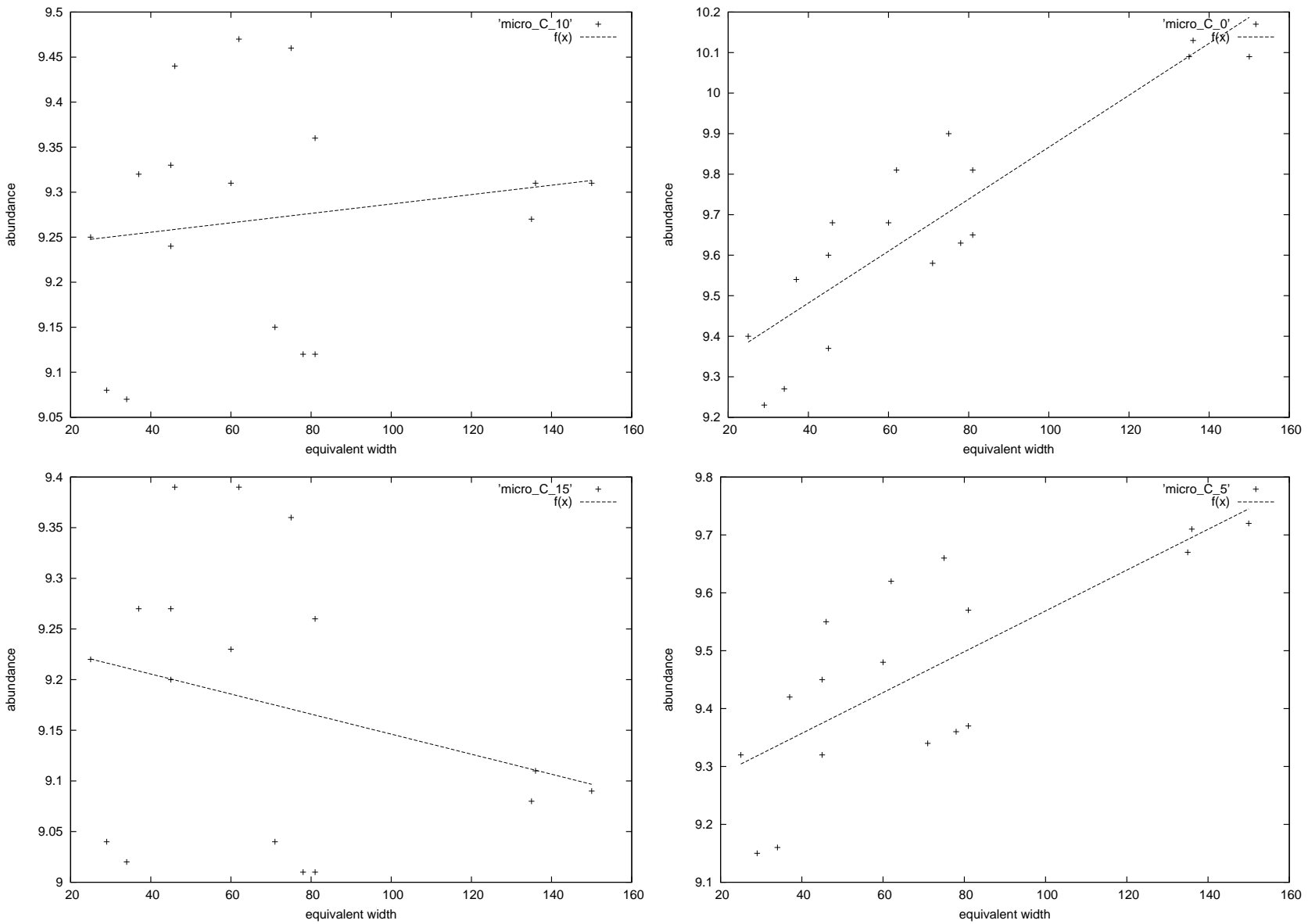


Figure B.5: Abundance measurement for different CII lines with  $v_{\text{turb}} = 0 \text{ km s}^{-1}$  (left top),  $v_{\text{turb}} = 5 \text{ km s}^{-1}$  (right top),  $v_{\text{turb}} = 10 \text{ km s}^{-1}$  (left bottom) and  $v_{\text{turb}} = 15 \text{ km s}^{-1}$  (right bottom) and a linear fit through the datapoints

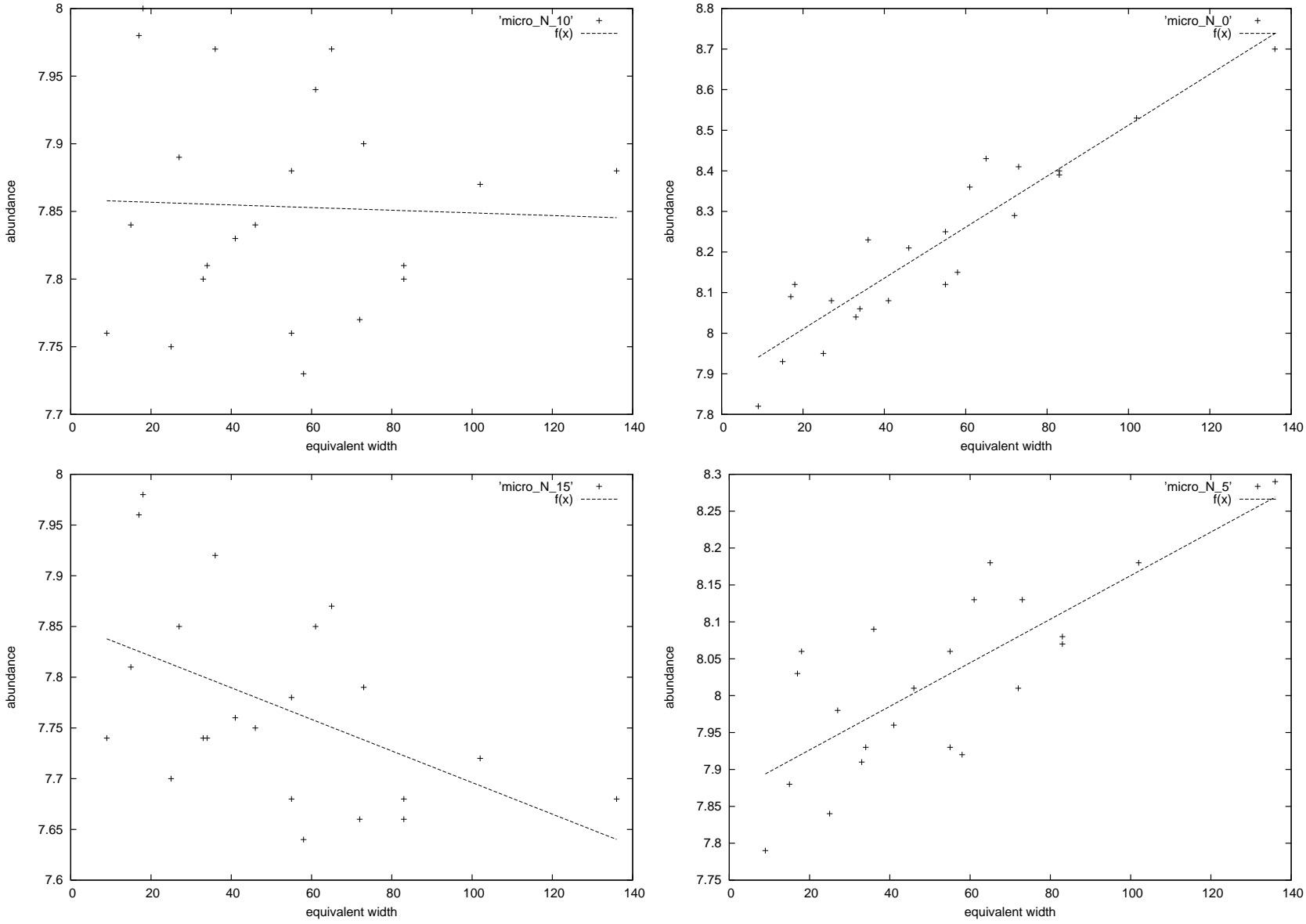


Figure B.6: Abundance measurement for different N II lines with  $v_{\text{turb}} = 0 \text{ km s}^{-1}$  (left top),  $v_{\text{turb}} = 5 \text{ km s}^{-1}$  (right top),  $v_{\text{turb}} = 10 \text{ km s}^{-1}$  (left bottom) and  $v_{\text{turb}} = 15 \text{ km s}^{-1}$  (right bottom) and a linear fit through the datapoints

## C Acknowledgements

Lot of people were involved to bring this work and my study to a final success. One page of this work will be dedicated to these people.

The first thing I want to mention is that the last three and a half years in the observatory belong to the most interesting parts of my study and of my life.

The first big thank you goes to my boss Uli Heber. He makes it possible for me to work in such a great environment not just for this work but also since three and a half years now when I started as a Hiwi. Thanks a lot for helping with my staying in Armagh, giving me the possibility to observe in Spain and Chile, having the door always open for a lot of questions and finally supervising this thesis about the really interesting topic Extreme Helium Stars. Another important person closely related to this thesis is Norbert Przybilla. Thanks for introducing me in ATLAS, DETAIL, SURFACE, answering the many questions about stellar atmospheres, doing the great work with the model atom and finally being referee of this thesis. A big thank you to Simon Jeffery who made it possible to have a great time in Armagh and being a patient supervisor when I did my first steps in analysing stellar spectra. Thanks to Natalie Behara to compute me all the STERNE models which I needed for this thesis.

A good deal for the great working atmosphere and therefore for the success of this work have my officemates, the guys from the Knigge room. Thanks to Stephan who gave me the great possibility to learn from him and work with him on binary subdwarf systems, for the great support before and during my observing trips to Chile and Spain but also for showing me that Bamberg has a lot of nice events like the "Sandkerwa", the "Bockbieranstiche" or the Christmas market. Thanks to Lew for his support during a lot of shared learning hours, for proof reading of this thesis and showing me that Vodka could be really tasteful. Thanks also to the rest of the Knigge guys Matthias with whom I still look forward to taste the "Bembel", Sebastian who brings a lot of fun in the office even if he has the worst jokes I ever heard and sorry I have to say that, a strange football opinion and thanks to the former member Heiko who has kindly given me his desk.

Thanks To Andreas Irrgang for a lot of fruitful discussions about data reduction, spectra analysing, for providing me a lot helpful ISIS routines which makes the work an many cases much easier and for proof reading of this thesis. The regular discussions about football not just about the second league were a great balancing to the daily work.

Heinz Edelman who showed me echelle data reduction and that MIDAS is a really powerful tool for data reduction, thanks for that.

Thanks to Ms Bues who enriches the institute still with regual visits and for proof reading of this thesis.

A big thank you to the rest of the actual and former members of the stellar group, Markus Firnstein, Veronika Schaffenroth, Eva Ziegerer, Alfred Tillich, Florian Schiller, Maria Fernanda Nieva, Stefan Nesslinger and Victoria Lohmann.

Thanks also to the X-ray guys who have a big part in the nice working environment in the observatory. Thanks for having the doors open for every ISIS problem I had.

Thanks to all the people in Armagh. Thanks to you, this time will always remain unforgettable for me.

Thanks to all my friends from university Babsi, Alex, Karsten, Dominik, Zeili, Thomas, Philip, Kerstin, Veit, MichiBu, Michi and Markus. The success of this study would not be possible without the many many not just learning hours you shared with me.

Thanks also to my closest friends in Happurg. I am always looking forward to come home. You are one reason for that. A thank you to Evi who supported me in all during a long time of my study.

A big thank you to my flatmates during the last year; Nina, Fabi, Tom, Vanni and Betti. Thanks for the nice evenings after sometimes long working days. You showed me that there is more to do than just astronomy in Bamberg. It is/was a pleasure for me to share the flat with you.

Marlies, thousands thanks for your great support during the last months, for pushing if necessary or just holding me if necessary. Without you I would never have done so well.

Die letzten Zeilen dieser Arbeit sollen den Menschen gehören ohne die diese Arbeit und mein Studium sicher nicht möglich gewesen wäre und die sicherlich die Wichtigsten in meinem Leben sind: Das sind Meine Eltern Angela und Wolfgang Kugler, meine Geschwister Timo, Franziska und Denise und meine Großeltern Heinz und Helga Kupfer. Vielen vielen Dank für jedes aufmunterte Wort nach anstrengenden Prüfungen, für Hilfe jeglicher Art, dafür dass ihr mich meinen Weg gehen lasst; einfach für alles!!

## D Bibliography

- Aerts, C., Puls, J., Godart, M., & Dupret, M. 2009, *A&A*, 508, 409
- Ahmad, A., Jeffery, C. S., & Fullerton, A. W. 2004, *A&A*, 418, 275
- Asplund, M., Grevesse, N., Sauval, A. J., & Scott, P. 2009, *ARA&A*, 47, 481
- Asplund, M., Gustafsson, B., Lambert, D. L., & Rao, N. K. 2000, *A&A*, 353, 287
- Avrett, E. H. & Loeser, R. 1966, *SAO Special Report*, 201
- Beals, C. S. 1938, *Trans. IAU*, 6, 248
- Behara, N. T. & Jeffery, C. S. 2006, *Baltic Astronomy*, 15, 115
- Berger, J. 1956, *Compt. rend. séances Acad. Sci.*, 242, 2300
- Bloecker, T. 1995, *A&A*, 299, 755
- Bloecker, T. 2001, *Ap&SS*, 275, 1
- Cohen, M., Hudson, H. S., Odell, S. L., & Stein, W. A. 1977, *MNRAS*, 181, 233
- Curtiss, R. H. 1916, *Publications of Michigan Observatory*, 2, 182
- Dreizler, S. 1993, *A&A*, 273, 212
- Dreizler, S. & Werner, K. 1996, in *Astronomical Society of the Pacific Conference Series*, Vol. 96, *Hydrogen Deficient Stars*, ed. C. S. Jeffery & U. Heber, 281–+
- Drilling, J. S. & Hill, P. W. 1986, in *Hydrogen Deficient Stars and Related Objects, Proceedings of IAU Colloq. 87, held in Mysore, India, Nov. 10-15, 1985*. Edited by Kurt Hunger, Detlef Schoenberner, and N. Kameswara Rao. Dordrecht, D. Reidel Publishing Co. (*Astrophysics and Space Science Library*. Volume 128), 1986., p.499, ed. K. Hunger, D. Schoenberner, & N. Kameswara Rao, 499–+
- Fleming, W. 1891, *AN*, 126, 165
- Green, R. F., Schmidt, M., & Liebert, J. 1986, *ApJS*, 61, 305
- Greenstein, J. L. 1966, *ApJ*, 144, 496
- Greenstein, J. L. & Matthews, M. S. 1957, *ApJ*, 126, 14
- Greenstein, J. L. & Münch, G. 1953, *Carnegie Inst. Washington Year Book*, 53, 11
- Hamann, W. 1996, in *Astronomical Society of the Pacific Conference Series*, Vol. 96, *Hydrogen Deficient Stars*, ed. C. S. Jeffery & U. Heber, 127–+
- Heber, U. 1983, *A&A*, 118, 39
- Heber, U., Dreizler, S., de Boer, K. S., Moehler, S., & Richtler, T. 1988, *Astron. Ges., Abstr. Ser.*, 1, 16

- Henize, K. G. & Fairall, A. P. 1981, *PASP*, 93, 435
- Herbig, G. H. 1964, *ApJ*, 140, 1317
- Herwig, F., Blöcker, T., Langer, N., & Driebe, T. 1999, *A&A*, 349, L5
- Hoffmeister, C. 1944, *Astronomische Nachrichten*, 274, 176
- Høg, E., Fabricius, C., Makarov, V. V., et al. 2000, *A&A*, 355, L27
- Humason, M. L. & Zwicky, F. 1947, *ApJ*, 105, 85
- Hunger, K. & Klinglesmith, D. 1969, *ApJ*, 157, 721
- Husfeld, D., Butler, K., Heber, U., & Drilling, J. S. 1989, *A&A*, 222, 150
- Iben, Jr., I. & Tutukov, A. V. 1984, *ApJS*, 54, 335
- Jeffery, C. S. 1996, in *Astronomical Society of the Pacific Conference Series*, Vol. 96, *Hydrogen Deficient Stars*, ed. C. S. Jeffery & U. Heber, 152–+
- Jeffery, C. S. 2000, in *Proceedings of the Workshop on Binary and Variable Stars*, ed. H. L. Malasan, O. Hashimoto, & K. Y., 32
- Jeffery, C. S. 2008a, in *Astronomical Society of the Pacific Conference Series*, Vol. 391, *Hydrogen-Deficient Stars*, ed. A. Werner & T. Rauch, 53–+
- Jeffery, C. S. 2008b, in *Astronomical Society of the Pacific Conference Series*, Vol. 391, *Hydrogen-Deficient Stars*, ed. A. Werner & T. Rauch, 3–+
- Jeffery, C. S. & Hamann, W. 2010, *MNRAS*, 460
- Jeffery, C. S., Starling, R. L. C., Hill, P. W., & Pollacco, D. 2001, *MNRAS*, 321, 111
- Kippenhahn, R. & Weigert, A. 1990, *Stellar Structure and Evolution*, ed. Kippenhahn, R. & Weigert, A.
- Klemola, A. R. 1961, *ApJ*, 134, 130
- Kurucz, R. L. 1970, *Atlas: A computer program for calculating model stellar atmospheres*, ed. Kurucz, R. L.
- Landolt, A. U. 1973, *PASP*, 85, 661
- Lucy, L. B. 1964, *SAO Special Report*, 167, 93
- Ludendorff, H. 1906, *AN*, 173, 3
- Luyten, W. J. 1952, *ApJ*, 116, 283
- McCook, G. P. & Sion, E. M. 1999, *ApJS*, 121, 1
- McGraw, J. T., Liebert, J., Starrfield, S. G., & Green, R. 1979, in *IAU Colloq. 53: White Dwarfs and Variable Degenerate Stars*, ed. H. M. van Horn & V. Weidemann, 377–381

- Moore, C. E. 1945, A multiplet table of astrophysical interest.
- Moore, C. E. 1970, Selected tables of atomic spectra, ed. C. E. Moore
- Pandey, G. 1999, PhD Thesis, Indian Institute of Astrophysics
- Pandey, G., Lambert, D. L., Jeffery, C. S., & Rao, N. K. 2006, *ApJ*, 638, 454
- Pigott, E. 1797, *Phil. Trans. R. Soc. London*, 1, 133
- Popper, D. M. 1942, *PASP*, 54, 160
- Przybilla, N., Butler, K., Heber, U., & Jeffery, C. S. 2005, *A&A*, 443, L25
- Przybilla, N., Nieva, M. F., Heber, U., & Jeffery, C. S. 2006, *Baltic Astronomy*, 15, 163
- Rufus, W. C. 1923, *Publications of Michigan Observatory*, 3, 257
- Saio, H. & Jeffery, C. S. 2002, *MNRAS*, 333, 121
- Smith, L. F. & Aller, L. H. 1969, *ApJ*, 157, 1245
- Warner, B. 1967, *MNRAS*, 137, 119
- Webbink, R. F. 1984, *ApJ*, 277, 355
- Wegner, G. & Nelan, E. P. 1987, *ApJ*, 319, 916
- Werner, K., Dreizler, S., Heber, U., & Rauch, T. 1996, in *Astronomical Society of the Pacific Conference Series*, Vol. 96, *Hydrogen Deficient Stars*, ed. C. S. Jeffery & U. Heber, 267–+
- Wesemael, F., Greenstein, J. L., Liebert, J., et al. 1993, *PASP*, 105, 761
- Wolf, C. & Rayet, G. 1867, *Comptes Rendus*, 65, 292
- Wolff, S. C., Pilachowski, C. A., & Wolstencroft, R. D. 1974, *ApJ*, 194, L83
- Woods, I. E. 1928, *Harvard College Observatory Bulletin*, 855, 22



# E Declaration

## DECLARATION

Hereby I declare that I wrote this diploma thesis autonomously and that I have not used other resources than those quoted in this work.

## ERKLÄRUNG

Hiermit erkläre ich, dass ich die Diplomarbeit selbstständig angefertigt und keine Hilfsmittel außer den in der Arbeit angegebenen benutzt habe.

Bamberg, October 2010

\_\_\_\_\_ (Thomas Kupfer)